DEVELOPMENT OF AN INTEGRATED SYSTEM FOR HUMAN SPINE DEFORMITY MEASUREMENT

ZHENG XIN

B. ENG.

A THESIS SUBMITTED

FOR THE DEGREE OF DOCTOR OF PHILOSOPHY

DEPARTMENT OF MECHANICAL ENGINEERING

NATIONAL UNIVERSITY OF SINGAPORE

NOVEMBER 2014

Declaration

I hereby declare that this thesis is my original work and it has been written by me in its entirety. I have duly acknowledged all the sources of information which have been used in the thesis.

This thesis has also not been submitted for any degree in any university previously.

Zheng Xin

20 November 2014

Acknowledgements

The author wishes to express his grateful gratitude to the supervisors, Prof. Andrew Nee Yeh Ching and Assoc. Prof. Ong Soh Khim from the Department of Mechanical Engineering, for their great help, encouragement and guidance throughout the research and study which is deeply appreciated.

The author also wishes to thank all the colleagues and fellow students in Stewart Platform research group and Augmented Reality research group, especially Dr. Ng Chee Chung, Dr. Vincensius Billy Saputra, Dr. Fang Hongchao and Mr. Yan Shijun for their inspiration, suggestions, research ideas and precious friendship for this research project. Besides, the author appreciates the technical assistance from the research staff and officers in the Advanced Manufacturing Laboratory, especially to Mr. Tan Choon Huat, Mr. Wong Chian Long, Mr. Ho Yan Chee, Mr. Lim Soon Cheong, Mr. Simon Tan Suan Beng and Mr. Lee Chiang Soon, for their support and machining the mechanical components for the research.

In addition, the author would like to acknowledge the contribution by the final year project student Mr. Tang Yongjie and SRP project participants, namely, the four junior college students (Yeo Jia Xuan, Sng Huina Julia, Madeline Ang Yen Yin and Xin Yi). They are very helpful and responsible in finishing their research project and working and cooperating with the author.

Last but not least, the author wants to thank his family and friends, directly or indirectly, for their supports and encouragement and the financial assistance provided by National University of Singapore during the research project.

Presented and Published Work Arising from the Thesis

The following presentations and publications resulting from the thesis were made prior to submission:

- X. Zheng, S.K. Ong, and A.Y.C. Nee (2014), "A Novel Evaluation Index for Adolescent Idiopathic Scoliosis Progression Measurement and Diagnosis," The International Journal of Medical Robotics and Computer Assisted Surgery, accepted on 15 Jan 2014.

- X. Zheng, S.K. Ong, and A.Y.C. Nee (2013), presented the paper of "An Innovative Approach for Assessing Adolescent Idiopathic scoliosis", at the 2013 World Congress on Advances in Nano, Biomechanics, Robotics, and Energy Research (ANBRE13), Seoul, Korea, 25-28 August 2013, p.137-154.

- X. Zheng, S.K. Ong, and A.Y.C. Nee (2014), "An Innovative Approach for Evaluating Adolescent Idiopathic Scoliosis through the Utilization of a Stewart Platform and Stereo Vision Technology", Advances in Biomechanics and Applications Journal, the paper was invited and was submitted on May 2014.

Table of Contents

Summary

Adult scoliosis is defined as a spinal deformity in a skeletally mature patient with the Cobb angle of more than 10 degrees in the coronal plane. Adolescent idiopathic scoliosis (AIS) is a long-term disease, affecting some 3% to 5% of children; it is defined as a lateral curvature of the spine greater than 10 degrees accompanied by vertebral rotation. Usually, a complex three-dimensional (3D) deformity of the spine will affect the quality of life during the period of rapid growth, leading to a damaged self-image, potential back pain, and pulmonary and cardiac complications in later life. A number of scientists reported that AIS is one of the most epidemic musculoskeletal diseases affecting children because of the vertebral rotation and deformity resulting in rib cage and flank muscle asymmetries. For diagnosis purposes, most children need to be monitored routinely using X-ray radiography after assessing by the Adams forward bending test as regularly as every three months, resulting in high and frequent exposure of radiation.

In order to reduce X-ray exposure and diagnosis cost, a mechanically-assisted system is a potential application in scoliosis measurement. The objective of this research is to build a non-contact and radiation-free system to evaluate and assess the severity of human spinal deformity. An innovative and integrative system consisting of a Stewart platform, which is a parallel manipulator, a controllable mechanical frame and motion capture technique is proposed in this research. The patient's posture is controlled precisely using the Stewart platform which assists the subject to bend his trunk and spine according to a series of pre-defined angles. The subject's bending postures are precisely controlled into 0˚, 30˚, 45˚, 60˚ and 90˚. For each of the postures, an image of the subject's back surface is captured with a

stereo camera system. The shapes of the spine and trunk are measured to evaluate the presence and severity of scoliosis through quantitative and reliable analysis before the subject is referred to the hospital for further inspection.

To complement the Cobb angle which is a standard parameter for scoliosis evaluation, two 2D novel evaluation indices, IVAS and MIVAS, for adolescent idiopathic scoliosis measurement and diagnosis are introduced to complement the existing assessment index, such as the Cobb angle, the differences of shoulder height, etc. Besides the IVAS and MIVAS parameters, a 3D parameter named 3DIVAS was designed for measuring the severity of scoliosis. A comparison between the Cobb angle and IVAS, the Cobb angle and MIVAS and the Cobb angle and 3DIVAS has been conducted in this thesis. The correlation coefficient is 0.9284 between IVAS and the Cobb angle, 0.9175 between MIVAS and the Cobb angle and 0.9116 between 3DIVAS and the Cobb angle. The high correlation found between the clinical variable (Cobb angle) and topographic variables (IVAS, MIVAS and 3DIVAS) shows that although different calculation methods are used for different deformities, they have the potential to be used as tools for supporting the traditional scoliosis measurement methods.

A data sample of 30 X-ray images of scoliotic spines from 30 patients including 22 C-shape spines and 8 S-shape spines was used in this research to evaluate and examine the usability and validity of the new index. The correlation between the Cobb angle and the indices was also determined, and a high correlation is found which demonstrated the usefulness of this proposed indices.

List of Figures

List of Tables

Chapter 1 Introduction

1.1 Overview

Adolescent idiopathic scoliosis (AIS) is a long-term spinal disease which affects some 3% to 5% of children in the at-risk population aged between 10–16 years. The human spine scoliosis is defined as a lateral curvature of the spine greater than 10 degrees accompanied by vertebral rotation. The etiology of this disorder remains unknown. It is thought to be a multi-gene dominant condition with variable phenotypic expression. Nowadays, this area is a much pursued research topic as more researchers and clinical doctors are working on spine scoliosis rehabilitation.

As reported, idiopathic scoliosis is a classic orthopedic disorder in which the etiology and pathogenesis still remain unidentified, although the genetic factor and spinal biomechanics have been shown to play an important role. Usually, a complex three-dimensional (3D) deformity of the spine will affect the quality of life during the period of rapid growth, leading to a damaged self-image, potential back pain, and pulmonary and cardiac complications in later life.

In school screening, in order to check the spinal shape and pre-inspect the occurrence of scoliosis for teenagers, a physical examination will be conducted in school before the teenagers need to be referred to hospitals or clinics. The Adams forward bending test, a popular evaluation technique used for school scoliosis screenings, is the most basic form of back-shape analysis method used to look for scoliosis in school-aged youngsters. However, according to reports, the Adams forward bending test fails to detect a significant number of scoliosis cases, especially when it is used as the sole screening method. Besides, this method also

suffers from the problem that it is not sensitive to abnormalities in the lower back, which is a very common site for scoliosis.

In clinics or hospitals, the traditional method for assessing scoliosis is the Cobb angle measurement. A radiograph of the spine is made in the coronal plane and the angle of any spinal curve is measured. The Cobb angle is an important measurement index in diagnosing scoliosis and determining the type of treatment. Several disadvantages should be noted. Biomechanically, scoliosis is a 3D deformity of the spine. However, the radiographic Cobb angle measurement only provides two-dimensional (2D) information, which makes this method unreliable. In order to track the growth of spinal deformity, the patients have to take radiographs regularly, which could lead to potential ill effects of radiation leading to genetic mutation.

In order to overcome the limitation of the traditional methods for human spine scoliosis measurement, an innovative and new methodology needs to be developed to reduce the potential radiation exposure and increase the measurement accuracy, which will be a key element for decision making by both surgeons and patients.

To sum up, this project aims to develop an innovative, non-contact and radiation-free system for human spine deformity measurement and assessment based on stereo vision technology and Stewart platform (SP) manipulation to precisely evaluate a patient's trunk topology, and this system can be considered for implementation in the schools for teenagers' health condition examination.

Furthermore, a set of innovative evaluation indices has been established and introduced for adolescent idiopathic scoliosis measurement and diagnosis for the

complementation of the existing evaluation parameters. The new evaluation index is based on the phenomenon of the tilt and deviation of the vertebras in a scoliotic spine, which forms the tile angles between each pair of adjacent vertebras.

To examine and estimate the usability and validity of the new indices, a data sample of 30 X-ray images of scoliotic spines was used in the preliminary experiment. The Cobb angle and the new indices were calculated and compared based on the same data sample. The correlation coefficient between the Cobb angle and the new indices was also determined. The correlation coefficient is 0.9284 between IVAS and the Cobb angle, 0.9175 between MIVAS and the Cobb angle and 0.9116 between 3DIVAS and the Cobb angle. And the high correlation is found which demonstrated the usefulness of these proposed indices. In this simulation, it has been shown that the newly-proposed indices have the potential to be used as a tool to support the traditional scoliosis measurement methods.

Using this system, a subject's bending posture can be obtained with high repeatability in a series of pre-defined angles, e.g., 0˚, 30˚, 45˚, and 90˚. For each posture, the images of the subject's back can be captured using stereo cameras and analyzed quantitatively to determine the presence and severity of scoliosis. Furthermore, all the data are stored in the database for further monitoring and assessment.

This research presents the design, development, construction of a spinal deformity measurement system for 3D spatial investigation of human spine shapes. To achieve better results and higher precision, three cameras are utilized simultaneously to attain sufficient redundancy to guarantee high accuracy and consistency of the measurement. By introducing information-driven assessment

tools, this research can help doctors and surgeons treat individual patients with greater safety, improved efficacy, and reduced morbidity in the measurement of scoliosis.

1.2 Background

As one of the major skeletal diseases in adolescents, where in the majority of cases it is manifested as a ‘C’ shape or ‘S’ shape (Willner 1974), scoliosis or spinal curvature occurs in three dimensions accompanied with the trunk rotation as the significant indications usually being changes in body symmetry and back surface shape. The regular examination by taking X-ray images exposes patients to high level of ionizing radiation which is potentially harmful to the patients’ health (Lonstein et al. 1989). Many previous works of orthopedists and researchers have made a great contribution to reduce the radiation exposure by exploring non-contact and radiation-free methods through discovering the correlation between the human back surface topology and the severity of spinal deformity (Hoffman et al. 1983), such as (1) a posterior-anterior projection, (2) specially designed leaded acrylic filters, (3) a high-speed screen-film system, (4) a specially designed cassette-holder and grid, (5) a breast-shield and (6) additional filtration in the x-ray tube. However, these techniques have not gained wide acceptance in the hospitals and clinics as they are assessed to be prone to biases caused by patients’ movements, breathing, posture and sway, limiting their practical utility.

In this thesis, the application of a combination of surface topology generation technique and a mechanical platform is described as a potential alternative valuation for adolescent idiopathic scoliosis patients. For most of the

patients, seemingly the inspiration of looking for treatment is to improve the appearance of the back and body shape rather than to correct the underlying spinal disease. Thus, the psychosocial and physical concerns and cosmetic impacts remain important aspects in the diagnosis decision-making process. Due to the current medical statistics, there is a growing need to quantify the body asymmetry and back surface shape aiming for producing a widely agreed methodology to be used in developing treatment plans and evaluating treatment outcomes. The purpose of the research is to develop an original, low cost and safe apparatus using stereo vision techniques and motion capture technology to acquire multiple locations of markers on a patient's back and other feature samples of the back surface shape to provide accurate results for quantitative and reliable analyses of the cosmetic defect and underlying impairment.

To examine the adolescent idiopathic scoliosis for school pupils, the opportunity to quantify routinely and reliably the cosmetic deficiency and decrease the radiation exposure would motivate more important studies for improving the quality of life for the affected children all over the country.

1.2.1 Adolescent Idiopathic Scoliosis

Different groups have different definitions of scoliosis, which are usually specified as larger than 10 degrees lateral curvature of the spine, as measured using the benchmark Cobb angle method, typically accompanied by vertebra rotation (Stokes 1994; Homocystinuria 2001). Nowadays, it is a popular research topic as increasingly more researchers and clinical doctors have committed to spine scoliosis rehabilitation. A number of scientists reported that AIS is one of the most

epidemic musculoskeletal diseases affecting children (Narayanan 2008) because of the vertebral rotation and deformity resulting in rib cage and flank muscle asymmetries (Dolan et al. 2008). In general, a serious 3D deformity of the spine will affect the appearance and the quality of life during a person's growing period, leading to a self-abased image, potential waist and back pain, and cardiac complication in later life (Moe et al. 1983).

1.2.2 Surface Topology Generation Technology

Surface topology (Eigensee et al. 1997) is the terminology most frequently used to study the properties that are preserved under continuous deformations including stretching and bending, but not tearing or gluing. The phrase surface topology is frequently used to explain the technology concentrating on the description of the position of the feature points in terms of coordinate system including altitude, latitude and longitude. Besides mathematics, surface topology generation techniques have been applied to other fields including bioengineering, rehabilitation research, fluid mechanics, etc.

The availability of motion capture techniques provides an opportunity to describe accurately the 3D position of multiple points and to investigate novel ways of enhancing the usefulness of existing topographical descriptions by introducing the capability of acquiring identified feature samples from distorted shapes and surfaces. The surface topography generation method was applied to the epidemic problem of scoliosis measurement by modifying the performance of self-built equipment and examining the applicability of the system.

Laulund et al. (1982) have attempted to apply the surface topography generation technology to school screening for structural scoliosis, which is a useful technique in the assessment of various trunk disorders, and have developed an apparatus to take an individual measurement of back surface contour and 3D information of the reflective markers from teenagers diagnosed with deformed spinal disease named adolescent idiopathic scoliosis. Many researchers have made outstanding contributions to the research of scoliosis diagnosis and treatment, such as the Moiré technique used by Takasaki and his team (Takasaki et al. 1970) and the ISIS system invented by the Oxford Orthopedics Engineering Centre (Patias et al. 2006). Although many distinguished scientists and groups have tried to develop and commercialize the human back surface topology generation apparatus and systems for use in the evaluation of the impact of scoliosis, none of them have gained wide clinical acceptance.

The main focus of the research is to monitor the progress of an affected child's trunk using radiation-free topology generation technology, and if necessary provide suggestions to stabilize the skeletal defect to prevent any deterioration condition. During the past few decades, there has been growing emphasis on the evaluation of the psychosocial impacts from the changes in body shapes and physical imbalance in order to generate an appropriate treatment plan. Overall, the surface topology generation technology could be potentially useful in the assessment of back surface shape and the severity of scoliosis through measuring multiple samples.

1. 3 Objective and Significance of the Research

The popular method of monitoring the progress of scoliosis and quantifying the degree of spinal deformity is to take measurements from full poster-anterior X-ray images. The Cobb angle is used as a standard measurement to determine and track the progression of scoliosis. Dr John Cobb invented this method in 1948 (Cobb 1948). Although the radiography technology and Cobb angle are still regarded as the "golden standard" against all the other newly developed methods, the radiography method and Cobb angle index have some limitations. Since the etiology and pathogenesis still remain unknown, several indirect scoliosis diagnosis and measurement approaches and systems have been proposed. The mechanisms become even more complex when different techniques, such as handheld devices (Thulbourne 1976; Bunnell 1984; Pun et al. 1987; Pearsall et al. 1992; Pruijs et al. 1995), optical-electronic techniques, Moiré fringe technique (Adair et al. 1977; Ruggerone and Austin 1986; Sahlstrand 1986; Poncet et al. 2001), X-ray technology, etc., are introduced to investigate the human back topology.

The research gaps of the previous methods of human spinal deformity measurement and trunk distortion evaluation index are summarized as follows:

• Although the pre-examined method of Adams forward bending test has been applied in the school screen program as the most commonly used approach, it bears the disadvantage of judgment subjectivity from doctors or orthopedists, which is usually called the inter-observer and intra-observer variations (Carman et al. 1990; Morrissy et al. 1990; W. Keessen 1994; Delorme et al. 2002; Stokes and Aronsson 2006). As reported, it is arguable whether this method is sufficiently reliable.

• In hospitals and clinics, the traditional method for assessing scoliosis, which uses the Cobb angle model and regular X-ray radiograph of the spine, is made

in the coronal plane that it is a 2D numerical representation of a 3D deformity, which is questionable (Stokes and Moreland 1989; Beauchamp et al. 1993). However, this method suffers from severe shortcomings of inaccuracy, potential harm from radiation exposure and high cost (Goldberg et al. 1996).

• Currently, there are few studies on methods that could allow the doctors to bend the patients in postures accurately to acquire fast and accurate results and to manipulate the output data in a database easily. There is hardly any reported work in the field of applying the SP in facilitating the measurement of scoliosis.

The main aim of this study is to develop a radiation-free non-contact methodology for human spinal deformity measurement based on stereo vision photography and SP manipulation. The specific objectives of the research are as follows.

• Propose an alternative method for accurate body trunk deformity assessment using surface measurement techniques.

• Design and construct a spinal deformity measurement apparatus and hardware system.

• Investigate the possibility to achieve precise human posture control with the use of SP.

• Design and validate a new evaluation index and parameter to represent the severity indication of human spine scoliosis.

The new methodology and results of this present study may have significant guidance and impact on both providing an alternative approach for human spine distortion evaluation and offering a new scoliosis evaluation indicator in the following aspects.

• First, the new measurement apparatus provides the methodology and practical application of using SP for human spine deformity assessment.

• Second, the proposal and theoretical application of specially designed estimation indices to present the trunk distortion and back surface topology quantitatively.

1.4 Outline of the Thesis

Chapter 2 gives a review and summary of the medical and orthopedic literature to describe the development, pathogenesis, observable characteristics of the adolescent idiopathic scoliosis and engineering literature to introduce the prevalent measurement technology to evaluate the severity and progression of the disease. In this chapter, different methods and technologies to assess human back scoliosis are introduced and the advantages and disadvantages of these methods are compared. A review of the early efforts by many researchers and doctors to minimize the ionizing exposure of X-ray radiation to the patients by using surface topology generation techniques is included in this part. As the SP plays important roles in the overall system, a short review on the development, design, and control of the SP is described. Furthermore, this chapter provides a literature review of different measurement parameters and indices for spinal deformity to assess the validity and potential usefulness of the existing measures to better describe body shape and back surface asymmetries.

Chapter 3 describes the design, development and construction of a mechanical apparatus based on the SP, motion capture techniques and stereo vision technology that is safe, and capable of obtaining the exact 3D spatial position of the

bony markers and back surface shape. In this chapter, both the simulation of the system and construction of the mechanical apparatus are introduced.

Chapter 4 focuses on the development of two novel evaluation parameters, namely, inter-vertebra angular separation index (IVAS) and modified inter-vertebra angular separation index (MIVAS), for adolescent idiopathic scoliosis progression measurement and diagnosis. A new 3D index of 3DIVAS is also developed. A data sample of several X-ray images of scoliotic spines is used in this research to evaluate and examine the validity of the new indices. The correlation between the Cobb angle and the IVAS index, MIVAS index and the 3DIVAS index is also determined. The correlation coefficient is 0.9284 between IVAS and the Cobb angle, 0.9175 between MIVAS and the Cobb angle and 0.9116 between 3DIVAS and the Cobb angle. The high correlation demonstrates the usefulness of these indices.

Chapter 5 introduces the performance testing process for the overall system and validates the test results to confirm that the apparatus is capable of being utilized, and the 3D locations of the feature points attached on the model's back surface can be reconstructed with clinically acceptable solutions. This chapter describes the setup of the overall system including the SP, the mechanical frames and the camera system. A trial experiment is performed using the system and the results are based on the data samples acquired from a physical spinal model.

Chapter 6 presents the process of system calibration and spinal deformity evaluation process optimization. The manufacturing and assembly tolerance is discussed to decrease the effect on the apparatus accuracy. The reflective markers and stereo cameras are used for positioning the location of the mechanical frame. The theoretical position of the frame calculated from the forward kinematic

algorithm and practical position of the frame are compared. The custom-built analysis software is designed in Matlab, including the user interface for controlling the SP, stereo camera system for motion capturing and the results interpretation interface.

Chapter 7 describes the experiments to evaluate the usability of the system using the physical spinal model following a series of forward bending angles precisely controlled by the mechanical frame. This chapter includes the calculation of the two proposed novel angular separation indices and other conventional parameters to describe the severity of deformity of back surface topology using the sample data. From these sample data and the novel angular separation indices, distorted surface data is constructed to simulate the occurrence of scoliosis.

Chapter 8 reviews the overall accomplishment in this study and discusses the results obtained. The results are compared with published data from conventional systems and are found to be comparable. In this chapter, further research and future potential applications are proposed to strengthen the clinical usefulness of surface topology generation technology for the evaluation of adolescent idiopathic scoliosis. References and appendices are presented after the main body of the thesis, including sample data, figures and tables in this research.

Chapter 2 Literature Review and Related Work

2.1 Adolescent Idiopathic Scoliosis

2.1.1 Definition and Brief Introduction of Scoliosis

Adolescent idiopathic scoliosis, simply defined as a lateral curvature of the spine, has been recognized clinically for centuries. The deformity is actually much more complicated, and to describe more completely and quantify scoliosis deformity, three planar and 3D terminology and measurements are required (Stokes 1994). However, for practical purposes, the deformity can be measured most conventionally from the standing coronal plane radiographs using the Cobb angle technique (Cobb 1948).

For certain patients, an underlying cause can be determined, including congenital changes, secondary changes related to neuropathic or myopathic conditions, or later in life from degenerative spondylosis. However, the cause of most of the scoliosis cases is not known (Kleinberg 1922). Adolescent idiopathic scoliosis is present in 3-5% of the children between 10 and 16 years of age (I. Busscher 2010). It is defined as a lateral curvature of the spine greater than 10 degrees accompanied by vertebral rotation. It is thought to be a multi-gene dominant condition with the variable phenotypic expression. Severe pain, a left thoracic curve or an abnormal neurologic examination are red flags that point to a secondary cause for spinal deformity. Specialty consultation and magnetic resonance imaging are needed if red flags are present.

Adolescent idiopathic scoliosis can probably be considered as a complicated genetic trait disorder. There is often a positive family history but the pattern of inherited susceptibility is not clear. Current information suggests that there is

genetic heterogeneity (Mao et al. 2013). This indicates that multiple potential factors are acting either dependently or independently in its pathogenesis (Lowe et al. 2000).

The prevalence of the rate of adolescent idiopathic scoliosis, using an angle of 10° or more, is approximately 2-2.5% (Kane 1977; Weinstein et al. 2008). Generally, 9.2% of the scoliosis has been reported although only 0.23% requires treatment (Nissinen et al. 1993). The differences that have been found between specific populations are thought to be due to genetic factors (Giampietro et al. 2003). In addition, environmental factors may also be a possible factor (Grivas et al. 2005).

The prevalence is very dependent on the curve size cut-off point, decreasing from 4.5% for curves of 6 degrees or more to only 0.29% for curves of 21° or more. It is also very dependent on sex, with one girl to one boy for curves of 6–10° but 5.4 girls to one boy for curves of 21° or more (Rogala et al. 1978).

The incidence, by year of birth, of treatment (brace or surgery) is remarkably stable averaging 0.26% (range, 0.14–0.43%) over a 23 year period from 1955 through 1977 (Montgomery and Willner 1997). The female to male ratio in this treatment (brace or surgery) series was 7 to 1. Although the ratio of braced to operated patients was not provided, it is generally thought that approximately 0.1% will warrant surgery (Asher and Burton 2006).

2.1.2 Classification of Spine Deformity

The Scoliosis Research Society has defined the scoliosis as deformity which occurs at the lateral side of the spine greater than 10 degrees as measured using the

Cobb method on a standing radiograph (Kane 1977). The idiopathic spine curvature is a structural curve with no clear underlying cause.

Idiopathic scoliosis is classified based on the age of the patient when it is first identified. Infantile scoliosis has an onset before 3 years of age. The infantile form accounts for less than 1% of all cases. Juvenile scoliosis contributes to 12% to 21% of all the patients with scoliosis (Dobbs and Weinstein 1999), which is first detected between 3 to 10 years old. Adolescent idiopathic scoliosis is found between 10 years old and growth maturity and this stage of spine deformity accounts for the majority of all the idiopathic scoliosis.

Idiopathic scoliosis has been sub-divided into three groups (James 1954) based on the practical observation as shown in Table 2.1.

Table 2.1: classification of idiopathic scoliosis patients according to age

Groups	Infantile Scoliosis	Juvenile Scoliosis	Adolescent Scoliosis
Age	Age before 3	Age 5 to 8	Age 10 until end of growth

This is the most widely used classification (Pehrsson et al. 1992; Robinson and McMaster 1996). Among all the cases of scoliosis, 80% or more is of the adolescent variety (Riseborough and Wynne-Davies 1973). As it is often not possible to determine the age of onset, it is likely that there is an overlap at the classification of infantile/juvenile interface and at the classification of juvenile/adolescent interface. The most common infantile curves presented are the left thoracic apex, and males are affected more frequently. The most common juvenile curves are the right thoracic apex and females are more frequently affected (McMaster 1983).

2.1.3 Effects of Spinal Deformity

Some of the bones in a scoliotic spine may have rotated slightly, making the person's waist or shoulders appear uneven. The scoliotic spine can cause serious effects on human breathing and heart function. Regarding the effects of scoliosis on bones, it can engender osteoporosis, a type of disease which makes one's bones extremely weak. Normally, the effect of scoliosis depends on how severe the curvature is. One thing for sure is that it is not life threatening.

In the mid-type of scoliosis, where the curvature is less than 20 degrees, there is no effect on the lungs whereas in the moderate type of scoliosis (25 to 70 degrees) there is some difficulty while exercising. In the case of severe scoliosis, problems can occur in the heart and lungs, e.g., one may experience problems while breathing and it can also cause pressure on the lungs (Dobbs and Weinstein 1999). One example of a patient with scoliosis is shown in Figure 2.1.

Figure 2.1: An example of comparison before and after treatment of scoliosis (http://bepainfreeforlife.com/2010/07/14/egoscue-and-scoliosis/)

2.1.4 Indicators for Spinal Deformity Diagnosis

Once a diagnosis of scoliosis has been decided, the primary concerns are whether there is an underlying cause and if the scoliosis will progress and deteriorate. There are several parameters to determine the spine deformity diagnosis.

In summary, the three main determinants of progression are patient gender, future growth potential and the curve magnitude at the time of diagnosis. In all cases, females have a risk of curve progression 10 times higher than males (Miller 1999).

Evaluation of growth potential is done by assessing the Tanner stage and the Risser grade. Tanner stages 2 to 3 occur just after the onset of the pubertal growth spurt and are the time of maximum progression of scoliosis (Renshaw 1993). The Risser grade (from 0 to 5) gives a useful estimate of how much skeletal growth remains by grading the progress of bony fusion of the iliac apophysis. The iliac apophysis ossifies in a predictable fashion from anterolateral to posteromedial along the iliac crest. Risser grades are used as follows: grade 0 signifies no ossification, grade 1 signifies up to 25% ossification, grade 2 signifies 26% to 50% ossification, grade 3 signifies 51% to 75% ossification, grade 4 signifies 76% up to 100% ossification and grade 5 signifies complete bony fusion of the apophysis (Lonstein 1994). Figure 2.2 is an example of Risser grades from 0 to 5. In one study (Lonstein and Carlson 1984), the Risser grade was found to be directly correlated with the risk of curve progression.

Figure 2.2: Risser grades 0 to 5. Grading is based on the degree of bony fusion of the iliac apophysis, from grade 0 (no ossification) to grade 5 (complete bony fusion) (Reamy et al. 2001)

The most commonly used clinical method to measure spine deformity is the Cobb angle, which is derived from a standard radiograph of the spine in a standing posture. This measurement is taken by first finding the most affected vertebra in the curve, called the apical vertebra. The apical vertebra is the spinal bone that has the most rotation and displacement from its ideal alignment. It also has the least amount of tilt, as measured by the angle of the endplates (top and bottom edges of vertebral body).

To come up with a number for the Cobb angle, the top and bottom vertebrae of the curve are identified. These bones have the most tilt, but the least amount of rotation and displacement.

In an X-ray radiograph, a line is drawn along the edge of the vertebrae and extended out. On the top bone, the line starts at the high side, and is drawn along the top edge and slopes downward according to the angle of the vertebra. On the

bottom vertebra, the line is drawn along the bottom edge and will slope in an upward direction. Perpendicular lines are then drawn from both lines so that they meet each other at the level of the apical vertebra identified in the first step and this process is shown in Figure 2.3.

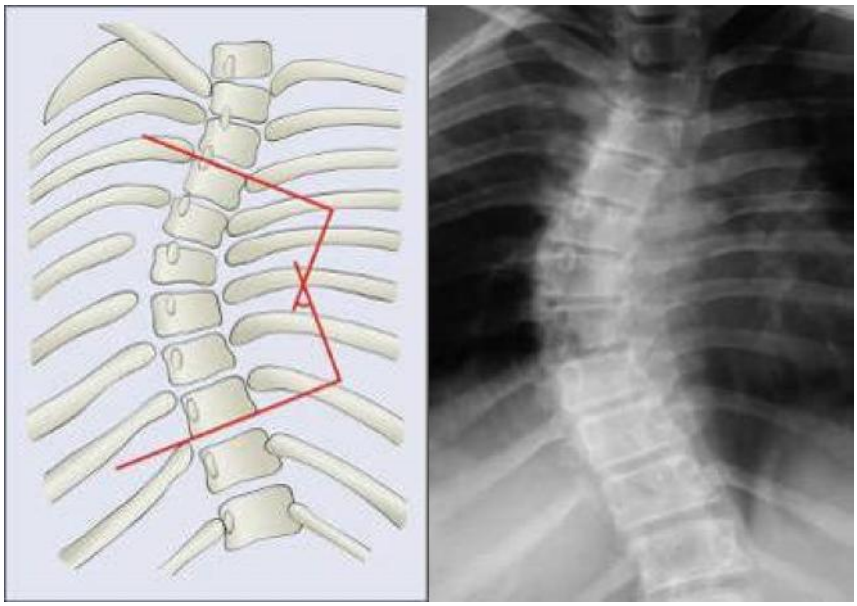

Figure 2.3: The Cobb angle method of measuring the degree of scoliosis. The physician chooses the most tilted vertebrae above and below the apex of the curve (http://www.e-radiography.net/radpath/c/cobbs-angle.htm).

The Cobb angle is found by measuring the angle of the two intersecting perpendicular lines. If the Cobb angle is 15 degrees or less, it is likely that one will need regular check-ups to see if the curve is progressing. If it is between 20 and 40 degrees, one will probably need a back brace. If it is over 40 degrees, the doctor will likely recommend surgery.

2.1.5 Adolescent Scoliosis Treatment

Adolescent idiopathic scoliosis is diagnosed and treated worldwide, and treatment approaches vary internationally. The treatment with bracing is to prevent progression of the curve until the patient reaches skeletal maturity, at which time the risk of curve progression (and hence the risk of surgery) greatly diminishes. Figure 2.4 shows an example of a teenager before and after brace implantation.

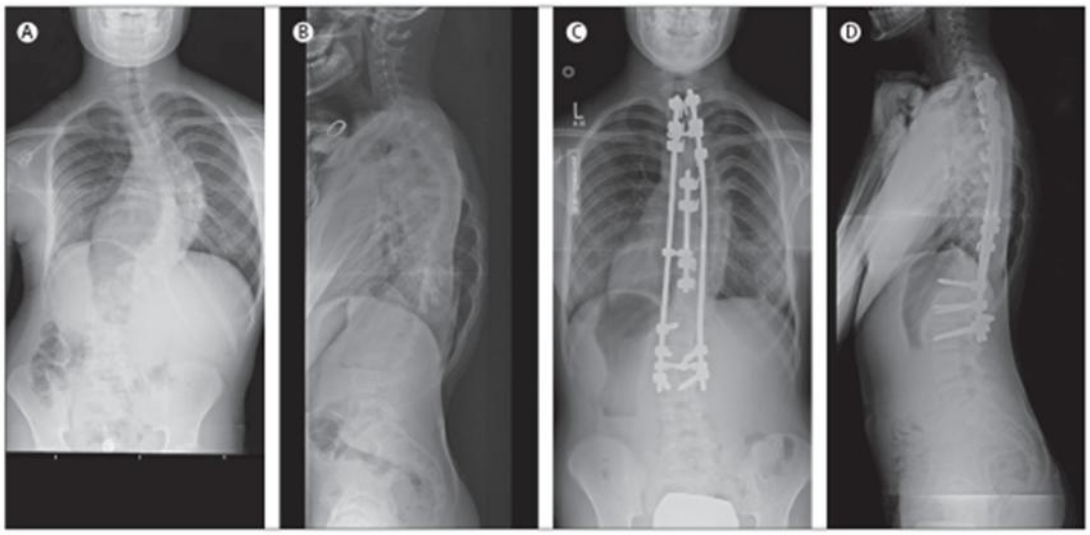

(a) (b) (c) (d)

Figure 2.4: Radiographs of a teenager with progressive AIS treated by posterior instrumentation by hybrid (rods, hooks, and screws) (a) Preoperative standing posterior-anterior (PA); (b) preoperative standing lateral; (c) postoperative standing PA; and (d) postoperative standing lateral (Weinstein et al. 2008).

2.1.6 Spinal Screening in Schools

School spinal screening has been developed to identify adolescents with small spinal curves and refer them for treatment before these curves become too severe. The school spinal screening for students uses school nurses and other trained

adults to screen all students. Careful training and understanding of spinal screening is essential for the success of this program.

The screening process identifies students who have some physical findings that suggest a spinal curve. However, the screening process does not diagnose a spinal deformity. A student showing these findings is referred to a physician who completes an extensive examination and takes x-rays to confirm whether or not the student has an abnormal spinal curve. At that point, the physician can provide recommendations for treatment.

The Adams forward bending test is the most commonly used method in schools for spinal screening.

The children bend forward dangling the arms, with the feet closed together and knees straight. The curve of structural scoliosis is more apparent when bending over. In a child with scoliosis, the examiner may observe an imbalanced rib cage, with one side being higher than the other, or other deformities.

A scoliometer is one type of inclinometer that is used to measure distortion of the torso. The scoliometer is placed on the back of the subject and it measures the apex (the highest point) of the upper back curve. The subject continues bending until the curve can be seen in the lower back (lumbar area). The apex of this curve is also measured.

After the regular assessment in the school for adolescent idiopathic scoliosis, the students and pupils who need further diagnosis will be sent to the hospitals for professional clinical tests or surgery if necessary.

2.2 Existing Human Back Surface Measurement Techniques

The human back surface measurement technologies are used for surface topology generation and detection before adolescent idiopathic scoliosis is diagnosed. As reported, for many patients with scoliosis and their family, the most important concern is directly related to the effects of their back shape and back surface cosmetic deformity rather than correction and treatment of the curvature. Therefore, the focus of human back surface measurement with potentially unneeded radiation exposure has encouraged many scientists and doctors to search for ways of quantifying deformity based on body shape and back asymmetry.

2.2.1 Simple Handheld Devices

Surface measurement techniques range from observational approaches to optic-electronic methods. A simple angle measurement device which is called a scoliometer for measuring the length of the human spine was first invented by Bunnell in early 1984 (Bunnell 1984; Bunnell 1993) in an attempt to compute the severity of deformity by measuring spine irregularity when a child is undertaking an Adams forward bending test. A scoliometer is a ruler with a U-shape concave gap as shown in Figure 2.5. Although this device is easy-to-use and inexpensive and could readily be used by experienced orthopaedic surgeons as an indicator for further diagnosis and treatment, it has the disadvantages of doctor's subjectivity and is inherently prone to postural and breathing bias, with significant inter and intra observer error (Côté et al. 1998).

Figure 2.5: An example of scoliometer for forward bending test (http://www.ortholutions.com/scoliosis-rsc-brace-treatment/measure-scoliosis-bunnell-adams-test-cobb/)

Distortions of the torso is another indicator for measuring scoliosis. An inclinometer (Scoliometer) measures distortions of the torso. The patient is asked to bend over, with arms dangling and palms pressed together, until a curve can be observed in the thoracic area (the upper back). The Scoliometer is placed on the back and used to measure the apex (the highest point) of the curve. In Figure 2.6, the method of measuring scoliosis has been presented including the Adams forward bending test using a scoliometer.

Pruijs and his colleagues (Pruijs et al. 1995) designed a new simple device named spinal rotation meter in 1995. Together with the scoliometer, the spinal rotation meter was applied to school screening programs in the Netherlands. However, both devices have the disadvantages that they are prone to be posturally affected with inter-observer and intra-observer variation and errors. These devices cannot replace the X-ray method to measure spinal changes over time.

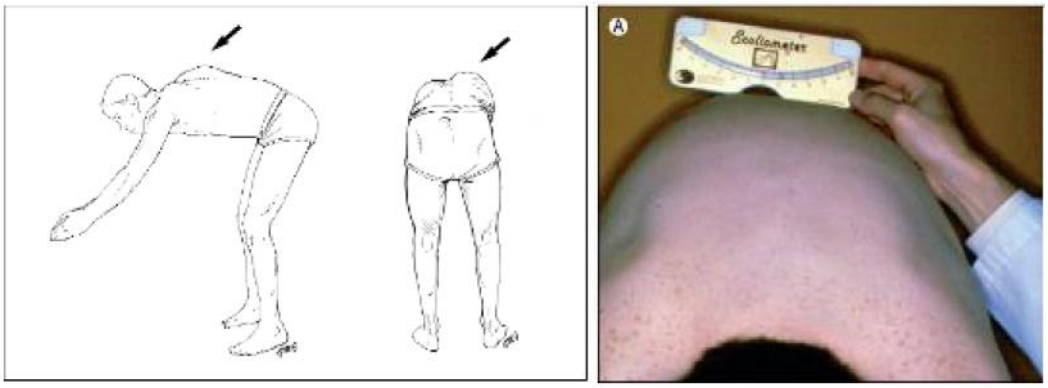

(a) (b)

Figure 2.6: (a) Adams forward bending test. (Left) As the patient bends over, the examiner looks from behind and from the side, horizontally along the contour of the back. (Right) A rotational deformity known as a rib hump (arrow) can be easily identified. (b) Measurement of trunk rotation with a scoliometer with patient in the forward bending position (Reamy et al. 2001).

2.2.2 Spinal Contour Detection Devices

During 1970's, another type of simple device has been developed with the purpose of assessing scoliosis through quantifying the rib hump on the back. Thulbourne and Gillespie (Thulbourne and Gillespie 1976) introduced a device consisting of several detachable and moveable parts and the shape of the rib hump can be generated when pressed against a subject's back and skin together with the Adam forward bending test. Pun et al. (1987) designed a similar device used together with two or more inter-independent manipulators measuring a single subject through a flexible curve detector. Although these spinal contour detection devices are easy to use and understand, they are time-consuming and may be subjective because the results are copied by hand to paper for analysis, and are not applied in most hospital and clinical diagnosis for long term observation.

2.2.3 Goniometers, Magnetometers and Ultrasonic Devices

Besides the simple handheld devices, numerous researchers have tried to exploit commercially available goniometers, magnetometers and ultrasonic devices and equipment to assess the 3D human body contour and deformed spine shape.

Goniometers are devices that are capable of quantifying the motion of rigid body in three-dimensional space. In 1996, Mior and his team (Kopansky-Giles et al. 1996) evaluated the goniometers of the Metrocom Skeletal Analysis System produced by Far Medical Technologies Inc., which can present signals to provide an accurate 3D positional measurement of feature points on the back surface. They reported that the electro-goniometric device was not suitable generally for long term clinical applications since the apparatus could not provide sufficiently precise position of the points and it could not acquire any surface topographical data including the measurement of the rib hump which has been assessed to be of limited practical value.

Similarly, ultrasonic-based equipment (Letts et al. 1988) and magnetic-based equipment (LeBlanc et al. 1997) were also clinically assessed to be prone to biases caused by patient's movement thus limiting their practical utility.

2.2.4 Moiré Patterns in Measuring Surface Topology

The Moiré (Willner 1979) pattern is an "interference pattern" created by intersecting lines, grids and shapes, and this phenomenon is caused by the optical interference when two graphic patterns are superimposed onto each other from different directions, and this pattern has applications in the generation of textiles

that originate a watery shape appearance and as a surface topography measurement tool. In late 1960's, a framework of horizontally parallel lines with equal distance was first described by Chiang (Chiang 1969) and this system generates images with the combination of parallel shadows projected onto a plane. Through mathematical relationships, the curve shape and the surface topology of an object can be deduced from the Moiré pattern for back shape analysis. Figure 2.7 presents an example of Moiré topography apparatus and Figure 2.8 shows an example of Moiré topology of a scoliosis patient (Kotwicki et al. 2007).

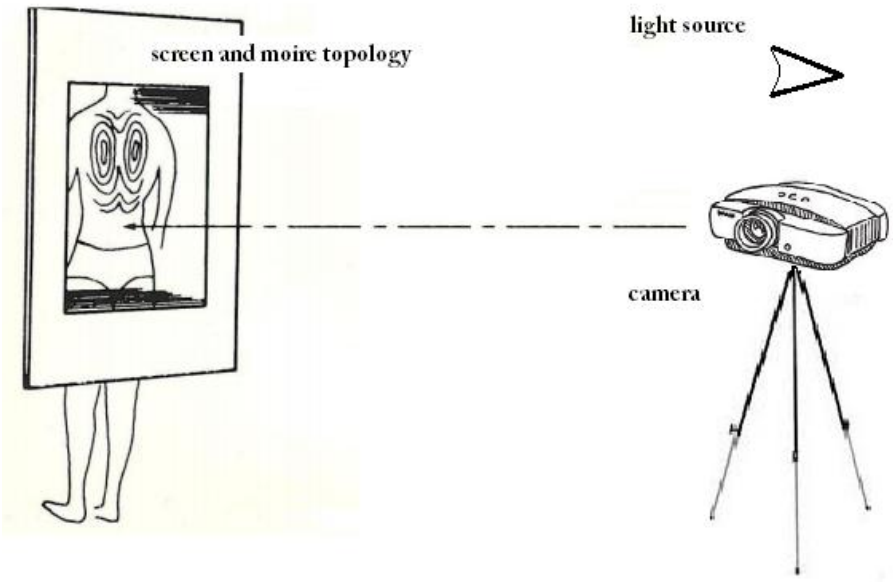

Figure 2.7 an example of Moiré topography apparatus (T.M.L Shannon 2008)

Figure 2.8 an example of Moiré topography of a scoliosis patient

(Kotwicki et al. 2007)

Takasaki and his team (Takasaki et al. 1970) developed an application based on the observation of the contour lines of an object using Moiré technique to measure the deformity of body surface. This technology has been used for scoliosis evaluation in Canada in 1977 (Adair et al. 1977) and Japan in 1981 (Harada et al. 1981). In their investigation, this method was proven to be more sensitive and accurate than the Adam's forward bending test. Besides, the results of the Moiré topography for individual patients can be permanently stored for future analysis.

The quantitative analysis of the Moiré topography usually involves the comparison of the relevant left and right maps of the back surface. Some quantitative linear and angular measurements are then derived. In order to analyze the surface Moiré topology, Stroke and Moreland (1989) constructed tangential lines across corresponding fringes on both the left and right sides of the patient back

which is shown in Figure 2.9. Their research aims to detect the presence, direction, magnitude and the therapeutic method of scoliosis.

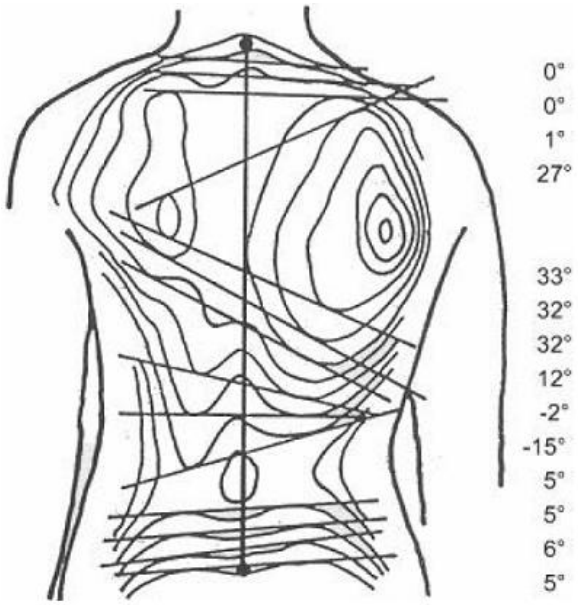

Figure 2.9 Moiré topography analysis: two tangent lines are drawn from corresponding contours and the angles between these contours are calculated (Stokes and Moreland 1989).

Some investigators reported that this method could identify most of the scoliosis cases reliably with high precision (Daruwalla and Balasubramaniam 1985), and the other advantage over the Adam's forward bending test is that the process is less influenced by the doctors' or nurses' subjective judgment for correct decision making (Suzuki et al. 1992). However, the Moiré technology suffers several problems. The formation of the Moiré fringes depends on the patient's body shape and standing posture and a slight change of the patient's stance may affect the results considerably, which may weaken this method and even become misleading. Thus, most researchers (Moran and Lipczynski 1994) have concluded that this

method has not found wide acceptance in the hospital and clinic examination environment but is still helpful for school screening programs.

2.2.5 ISIS System

The ISIS (Integrated Shape Imaging System) was one of the earliest designed and extensively applied commercial systems for optical scanning and measuring human back shape in the clinical environment (Turner-Smith and De Roguin 1984; Turner-Smith et al. 1988; Weisz et al. 1988; Carr et al. 1991). In the early 1980s, the Oxford Orthopedics Engineering Centre, University of Oxford developed this system and later was commercialized by Oxford Metric Limited, UK (Turner-Smith 1988; Sweatt et al. 1998; Patias et al. 2006).

The ISIS apparatus consists of a projector to project a structured light pattern onto the scoliotic patient's back surface using digital and video camera technology with micro-processors and personal computers. The projector emits a horizontal blade of light which is swept beyond the back surface from the neck to the buttocks and a camera is mounted below the projector to capture the 3D position of the light blade, and the spatial coordinates are digitalized. Figure 2.10 shows the commercial ISIS system. The advantage of this system is that by placing the scanning apparatus with the projector and camera, it allows patients with severe scoliosis and kyphosis to be measured; reducing the overall inspection time to less than 10 seconds, hence decreasing the influence of sway and breathing. In the commercial ISIS system, bony landmarks are also used to establish the shape of the patient's back surface by calculating the orientation and coordinates of the landmarks.

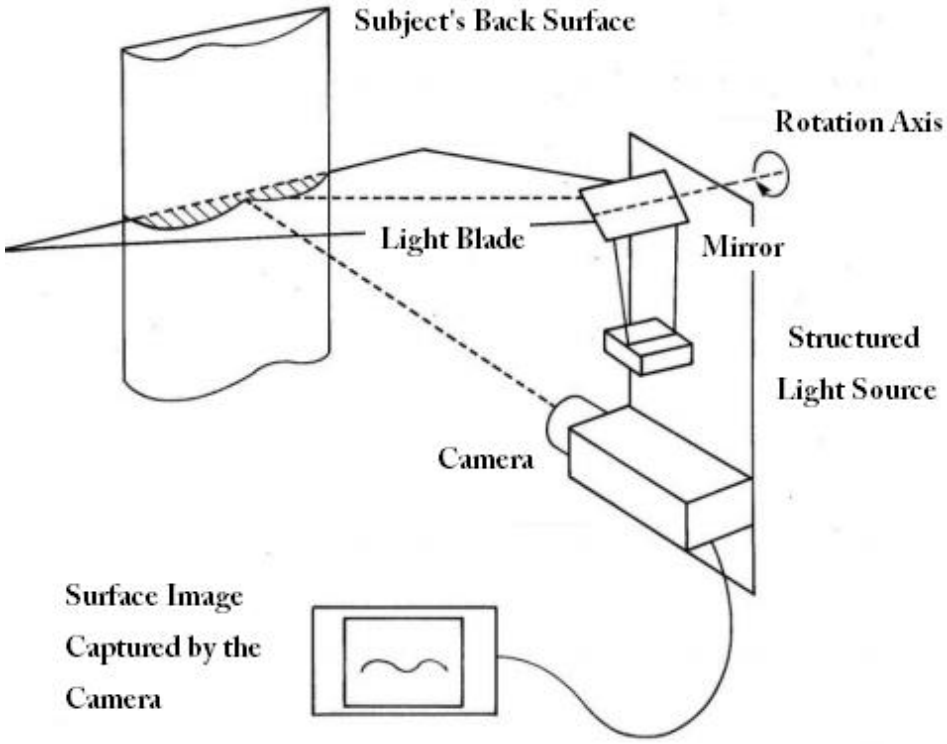

Figure 2.10 The commercial ISIS system (Berryman et al. 2008)

The ISIS system has been proven to be a useful method in the evaluation of scoliosis and has been supported by some researchers (Weisz et al. 1988; Theologis et al. 1997). The system could also support the nurses by producing a printed report (Legaye et al. 1992). The production of the ISIS system began in 1985 and ends in 1988 with only 60 systems purchased all over the world. This system has not been widely accepted by the clinics and hospitals because Oxford Metrics Limited was unable to obtain medical insurance imbursement codes in United States for the technology and the researchers were dubious if this system could become a substitute to radiography completely (Weiss and Seibel 2008).

2.2.6 ISIS2 System

The ISIS2 system comes from the original ISIS system. The ISIS system has been modified and redesigned with new evaluation parameters (Berryman et al. 2008), and has been utilized at the Nuffield Orthopaedic Centre (Oxford) in 2006 and at the Royal Orthopaedic Hospital (Birmingham) in 2008.

The ISIS2 system consists of a projector, a digital camera, a telescopic column and actuator, a personal computer to control the projector and the camera.

The ISIS2 system overcomes the major disadvantage of the original ISIS system in that it uses a digital camera to take photographs every 100ms rather than using the structured light to scan the back surface every 0.5s, which could minimize the impact and errors from breathing and sway during the process of measurement. During the measurement, the patient is asked to put on a black neckband and apron to provide a clean and clear background for taking the photograph. The clinicians attach several small coloured paper-made stickers on the prominent positions of the scoliotic subject's back. In general, 7 to 12 stickers with the size of 9 ×15mm^2 are used (Berryman et al. 2008) and Fourier transform profilometry is also applied to convert the distortion of the parallel grid into a 3D map of the back surface (Berryman 2004).

The ISIS2 system has not been commercialized but is now in use for research within the Nuffield Orthopaedic Centre (Oxford, UK) since 2006. Similar to the original ISIS system, ISIS2 provides quite a useful and complementary tool for radiographic examination (Zubović et al. 2007; Pynsent et al. 2008), but it can still be influenced by breathing, stance and postural variations.

2.2.7 Quantec System

In the early 1990s, Quantec Image Processing Ltd. (Liverpool, United Kingdom) developed the Quantec system (Curran and Groves 1990; Wojcik et al. 1994) employing raster stereography technology and using a pattern of horizontally structured lines onto the subject's back surface (Oxborrow 2000). This system also uses bony markers attached over the prominent points of T1, T12, posterior superior iliac spines (PSIS) and other spinal processes. The Quantec system can capture the whole body area in less than one second, which is a considerable advantage beyond the ISIS system in order to better decrease the effect of breathing and sway variations. The system could produce a point cloud of bony markers to present the 3D surface together with the clinical parameter calculations for spinal deformity evaluation of lordosis, kyphosis and scoliosis (Liu et al. 2001).

Some of the clinicians and researchers studying comparable investigation have established the relationship between the Quantec parameters, scoliometer and the Cobb angle (Thometz et al. 1999; Liu et al. 1999; Lamdan et al. 2000). However, the apparatus seldom considers the orientation of the patient related to the reference plane and the camera, which may introduce variations to the measurement process. Algorithms have been developed by averaging some output results to overcome the system deficiency (Goldberg et al. 1997; Griffiths et al. 1997; Goldberg et al. 1999). However, due to these shortcomings, the Quantec system has not been widely accepted in routine clinical diagnosis although some enthusiasts still use it until today.

2.2.8 Formetric System

In 1999, Diers® International GmbH (Schlangenbad, Germany) designed and manufactured the Formetric 3D system for human back topology generation. Goh and his team (Goh et al. 1999) tested and evaluated this system for thoracic kyphosis measurement. It was found that the reliability and feasibility of the Formetric 3D system relies largely on the subject's postural and breathing. The commercialized Formetric 3D system is based on the study from Hierholzer et al. (Frobin and Hierholzer 1982; Drerup and Hierholzer 1987; Frobin and Hierholzer 1991; Drerup and Hierholzer 1994) at the Centre of Orthopaedics at the University of Münster (Germany). In their research, the raster stereography technique was used by projecting structured light and pattern of horizontal grids onto the subject's back to simulate the back surface through analyzing distorted line patterns.

Diers International GmbH has developed another Formetric 4D system which permits rapid static and dynamic optical measurement of human back and spine and the Formetric 4D Motion system to visualize the complex motion pattern of the spine and pelvic during walking and running. Figure 2.11 shows an example of the Formetric human back surface measurement system.

Figure 2.11 DIERS 4D motion® system for dynamic spine and posture analysis (http://www.diersmedical.com/ProductPage.aspx?p=23)

2.2.9 Other Systems

Some other techniques including laser scanning for surface analysis (Aliverti et al. 1993; Aliverti et al. 1995; Ronald 1999; Treuillet et al. 2002) have been used in the system design for spinal deformity evaluation. However, high cost and low scanning speed restrict their application in routine diagnosis. Furthermore, a few commercial 3D scanning systems are also available, such as the COMOT system (www.metos.org), LASS, Vitus 3D Body Scanner (Daniell 2007), Minolta Vivid Laser Scanner, Cyberware Rapid 3D Prototype, Inspeck Scanning System, etc.

The research team from the University of Alberta and the Glenrose Rehabilitation Hospital in Edmonton Canada (Durdle et al. 1995) developed a

surface modeling system running on an IBM RISC6000 engineering workstation using triangulation based on multiple cameras. Work by Ajemba and his group found that torso deformity plays an important role in connecting back surface changes to inner spinal scoliosis (Ajemba et al. 2007; Ajemba et al. 2008; Ajemba et al. 2009).

However, all these existing commercial systems and systems in development are not publicly used in routine clinical application because of the complexity of the implementation, high equipment cost and the likelihood to be affected by the patient's breathing, sway and stance posture during the measurement process.

Besides the system for spinal curvature measurement, some parameters or indices are necessary and helpful to define the severity of the scoliosis. A review about the existing scoliosis measurement parameters was introduced in the next section.

2.3 Review of Existing Scoliosis Measurement Indices

As an epidemic spinal syndrome, adolescent idiopathic scoliosis affects approximately 3% to 5% of children worldwide. The occurrence of scoliosis happens in three dimensions in the sagittal and coronal planes with rotation in the transverse plane, and with initial indications of body asymmetry and back shape unbalance. For most of the cases, the motivation in seeking treatment is to correct the trunk deformity and improve the cosmetic appearance. Formal structured training programs may help the patients enhance their medical knowledge and maintain good spine care. The understanding of the physical and psychological

concerns of scoliosis plays an important role in the clinical decision-making procedure.

One of the most important questions about the numerous types of spinal shapes is the method to define and examine the severity of the scoliotic spine. Different scoliosis evaluation indices have been created, such as the Cobb angle (Cobb 1948), factors that affect shoulder balance Hong et al. (2013), Sun et al. (2011) designed and developed the "X-factor" index for evaluation of adolescent idiopathic scoliosis correction. Samagh et al. (2011) and Mangone et al. (2012) considered the important role of spinal axial rotation and the methods of determination of axial rotation center. Benneker et al. found that radiographic evaluation parameters were able to distinguish different stages of degeneration, whereas MRI evaluation parameters could only detect the advanced stages of disc degeneration (Benneker, et al. 2005). The aim of an evaluation index for scoliosis is to provide an indication of the progression of scoliosis, assess treatment outcomes and attempt to establish the relationship between the back shape and the underlying skeletal deformity. Most of the existing indices are calculated using the 2D images. Until recently, the conventional and most widely-used method for assessing the degree of scoliosis is the Cobb angle, which is considered the golden standard for the spinal deformity measurement. Other existing spinal deformity indices also play important roles in assisting scoliosis diagnosis and assessment, such as the 3D evaluation method for lumbar mobility and overall back shape (Tuong et al. 1998) which can help the patients and their families assess trunk deformity cost-effectively with reduction of X-ray exposure when monitoring spinal shape changes.

There are several scoliosis evaluation parameters using surface topology techniques other than the radiography images and they will be reviewed next.

The Cobb Angle. The Cobb angle was originally used by the American orthopaedic surgeon John Robert Cobb in 1948 to determine coronal plane deformity in the classification of scoliosis (Berryman et al. 2008). To calculate the Cobb angle, the apical vertebra is first identified, which is the most likely to have displaced and rotated with the least tilted vertebra. The top and end vertebra are then identified, which are the most superior and inferior vertebra that are least displaced and rotated and have the maximally tilted the end plates. Two lines are drawn along the superior end plate of the superior end vertebra and along the inferior end plate of the inferior end vertebra. If the end plates are indistinct, the lines may be drawn through the pedicles. The angle between these two lines (or lines drawn perpendicular to them) is measured as the Cobb angle as shown in Figure 2.12.

Figure 2.12 The Cobb angle index (62 degrees for this example) (Syndrome Homocystinuria 2001)

The Walter Reed Assessment Scale. The Walter Reed Assessment Scale (Turner-Smith et al. 1988) is a group of figures symbolizing seven aspects of spinal deformity. The scale describes the body curve, rib prominence, flank prominence, the relative position of the head to the rib cage and to the pelvis, the relative position of the head to the pelvis, the shoulder level, and the scapular rotation. For each aspect, five levels of figures according to the order of increasing levels are scored from left to right. The final result is calculated as the sum of the seven aspects and Figure 2.13 shows the Walter Reed Assessment Scale (Polly Jr et al. 2003; Bago et al. 2007).

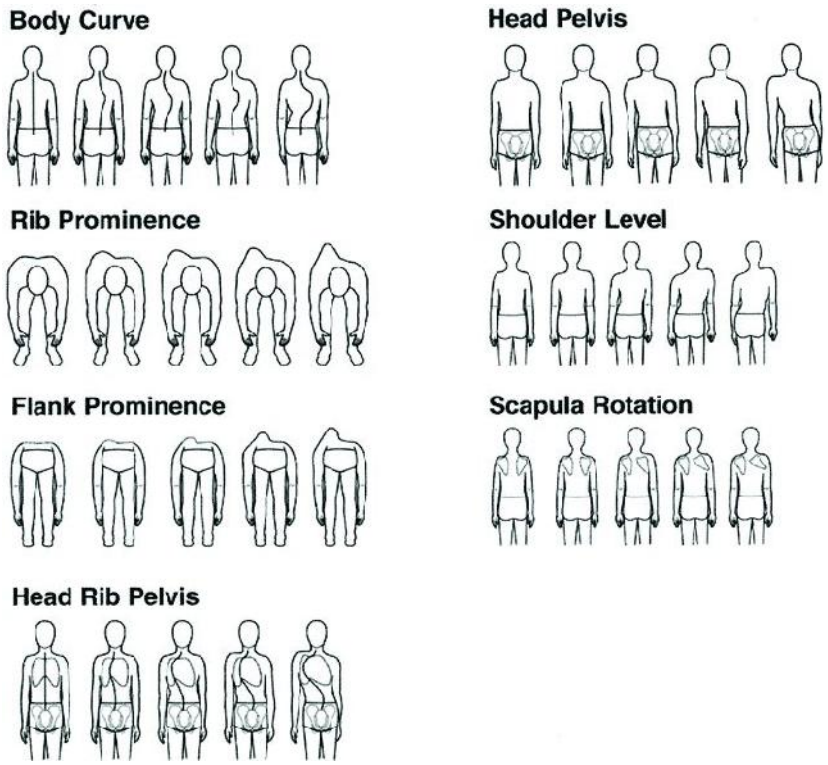

Figure 2.13 Walter Reed Assessment Scale (Polly Jr et al. 2003; Bago et al. 2007)

The Posterior Trunk Symmetry Index (POTSI). The Posterior Trunk Symmetry Index (POTSI) was first introduced by Suzuki et al. (1999) to assess

body asymmetry in scoliotic patients. This method includes several indices for trunk deformity evaluation as shown in Figure 2.14 and Figure 2.15. In Figure 2.14, the Frontal Asymmetry Index (FAI) is measured by calculating the medio-lateral differences at the axilla and the difference between the locations of the vertebra prominence and gluteal furrow. The FAI-C7 is the imbalance index, which is calculated by dividing the distance between the vertebras prominences (C7) to the central line by the width of the back defined as the distance between the two axillae. The axilla index FAI-A is defined by dividing the absolute value of the distance from the axillae to the vertical central line by the axilla width. The trunk index FAI-T is calculated by dividing the absolute value of the distance from the back edge to the vertical central line by the back width. In Figure 2.15, the Height Differences Index (HDI) is presented. The HDI-S is the height difference between the two shoulders. The HDI-A is calculated as the height difference between the two positions of the axillae. The HDI-T is defined as the height difference between the trunk and it is calculated as the height difference between the narrowest parts of the trunk.

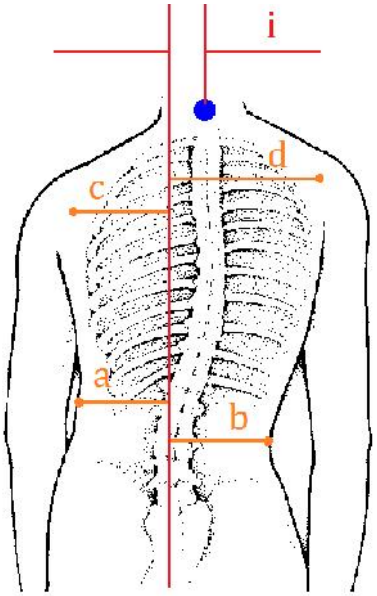

Frontal Asymmetry Index:

$$\text{FAI} - \text{C7: C7} = \frac{\text{i}}{\text{c} + \text{d}} \times 100$$

$$\text{FAI} - \text{A: Axilla} = \frac{|\text{c} - \text{d}|}{\text{c} + \text{d}} \times 100$$

$$\text{FAI} - \text{T: Trunk} = \frac{|\text{a} - \text{b}|}{\text{a} + \text{b}} \times 100$$

Figure 2.14 Frontal Asymmetry Index (FAI-C7, FAI-A, FAI-T) (Suzuki et al. 1999)

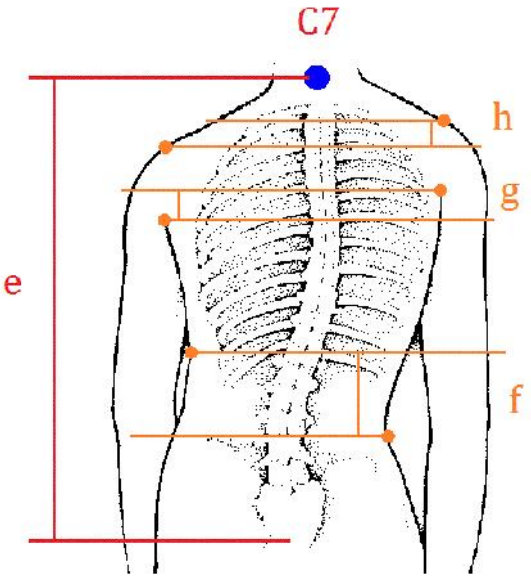

Height Asymmetry Index:

$$\text{HDI} - \text{S: Shoulder} = \frac{\text{h}}{\text{e}} \times 100$$

$$\text{HDI} - \text{A: Axilla} = \frac{\text{g}}{\text{e}} \times 100$$

$$\text{HDI} - \text{T: Trunk} = \frac{\text{f}}{\text{e}} \times 100$$

Figure 2.15 Height Asymmetry Index (HDI-S, HDI-A, HDI-T) (Suzuki et al. 1999)

The posterior trunk symmetry index (POTSI) is calculated as the summation of the FAI and HAI, which includes six indices, as follows.

$$\text{POTSI} = [(\text{FAI-C7}) + (\text{FAI-A}) + (\text{FAI-T}) + (\text{HDI-S}) + (\text{HDI-A}) + (\text{HDI-T})] \times 100\% \quad (1)$$

In 1999, Inami et al. (1999) found that although the correlation between POTSI and the benchmark method of the Cobb angle was weak, $r=0.435$ and $p<0.0001$, where "r" is the correlation coefficient and p is the P-value in Significance Test, POTSI is still a quantifiable and useful indicator in clinical diagnosis to evaluate scoliosis treatment with the emphasis on cosmetic defects.

Deformity in the Axial Plane Index (DAPI). In 2007, Minguez et al. (2007) introduced another series of indices which do not depend on the radiography images. DAPI indices are built by computing the differences in the surface depths at the position of the scapulae and the waist location to define the level of severity of the deformity, as shown in Figure 2.16. In Figure 2.16, the meanings of some symbols are shown.

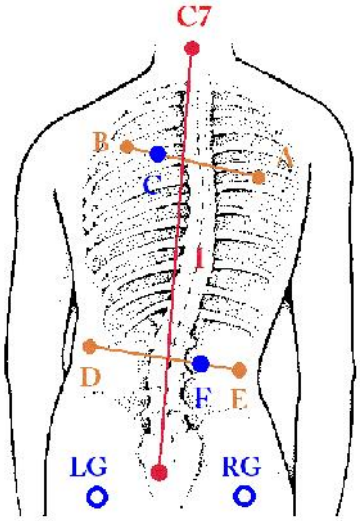

Deformity in the Axial Plane Index:

I: the distance between the vertebras prominence C7 and the apex of the inter gluteal furrow.
A: Most prominent point on the right scapula.
B: Most prominent point on the left scapula.
C: Most prominent point on the line AB.
D: Least prominent point on the right waist.
E: Least prominent point on the left waist.
F: Most prominent point on the line DE.
LG: Most prominent point on the left gluteus.
RG: Most prominent point on the right gluteus.

Figure 2.16 Deformities in the axial plane index (DAPI) (Asher et al. 2004)

The index of deformity in the axial plane includes the scapula index and the waist index, which are defined as follows (|A-C| and |D-F| are the absolute distances of the value between the two points).

$$\text{Scapula Index} = \frac{|A-C|}{I} \times 100\% \quad (2)$$

$$\text{Waist Index} = \frac{|D-F|}{I} \times 100\% \quad (3)$$

The Deformity in the Axial Plane Index is the summation of the two elements.

$$\text{DAPI} = \text{Scapula Index} + \text{Waist Index} = \left(\frac{|A-C|}{I} + \frac{|D-F|}{I}\right) 100\% \quad (4)$$

It was found that the DAPI scoliosis index has high correlation with the POTSI and the Cobb angle (Perdriolle and Vidal 1985). The coefficients for DAPI to the Cobb angle is r=0.668, which indicates that the DAPI is a useful parameter for human spinal deformity evaluation.

In order to obtaining the coordinates of the markers to interpolate the spinal shape, the hardware and apparatus were designed in the system. The hardware and apparatus is a type of parallel robotic manipulator which is named Stewart platform. A review about the parallel robotic manipulator was introduced in the next section.

2.4 Review of Parallel Robotic Manipulator and Stewart Platform

In this research, a parallel robotic manipulator is used to control the overall movement of the hardware system. Currently, there are three epidemic types of robotic mechanisms, which are serial manipulators, parallel manipulators and hybrid manipulators.

A serial manipulator is the most common robotic mechanism which is designed to link the fixed base to the end-effector using a series of links connected by motor-driven joints. A parallel manipulator is a mechanism that uses several parallel chains or parallel linear actuators to support the end-effector to achieve a spatial movement. A hybrid manipulator is a serial-parallel connection robot that gives rise to a multitude of highly articulate robotic manipulator. In this research, a parallel manipulator, or generally called a Stewart platform (SP) or Gough-Stewart platform, is applied to control the movement of the system and the posture of the scoliotic subject.

It is helpful to introduce the benefits and advantages of using the Stewart platform (SP) in the system over the other robotic arms.

- Comparing to other 6-DOF robotic arms, SP which is a type of parallel manipulator has high load/weight ratio because SP could distribute its load to the six legs and joints. This mean SP can support higher load with small mass of the

manipulator. In this research, the SP supports the weight of the mechanical frame and the patient's weight.

◆ Comparing to other 6-DOF robot arm, SP has the benefit of owning high rigidity and inherent stiffness. A high rigidity may be obtained with a small mass of the manipulator. This allows high precision and high speed of movements, and motivates the use of parallel manipulators in medical usages and applications.

◆ Comparing to the other type of parallel manipulator, SP is most widely used and in a central status in the literature on parallel manipulator in the past twenty years and has been applied to various fields such as robotics, numerically controlled machine, etc.

◆ In this research, the generalized Stewart platform is used, which could be considered as the most general form of parallel manipulators with six DOFs in certain sense.

◆ The SP system or similar apparatus is necessary in this research and it can bring advantages. The routine approach in evaluating and monitoring the progress of scoliosis is the forward bending test which is not accurate. Using the SP apparatus, the patients' bending angles can be precisely controlled by the SP and computer.

2.4.1 The Origin and Definition of Stewart Platform

The Stewart platform is a classic mechanical design for position and motion control. This device is originally designed and proposed by Stewart in 1965 as a flight simulator, and is still commonly used for this purpose (Stewart 1965). A wide range of applications have benefited from the usage of the Stewart platform, e.g.,

aerospace technology, automotive industry and machine tools manufacturing. The Stewart platform has also been used to simulate flight, model a lunar rover, build bridges, support vehicle maintenance, design crane hoist mechanisms, and position satellite communication dishes and telescopes, among other tasks. The Stewart platform consists of a base, a moving platform, six links or legs, several joints and actuators as shown in Figure 2.19. By changing the lengths of each of the six legs, the orientation and position of the moving platform can be controlled.

The invention of the first parallel manipulator has triggered developments in many research and industry fields, such as satellite positioning, underwater explorations, medical operation, flight simulators, etc. Another well-known parallel platform structure is the Gough Platform (Gough and Whitehall 1962) shown in Figure 2.17.

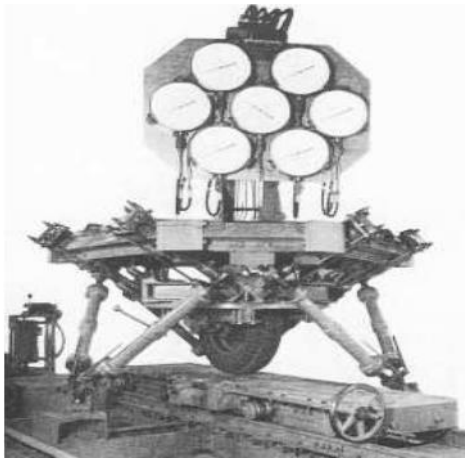

Figure 2.17 The first octahedral hexapod or the original Gough platform (Proc. IMechE, 1965-66)

The structure of a Stewart platform is similar to the Gough platform. Other types of motion manipulators based on the same principle as the Stewart platform

have been proposed. Some researchers have demonstrated that the Stewart platform could be implemented not only as motion generators, but other forms of simulators. In the last few decades, many scientific works on the characteristics and physical behaviors of parallel manipulators have also been reported. Stewart platform, the most prevalent parallel mechanical structure, has been extensively studied and applied in many fields, such as in machining motion planning. The Ingersoll Octahedral Hexapod machining centre is shown in Figure 2.18.

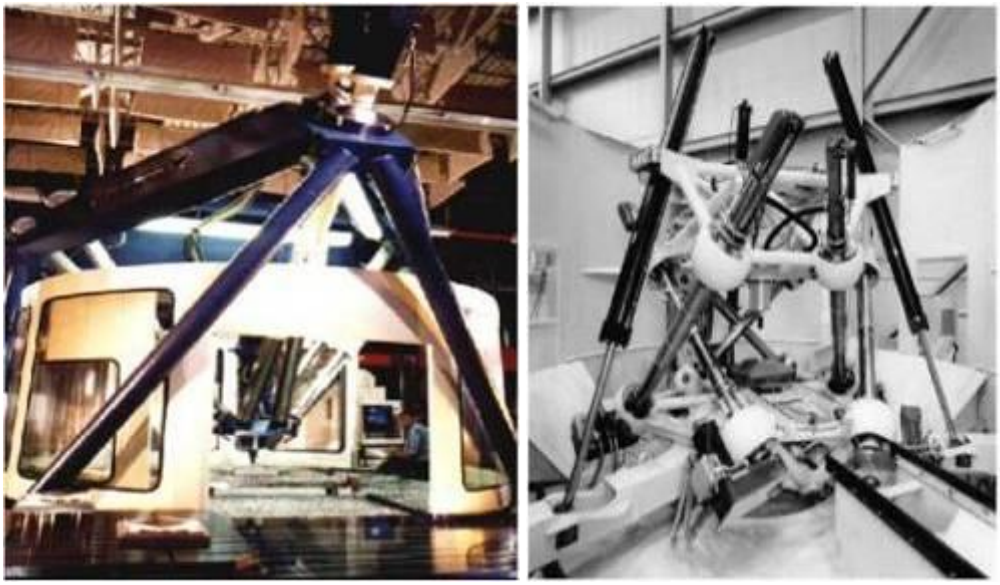

Figure 2.18 The Ingersoll Octahedral Hexapod machining center

(Shankar et al. 1998)

The motivation behind designing machine tools based on parallel structures can be found in their outstanding characteristics. Currently, most common types of machine tools consist of a succession of rigid bodies, links or joints, each connected to its predecessor by a joint. In the serial kinematic chains, each leg has to support the load in addition to the weight of the components of the platform. This is

especially critical in multi-axis machining that requires more degrees of freedom (DOFs), thus requiring longer chains and more space from the base to the tool. With a parallel mechanism or parallel kinematic chains, the construction of the multi-axis machine tool requires fewer numbers of chains. In the Stewart platform, each leg is composed of the same components and only supports the weight of the moving platform plus the load. Therefore, it offers higher stiffness, accuracy and payload as the load is divided among the legs. An example of a SP mechanism is shown in Figure 2.19.

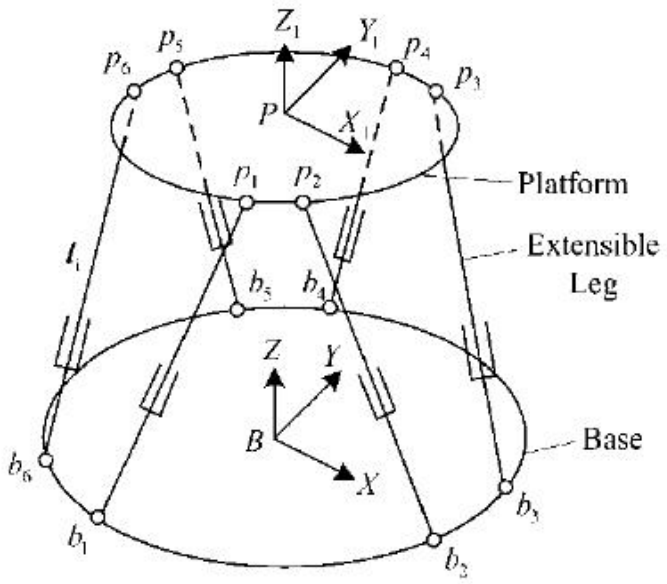

Figure 2.19 A schematic diagram of the SP manipulator mechanism

(Guo and Li 2006)

As compared to serial mechanical structures of comparable size, the workspace of a parallel manipulator is smaller. In addition, parallel structures have other disadvantages including difficulties in designing the control strategies,

complicated forward kinematics, variable performance over the workspace and the occurrence of singular configurations.

The general structure of the SP mechanism is composed of a moving plate on which the six legs are attached. As shown in Figure 2.20, the other ends of the legs (also referred to as actuators) are connected to the base plate of the platform. Each actuator links the moving plate to the base by either a 3-DOF joint with a 2-DOF joint, or two 3-DOF joints. The 6-DOF positioning capabilities of the SP is contributed by the linear extension and retraction of the six legs, including three rotational DOF (roll, pitch and yaw) and three translational DOF (X, Y and Z axes).

2.4.2 Hybrid Manipulators

Some researchers have designed and explored the combination of parallel and serial manipulators to obtain the advantages from both the parallel and serial structures. SP is one kind of parallel manipulator that possesses many connections between the base and the tool, thus providing for a much stiffer structure while sacrificing workspace relative to serial manipulators.

Some promising results have been reported, such as the Logabex LX4 robot (Cortés and Siméon 2005) (Figure 2.20 (a) and (b)) and the robotic arm designed at California Institute of Technology (Tanev 2000) (Figure 2.20 (c)). These mechanical manipulators consist of a combination of identical parallel mechanisms, leading to a larger workspace and a good ratio of load capacity to manipulator mass.

Recently, more hybrid manipulators have been applied in a wide range of applications, such as micro-machining, medical surgery, deep-sea mining and assembly operations (Chai and Young 2001; Callegari and Suardi 2003; Zheng, et

al. 2004; Carbone and Ceccarelli 2005; Harib et al. 2007). In some combinations of SPs, the mechanism is usually designed such that one platform performs pure orientation and the other performs pure translation so as to simplify the control algorithm (Lallemand et al. 1997; Tsai and Joshi 2002). Nevertheless, research on hybrid structures is still in the early stage and limited literature has been published.

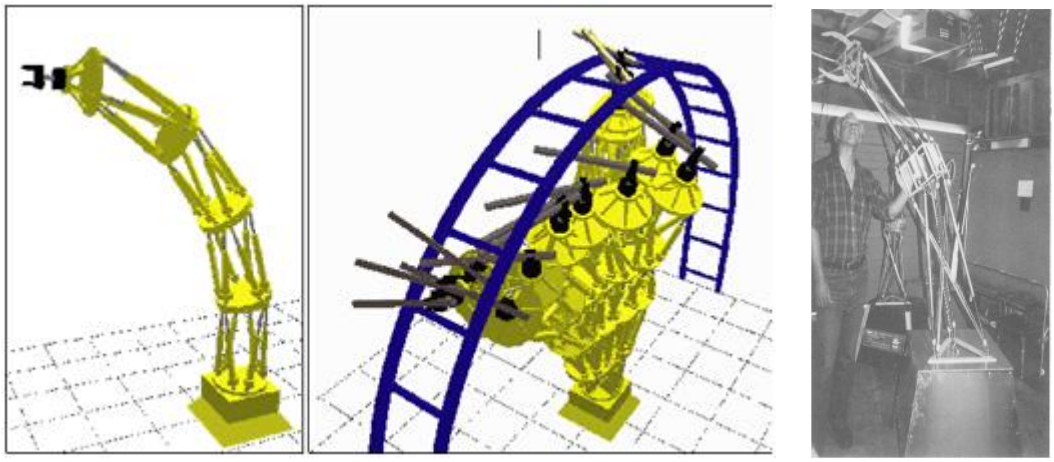

(a) (b) (c)

Figure 2.20 (a) (b) Model of the robot Logabex-LX4, composed of four Gough-Stewart platforms connected in series, and trace of a collision-free path (Cortés and Siméon 2005); (c) Operational model of hybrid robotic arm (Tanev 2000)

2.4.3 Kinematics of the Stewart Platform

The kinematics of the SP mechanism, like all robotic manipulators in general, is a study of the physical geometry of the motions of the end-effectors and the actuating joints, and the relationships between the motions of the mechanical inputs and the motions of the end-effectors without considering the forces and torques. There are two types of kinematics, namely, forward kinematics and inverse kinematics for these hexapod parallel manipulators.

Inverse kinematics for hexapod parallel manipulators can be defined as finding the leg lengths of three or six legs needed to position the moveable platform in a certain position with a desired orientation. The solution to this problem is straightforward and not complex for parallel kinematics machines (PKM). Furthermore, the computation of the length for each leg can be carried out independently in parallel, which can speed up the process.

On the contrary, the forward kinematics or direct kinematics of a parallel manipulator involves finding the position and orientation of the moveable platform when the three or six leg lengths are given. This problem has no known closed form solution for the most general 6-6 form of hexapod manipulators (with six joints on the base and six joints on the mobile platform). For a general SP, 40 assembly modes (i.e., direct model solutions) can exist (Dietmaier 1998). In practice, the use of numerical methods has been proposed, which assume that an estimated solution is known (Nguyen et al. 1991; Parikh and Lam 2005; Wang 2006). Another method is to use a larger number of sensors than the number of DOFs so that additional information can be used to improve the direct kinematics algorithm (Cheok et al. 1993; Parenti-Castelli and Di Gregorio 1999; Parenti-Castelli and Di Gregorio 2000; Chen and Fu 2006). It has been shown that the computation of forward kinematics is more efficient with an additional off-line pre-processing phase (Tarokh 2007).

2.4.4 Calibration and Accuracy

Parallel kinematic manipulators (PKMs) are introduced because of their higher accuracy as compared to conventional robots and better stiffness in the same range as the machine tools. Due to the complicated kinematic chains in a PKM, it

is difficult to achieve the required accuracy. Masory (Masory et al. 1996) has studied the influence of the sensor errors and the manufacturing tolerances on the locations of the joint centres. A more thorough analysis has been proposed by Ehmann et al. (Patel and Ehmann 1997; Wang and Ehmann 2002), which includes the location errors of the passive joint centres, errors in the leg lengths, and the imperfect motions of the ball joints. Tischler and Samuel (1998) proposed a numerical approach for determining the influence of the backlash of the joints, while Meng and Li (2005) and Wolhart (1999) proposed an analysis of the effect of the joint clearances on the trajectories followed by serial and parallel manipulators. Other sources of errors, such as thermal errors, gravity induced errors, and dynamics errors (Pritschow et al. 2002; Niaritsiry et al. 2004; Clavel et al. 2005), have also been studied.

The method of kinematic calibration can reduce the geometric errors, which is also called the kinematic errors. In kinematic calibration, various methods have been proposed, e.g., optimization methods (Zhuang and Roth 1993), linearization method (Geng and Haynes 1994), and partial differentiation (Ropponen and Arai 1995). Merlet (2006) distinguished three main types of calibration methods:

1. **External calibration:** an external measurement device is used to determine (completely or partially) the real pose of the platform for different desired configurations. The difference between the measured pose and the desired pose gives an error signal that is used for the calibration.
2. **Constrained Calibration:** methods that rely on a devoted mechanical system that constrains the robot motion during the calibration process.

3. **Auto-calibration or self-calibration:** the platform has extra sensors and only the manipulator measurements are used for the calibration.

In addition, there is another group of calibration methods that make use of interesting geometrical properties. Huang et al. (2005) proposed using specific motion characteristics, e.g., flatness and straightness which can be measured easily using dial gauges. Takeda et al. (2004) proposed using a double-ball-bar measuring device. In the machining field, calibration can be conducted using machining experiments (Chanal et al. 2007). Recent research shows a trend of using computer vision methods for calibration, which can produce good accuracy with relatively low cost (Andreff et al. 2004; Dallej et al. 2006; Daney et al. 2006; Renaud et al. 2006; Tanaka et al. 2006).

2.4.5 Motion Planning and Redundancies

Motion planning is a classical problem to avoid obstacles. For parallel manipulators, many factors should be considered, such as the limited workspace, singularities, and other performance requirements. Figure 2.21 shows the simulation of motion planning on a SP.

Merlet (1994) presented a method for checking whether a trajectory lies within the workspace of a manipulator. Harris (1995) dealt with motion planning between two poses, looking for the parameters of the screw motion linking the two poses, and reckoned that this motion should be able to minimize the changes in the link lengths. Gosselin and Angeles (1990) presented an algorithm that can find the orientation of the manipulator with the best accuracy in some specific poses along the path. Recently, probabilistic path planning has emerged as one of the most

promising approaches for path planning of manipulators with large DOFs. A most prominent research in this field for parallel manipulators is the probabilistic roadmap approach (Cortes and Simeon 2003), but this approach does not consider singularity or multiple solutions for the direct kinematics, which may prohibit the use of the trajectory.

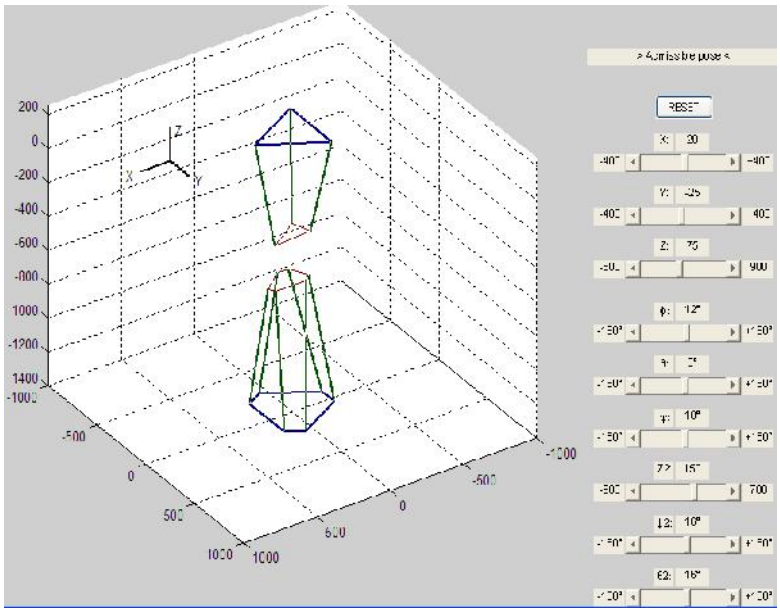

Figure 2.21 A design of GUI for the simulation of motion planning

Redundant manipulators are of significant importance because of their advantages when task versatility and manipulator performances are required. Redundant manipulators possess ‘additional inputs’ that offer a means to improve their performance and increase their versatility. Marquet, et al. (2001) distinguished three different types of redundancies:

1. **Kinematic redundancy:** at least one of the legs is a motion generator with a larger number of DOFs than necessary. This is used for enlarging the workspace (Liu et al. 2001).

2. **Actuation redundancy:** the end-effector is over constrained by the actuators. The number of actuators is more than the number of DOFs. Such redundancy is mostly used for singularity avoidance (Wang and Gosselin 2004).
3. **Measurement redundancy:** the number of sensors is larger than the number of actuated joints. This redundancy plays a role in solving the forward kinematic problem to reduce the positioning errors and for calibration (Marquet et al. 2002).

With the application of one SP manipulator to control a patient during spine deformity measurement, there are too many DOFs caused by the three positional DOFs and three rotational DOFs working altogether. Thus, there is a need to determine the best use of these DOFs.

2.4.6 Dynamics and Control

Dynamics is the determination of the relationship between the generalized accelerations, velocities, coordinates of the end-effector and the joints. Dynamics analysis of PKMs is complicated by the existence of multiple closed-loop chains. The earliest research regarding this can be found in the work by Fichter (Fichter 1986), where the leg inertia and the joint friction are assumed to be negligible.

There were three major approaches for computing the dynamics, including the Newton-Euler formulation (Codourey and Burdet 1997; Dasgupta and Choudhury 1999; Harib and Srinivasan 2003), the Lagrangian formulation (Nguyen and Pooran 1989; Geng et al. 1992; Liu et al. 1993), and the principle of virtual work (Wang and Gosselin 1998; Tsai 2000; Gallardo et al. 2003). Some researchers

(Reboulet and Berthomieu 1991; Kim and Lee 1992; Kock and Schumacher 2000) concluded that the dynamics model needs to be simplified in order to be used in a real-time control system. Different methods can be applied depending on the situation and the requirements, i.e., whether the dynamics has to be calculated for control, evaluation or simulation purposes.

Accurate control of a SP manipulator is still an open research issue and the works reported are not rigorous. In the field of machine tools, the trend is to adopt existing hardware for controlling the parallel manipulators. However, the use of existing hardware for controlling these manipulators will drastically penalize the performance of the system in the long term. Some researchers have suggested that each actuator can be controlled independently and robustly with a control law other than the simple PID control (Chiacchio et al. 1993). Another approach implemented an optimization scheme on top of a PD control (Yurt et al. 2002). Wang et al. (1995) and Geng and Hayes (1993) presented a neural network control scheme and showed its superiority over kinematic control. A model reference adaptive control scheme has been proposed (Li et al. 2003) to control a machine tool, and the Popov hyperstable theory is utilized as the adaptive control law. Recently, a more advanced tracking control scheme has been proposed (Huang et al. 2004; Huang and Fu 2004) and feedback using a camera (visual-serving) has been implemented (Zuo et al. 2002; Dallej et al. 2006; Andreff et al. 2007). Lastly, the combination of more than one single control strategy that takes advantage of multiple coordinated parallel structures (hybrid manipulators) is another important field that is relatively unexplored.

2.5 Significance of the Study

The goal of the research on a human spinal deformity measurement system is to be able to identify the small progressive curvatures of the human spine. This system is developed to identify adolescents with small spinal curvature and refer them for treatment before the curvature becomes too severe.

Although the Adams forward bending test is widely implemented, it still suffers from some problems. It is not sensitive to abnormalities in the lower back, which is a very common site for scoliosis. Since the test misses about 15% of scoliosis cases, many experts do not recommend it as the sole method for screening for scoliosis. In addition, the nurses or trained technicians need to go to schools to conduct the screening program which is human resource intensive.

Using a stereo vision camera system, the system could obtain the 3D information easily about back surface. By implementing marker-based tracking, the operator could attain the contour of a spine with image processing technology. Much work has been done on measuring the surface of the human back for assessing the degree of deformity in scoliosis patients. After obtaining the shape contour of the human spine, some evaluation parameters related to the severity of human spine deformity can be created or designed. The spinal curvature can be assessed by calculating these evaluation parameters.

In addition, a complete integrated system from measurement to data interpretation and diagnosis, storage, and record building will be developed. The

data has to be presented according to the specifications required by the orthopedic surgeons.

Chapter 3 Research Methodology and Development of Apparatus

The proposed spinal deformity measurement system is built by combining the mechanical and hardware sub-system and the control sub-system. The mechanical and hardware sub-system is used to achieve the functions of controlling the postures and motions of the subjects, taking stereo pictures, processing the images for information extraction, etc. The control sub-system is mainly designed for manipulating the SP and the mechanical frame, and storing and editing the measurement output data. One user can log in to the central server database, from which a standard diagnosis report is available, to check his/her results and follow his/her spinal deformity progress.

3.1 Spinal Deformity Measuring System Design

3.1.1 System Architecture

The mechanical and hardware sub-system of the spinal deformity measurement system is composed of a SP manipulator which movement is controlled using the MatLab program, a stereo vision camera from NaturalPoint, Inc. (Oregon, US), a specially designed mechanical frame for positioning the subject and a personal computer for processing spine images and data storing using MatLab program and visual C++. Figure 3.1 shows the components of the system and the system architecture is also shown in Figure 3.2.

In the commonly used diagnosis and measurement methods for human spine scoliosis, such as the Adam forward bending method or the X-ray radiography, the patient is usually in a static state or posture (Fairbank 2004). As the patient moves, such as stooping down, the human back and spine shape may present relatively

different topologies. If the subject bends into different angles from the standing position to bending forward, the curve of structure scoliosis becomes more distinct and can display different patterns. The patients' forward bending angles and postures are controlled precisely by the movement of the SP.

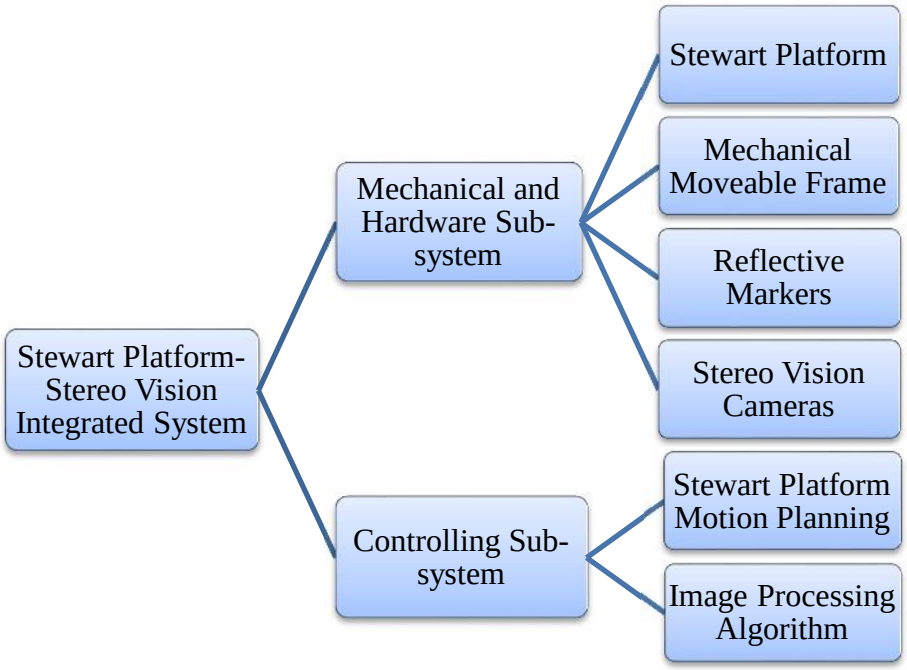

Figure 3.1 Components of the spinal deformity measurement system

In this system, the model's posture is controlled accurately by a specially designed apparatus and equipment. The model is standing in front of the apparatus, holding the handles on the side of the apparatus with his/her hands and hanging down onto the moveable frame of the apparatus. The apparatus is designed to achieve accurate bending movements at various bending angles.

The SP system or similar apparatus is used in this research and it has several advantages. The routine approach in evaluating and monitoring the progress of

scoliosis at school or in clinics is the forward bending test which is not accurate and subjective. Using the SP apparatus, the patients' bending postures can be precisely controlled by the SP and computer. In the system, SP provide accurate postures and positions for the patients during movement, in which the subject's spinal contour is probably different.

Comparing to serial robotic manipulator, this type of parallel manipulator has high load/weight ratio, high rigidity and inherent stiffness, which means that the SP could support the subject's weight with high stabilization. In summary, SP is used in the integrated system to accurate control the patient's forward bending postures.

During the test for scoliotic spinal deformity, the bending is needed and necessary because when the patient tries best to bend hard, the asymmetry of the back and imbalance of the shoulders become more and more obvious and prominent. The forward bend test is used most often in schools and doctor's offices to screen for scoliosis. During the test in school, the subject bends forward with the feet together and knees straight while dangling the arms. Any imbalances in the rib cage or other deformities along the back could be a sign of scoliosis.

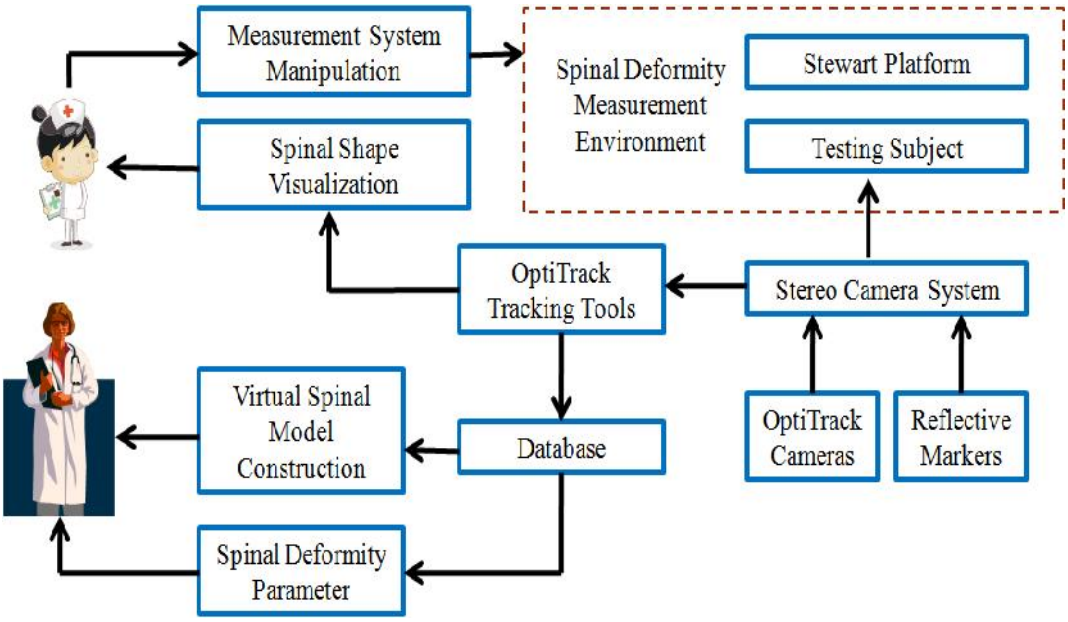

Figure 3.2 The architecture design for the spinal deformity measurement system

In the system, a commercial stereo camera system is used for capturing the shape of the subject's spine. The motion-capturing system which is composed of three OptiTrack cameras and several round reflective markers are used to obtain the trajectory of the human movement. The markers are made from reflective material that can be tracked by the cameras, and they are attached to the articulation of the human spine. In order to track the markers, three OptiTrack cameras are arranged to have overlapping fields of view. For best calibration and tracking results, it is necessary to avoid placing all the three cameras aligned or in the same plane, but to position the cameras at different angles. This creates an area called a captured volume in which tracking can occur. A design illustration of the system with the part names is shown in Figure 3.3.

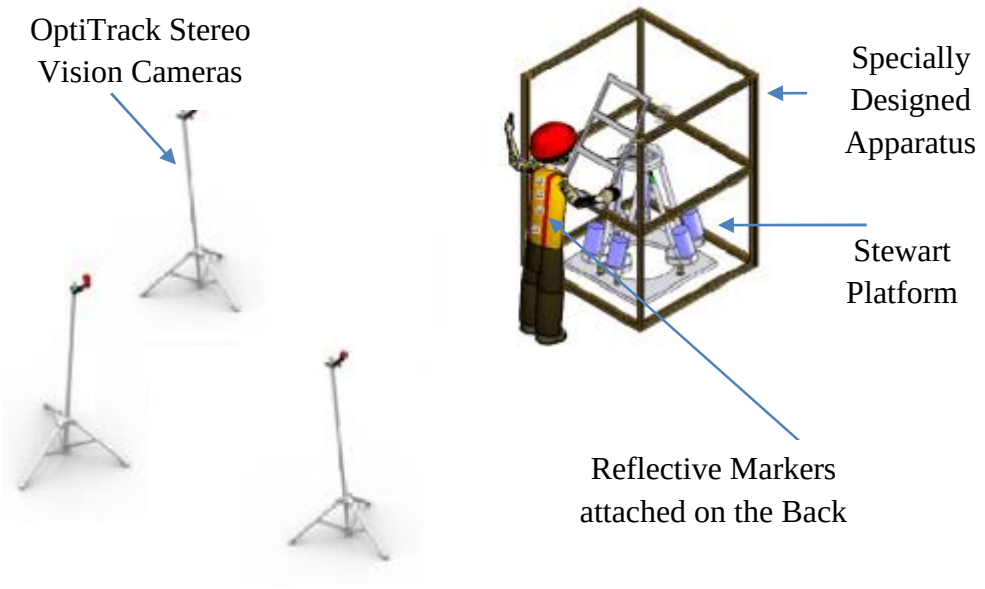

Figure 3.3 Design illustrations for the spinal deformity measurement system

In this research, the process of spinal deformity measurement follows the flow diagram and steps shown in Figure 3.4.

In the first step before the spinal measurement process starts, the SP and the 3D camera system are set up and trial movements are carried out to ensure the system works smoothly. The SP is calibrated by adjusting the length of six legs and the camera system is next calibrated by swinging the OptiWand Kit and processing by the pre-programmed algorithm in the camera system to improve the accuracy and precision of the image capturing process.

The calibration process of the SP generally consists of four basic steps, namely (1) development of a kinematic model that contains a set of parameters to determine the relationship between the actuated joint angles and the end-effector pose, (2) measurement and recording of the manipulator poses, (3) error minimization through searching for the optimum kinematic model parameters of the manipulator from the pose measurements and manipulator actuated joint angles,

and (4) correction for the geometric parameter errors in the manipulator kinematic model. And the calibration of the camera system is done automatically in the OptiTrack system by inputting large number of sample marker points with error compensation algorithm.

The second step is the preparation stage, where the subject or patient would need to remove the shirt and expose the bare back for measurement. 8 to 10 round reflective markers are prepared and attached onto the prominence points of the subject's back.

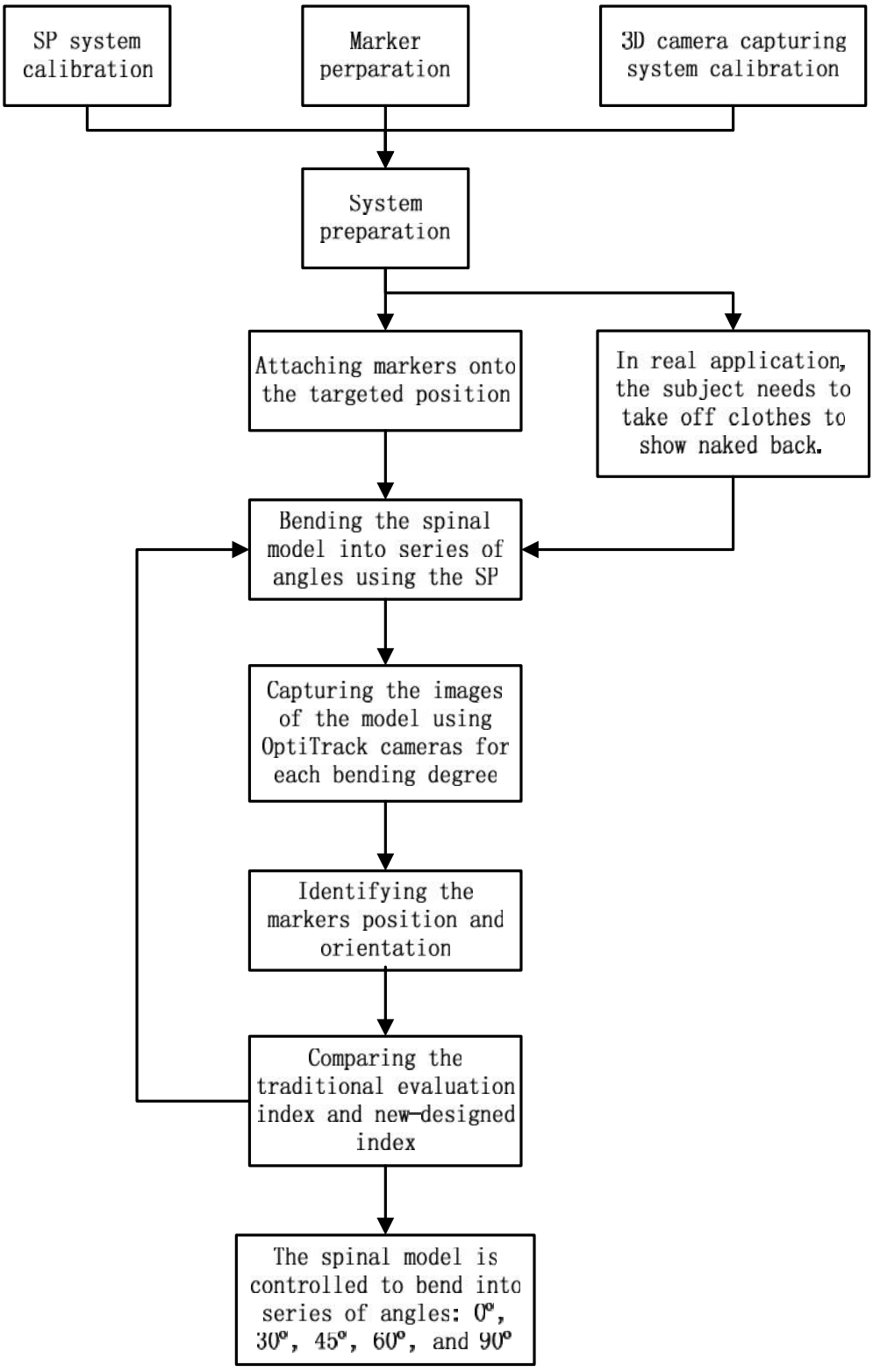

Figure 3.4 The flow diagram and process followed in the measurement process

The system is then activatedand the subject is bent in series of angles of 0°, 30°, 45°, 60°, and 90° by precisely controlling the movement of the SP. When the patient bends in 0°, this means that the patient is standing upright on the ground, and bends in 90° would mean the patient is almost lying down onto the frame. For each bending angle and posture, the back images are captured using the three 3D cameras. In each image captured, the position and orientation of each reflective marker are identified to indicate the spinal prominence. The spine shape and degree of spinal deformity are presented by analyzing the marker positions and orientations. Finally, all the data is stored in the patient's database which can be analyzed for monitoring the progression of the deformity.

When the subject bends into 90°, some markers on the subject's back may be blocked, the three cameras are put higher facing to the patient's back with a downward tilt angle. This assures that when the subject bends with large angle, field of view of the cameras can still cover the whole back.

3.1.2 Requirements and Specifications of Apparatus Development

Based upon the research and previous work published on existing surface measurement techniques and apparatus construction (Sanes and Zipursky 2010; Chen et al. 2000), the proposed mechanical and hardware apparatus has the following requirements and specifications:

1) Inherently safe and does not introduce any ionizing radiation.
2) Minimize the inclusion of any measurement error and variation during data acquisition.

3) The subjects are allowed to stand, pose and move naturally within the defined capture volume by the cameras without compromising measurement accuracy.
4) During acquisition, the comfort of the subject or patient should be ensured.
5) The accuracy of the bony markers recognition and surface measurement reconstruction do not exceed 1mm mean and standard deviation in all the three axes.
6) Pre-defined, independently validated and measureable parameters need to be defined.
7) During each bending session for image capture, the time for capturing the bony markers and generating the back surface shape is within 30 seconds.
8) The overall time of the spinal deformity measurement process is limited to be no more than 10 minutes in acquisition duration (the time includes the process of patient's height measurement and preparation, attaching the markers and spinal shape measurement. The spine measurement process will be controlled within 5 minutes).
9) In the apparatus development, low cost, readily available materials will be used to commensurate with the measurement requirements and specifications.

3.2 Stewart Platform and Specially-Designed Frames

3.2.1 Design of the Stewart Platform and Mechanical Frames

In this research, the components of the hardware of the human spine deformity measurement system include the SP, a moveable mechanical frame,

OptiTrack stereo vision cameras and image processing packages. The posture of the model is controlled using the SP, which activates the movable mechanical frame. The components are described next. By operating the customized apparatus, the subject could bend his or her back accurately in precise angles. The design of the system is shown in Figure 3.5.

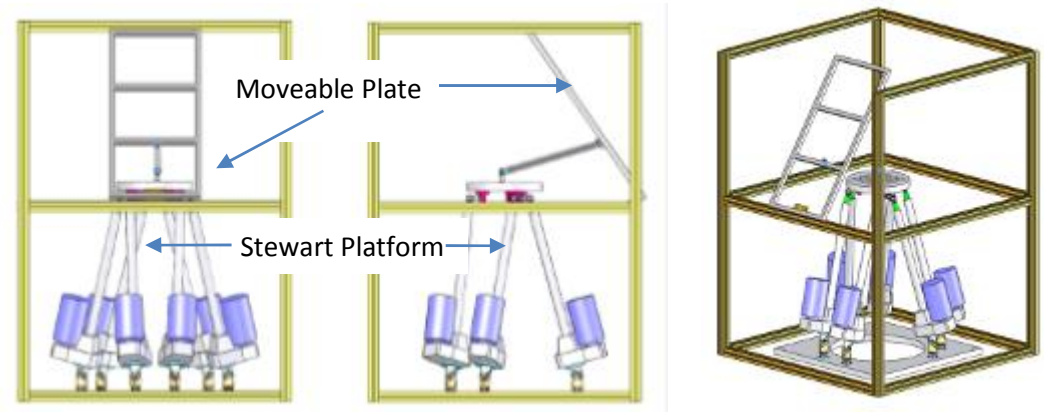

Figure 3.5 The design illustration of overall human spine deformity measurement system

In the SP, the six legs are controlled and activated by individual actuators to achieve six DOFs, which are the three linear movements along the x-axis, y-axis, and z-axis and the three rotational movements, namely pitch, roll and yaw. The specially designed moveable frame is placed on top of the mobile plate of the SP which controls the movement of the subject who is holding onto the handle of the frame.

As the SP moves horizontally, the rectangular aluminum frame is manipulated to rotate along the hinge such that the intersection angle between the

rectangular aluminum frame and the horizontal plane can be controlled accurately as shown in Figure 3.6, and Figure 3.7 shows the details of the structure of the SP.

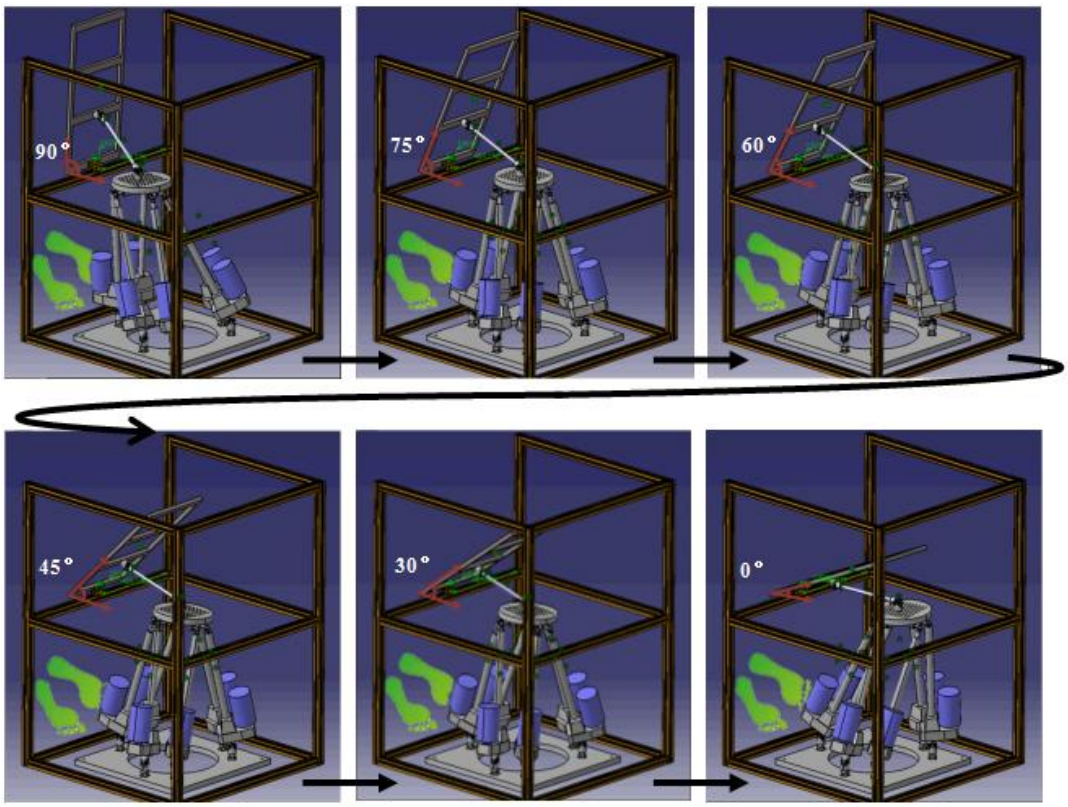

Figure 3.6 Simulation of the dynamic movement of the Stewart platform with standing position and the rectangular aluminum frame

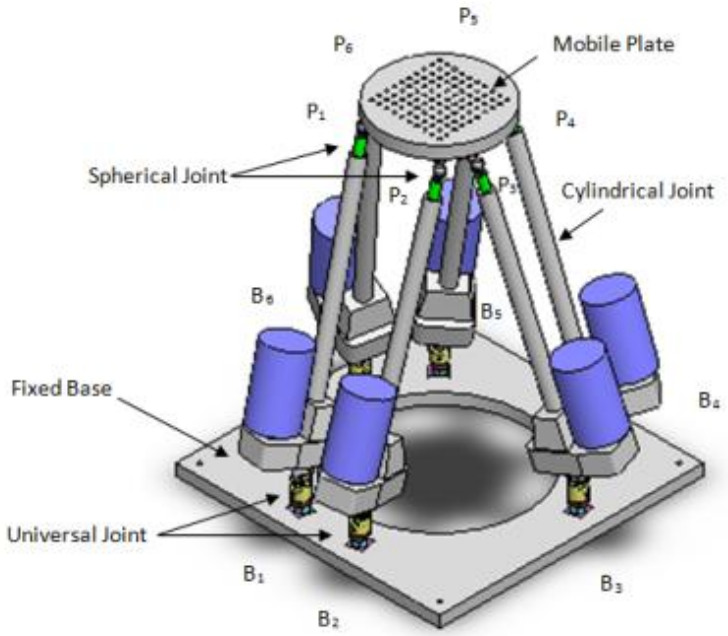

Figure 3.7 Model of Structure of the Stewart Platform

In the design of the existing SP system, the mechanical frame leads the subject bend into serial of angles as shown in Figure 3.6. The subject stands closely to the frame and lay down his or her body onto the frame. During the measurement, the subject holds the handles and tries to be relax.

However, the mechanical frame probably also restrict the bending of the upper part of the subject's body. While the frame moves, the upper body of the subject lay down onto the frame and become a flat rigid body. Therefore, in order to include the movement of rotation of the subject's body, not only the bending postures, a new conceptual design is proposed.

Figure 3.8 shows a new system design and this design includes both the bending motion and rotation motion of the subject's upper body. In this is design, the subject's upper body can freely bending and rotating, while the waist is attached to the frame which is a saddle-shape component. Figure 3.9 shows the comparison of the existing design of the system and conceptual design 2 of the system. In

conceptual design 2, the frame is replace by smaller frame. During the test, the subject stands at the position of footprint and make the subject's waist attach to the saddle-shape component. Using this design, the movement of forward bending and rotation of the upper body are included.

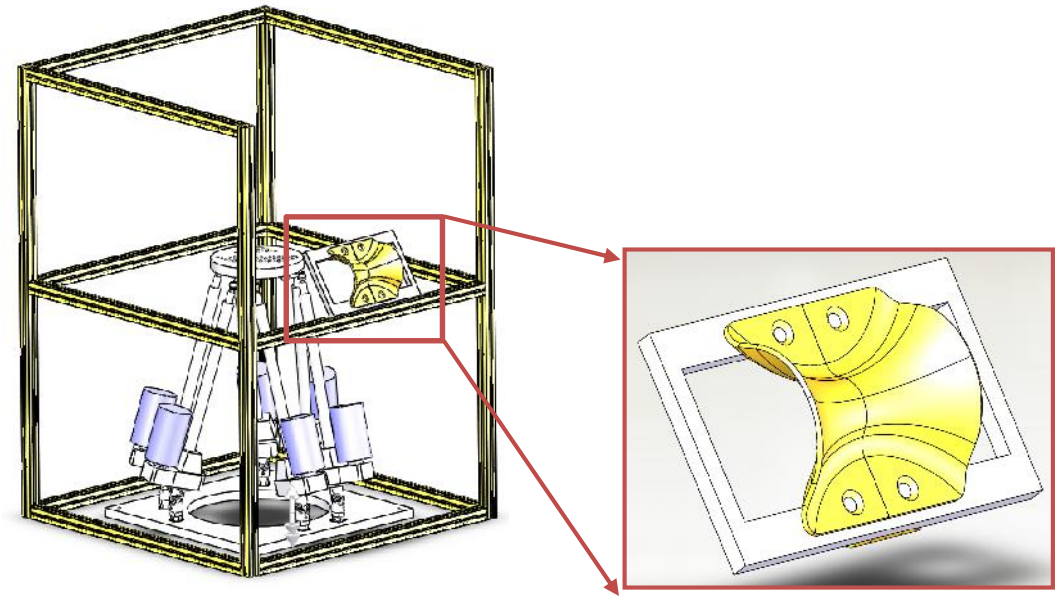

Figure 3.8 A new design of the system to include the forward bending and rotation movement of the subject's upper body

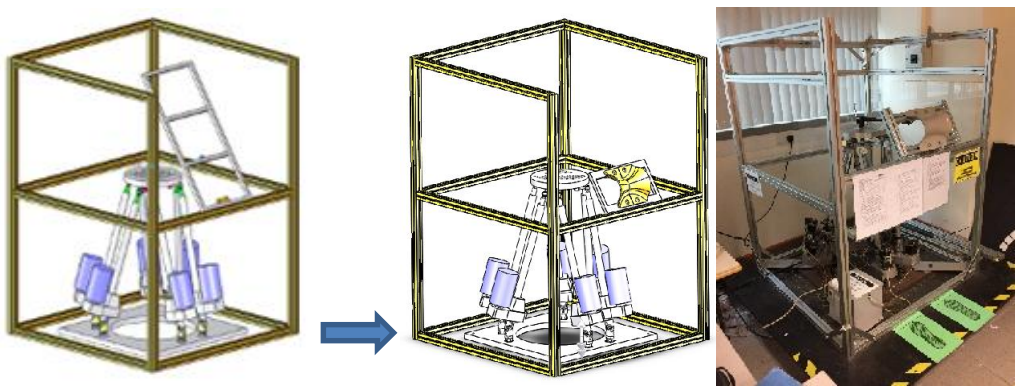

Figure 3.9 The comparison of the existing design of the system and a new conceptual design of the system

3.2.2 Motion Control of the Stewart Platform

The trajectory control of the apparatus is achieved using forward and inverse kinematics. It is the motion analysis of an object without considering forces and torques (Tsai 1999). The kinematics of a rigid body is determined by the configuration of the joints and the position, while the velocity and acceleration of the rigid body are investigated in motion control.

The forward kinematics algorithms are used to control the motion of the SP and calculate the position and orientation of the mobile platform while knowing the joint positions and the six leg lengths. The inverse kinematics algorithms are applied in this study to compute the six leg lengths given the orientation and position of the end-effector of the SP. In short, forward kinematics and inverse kinematics are the mapping of the vectors of the joint coordinates and the vectors of the mobile plate.

a) Forward Kinematics

In the definition of the motion of the SP using forward kinematics (Jakobovic and Jelenkovic 2002), the rotation angles of the mobile platform (end-effector) is defined by the roll-pitch-yaw vector (α, β, γ), which means the consecutive rotations around the *x*, *y*, and *z* axes respectively. The positional coordinates of the centre of the mobile platform is defined by the vector $\vec{t}$ as:

$$\vec{t} = \begin{bmatrix} t_x \\ t_y \\ t_z \end{bmatrix} \tag{3.1}$$

Assume the local coordinates of the mobile platform and the base are shown in Figure 3.10.

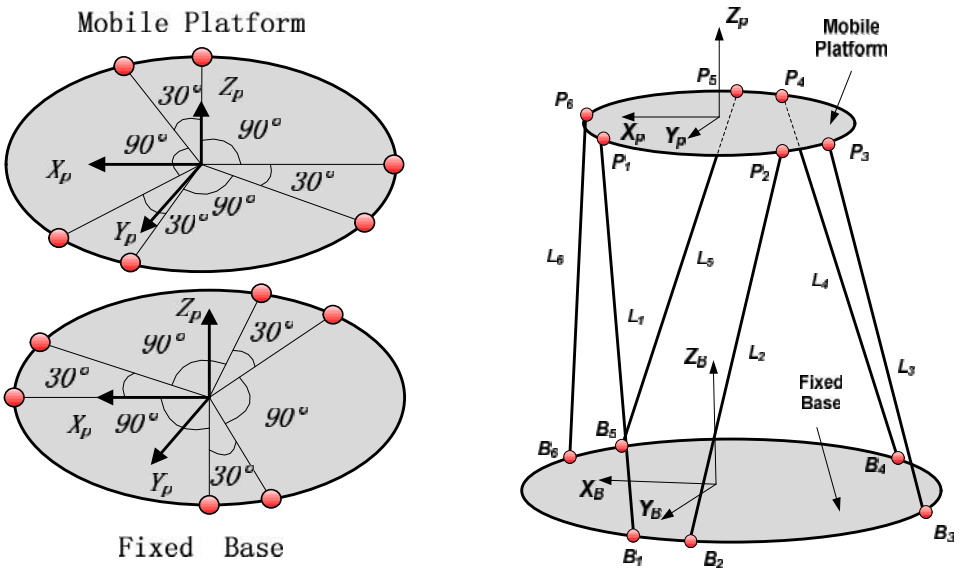

Figure 3.10 Local coordinate system of the Stewart platform

As shown in Figure 3.7, the six joints on the base and mobile platform are defined as six vectors. The coordinates of the joints on the base are represented by $\vec{B}$ and the coordinates of the joints on the mobile platform are represented by $\vec{P}$. Since the base and mobile platform are assumed to be flat, the *z*-coordinates of the vectors $\vec{B}$ and $\vec{P}$ are 0 from the top view.

$$\vec{B}_i = \begin{pmatrix} B_{ix} \\ B_{iy} \\ 0 \end{pmatrix} \text{ and } \vec{P}_i = \begin{pmatrix} P_{ix} \\ P_{iy} \\ 0 \end{pmatrix}, i = 1, \ldots, 6 \tag{3.2}$$

The vectors of the links or legs of the SP can be expressed as $\vec{l}_i$ (Jakobovic and Jelenkovic 2002).

$$\vec{l}_i = -\vec{B}_i + \vec{t} + R \cdot \vec{P}_i, i = 1, \ldots, 6 \tag{3.3}$$

R is the rotational matrix representing the orientation of the centre of the mobile platform. The resultant Eulerian rotation was introduced by Craig (2004).

$$R_X \quad (\gamma, \beta, \alpha) = R_{Z,\alpha} R_{Y,\beta} R_{X,\gamma} =$$

$$\begin{bmatrix} \cos\alpha & -\sin\alpha & 0 \\ \sin\alpha & \cos\alpha & 0 \\ 0 & 0 & 1 \end{bmatrix} \begin{bmatrix} \cos\beta & 0 & \sin\beta \\ 0 & 1 & 0 \\ -\sin\beta & 0 & \cos\beta \end{bmatrix} \begin{bmatrix} 1 & 0 & 0 \\ 0 & \cos\gamma & -\sin\gamma \\ 0 & \sin\gamma & \cos\gamma \end{bmatrix} =$$

$$\begin{bmatrix} \cos\alpha\cos\beta & \cos\alpha\sin\beta\sin\gamma - \sin\alpha\cos\gamma & \cos\alpha\sin\beta\cos\gamma + \sin\alpha\sin\gamma \\ \sin\alpha\cos\beta & \sin\alpha\sin\beta\sin\gamma + \cos\alpha\cos\gamma & \sin\alpha\sin\beta\cos\gamma - \cos\alpha\sin\gamma \\ -\sin\beta & \cos\beta\sin\gamma & \cos\beta\cos\gamma \end{bmatrix} \quad (3.4)$$

The length of each of the leg can be calculated and derived from the Euclidean distance function between two vectors.

$$l_i = \mathrm{d}\left(\vec{B}_i, \vec{t} + R \cdot \vec{P}_i\right), i = 1,2,\ldots,6 \quad (3.5)$$

By calculating the summation of the squares of the disparity between the actual and theoretical positions of the mobile platform, the kinematics errors can be expressed and the first optimization function can be written as follows.

$$F_1 = \sum_{i-1}^{6} \left[\mathrm{d}\left(\vec{B}_i, \vec{t} + R \cdot \vec{P}_i\right)^2 - {l_i}^2\right]^2 \quad (3.6)$$

The translation and orientation vector of the platform is $\vec{X}$.

$$\vec{X} = \left[t_x, t_y, t_z, \gamma, \alpha, \beta\right]^T \quad (3.7)$$

b) Inverse Kinematics

Inverse kinematics refers to the solution of the kinematics equations of the SP to determine the joint parameters that provide a desired position of the end-effector. There are a number of methods to find the solution.

Each of the six joints on the base is described by the position vector, $\overrightarrow{B_i^b}$ according to the local coordinate system, and each of the six joints on the mobile

platform is denoted by $\overrightarrow{P_i^p}$. The left superscripts *b* and *p* represent the vector that is referenced to the base coordinate system and the mobile platform coordinate system.

The most important set of parameters include the minimal and maximal leg lengths of the links which are defined as (l_{i_m}, l_{i_m}), the radii of the base and mobile platform (r_b, r_p), the joint placement which is defined as the angle between the closest joints for both the platform and the base, the workspace and the moving volume of the SP. As assumed previously, the vector $\vec{B}_i$ represents the coordinates of the joints on the base and $\vec{P}_i$ represents the coordinates of the joints on the mobile platform. The inverse kinematics algorithm is described as follows.

$$\vec{P}_i = \vec{t} + R \cdot \vec{p}_i \tag{3.8}$$

$$l_i = d(\vec{P}_i, \vec{B}_i) \tag{3.9}$$

The matrix *R* is written in the following format (Innocenti 2001).

$$R = \begin{bmatrix} \alpha_x & \beta_x & \gamma_x \\ \alpha_y & \beta_y & \gamma_y \\ \alpha_z & \beta_z & \gamma_z \end{bmatrix} \tag{3.10}$$

The orientation of the base with respect to the platform, R^p, is derived as:

$$R^p = R^{-1} = R^T = \begin{bmatrix} \alpha_x & \alpha_y & \alpha_z \\ \beta_x & \beta_y & \beta_z \\ \gamma_x & \gamma_y & \gamma_z \end{bmatrix} \tag{3.11}$$

The vector of the *i*th leg or *i*th link is expressed from the mobile platform joint $\vec{P}_i$ to the base joint $\vec{B}_i$, which means $\vec{P}_i$ is referenced to the base coordinate system.

$$l_i = d(\vec{P}_i, \vec{B}_i) = \vec{P}_i - \vec{B}_i \tag{3.12}$$

Hence, from equations 3.8 and 3.12,

$$l_i = \vec{P}_i - \vec{B}_i = \vec{t} + R \cdot \vec{p}_i - \vec{B}_i \tag{3.13}$$

In the design of the SP, assume the radius of the base plate is r_B and the radius of the mobile platform is r_P. As shown in Figure 3.7, the six universal joints are located at the base and the six spherical joints at the mobile platform with 15° symmetry on both sides of each of the 120° line of the platform. Each pair of the adjacent mobile platform joints p_i with 30° disparity forms a triangle with two adjacent base joints b_i of 90° disparity. Thus,

$$B_i = r_B\left[\cos\left(Angle_{B_i}\right),\ \sin\left(Angle_{B_i}\right),\ 0\right] \tag{3.14}$$

$$P_i = r_P\left[\cos\left(Angle_{P_i}\right),\ \sin\left(Angle_{P_i}\right),\ 0\right] \tag{3.15}$$

Therefore, the coordinates of the position of the link l_i is derived in the scalar function as follows.

$$l_{ix} = r_p\left[\alpha_x \cdot \cos\left(Angle_{P_i}\right) + \beta_x \cdot \sin\left(Angle_{P_i}\right)\right] + T_x - r_B \cdot \cos\left(Angle_{B_i}\right) \tag{3.16}$$

$$l_{iy} = r_p\left[\alpha_y \cdot \cos\left(Angle_{P_i}\right) + \beta_y \cdot \sin\left(Angle_{P_i}\right)\right] + T_y - r_B \cdot \cos\left(Angle_{B_i}\right) \tag{3.17}$$

$$l_{iz} = r_p\left[\alpha_z \cdot \cos\left(Angle_{P_i}\right) + \beta_z \cdot \sin\left(Angle_{P_i}\right)\right] + T_z \tag{3.18}$$

The length of leg l_i is calculated as the magnitude of the component vectors.

$$|l_i| = \sqrt{l_{ix}{}^2 + l_{iy}{}^2 + l_{iz}{}^2} \tag{3.19}$$

3.2.3 User Interface for the Control of the Stewart Platform

A graphic user interface (GUI) has been designed and developed to control the position and movement of the SP for achieving the postures of the scoliotic subject. Before designing the GUI, all the internal control algorithms have been accomplished as previously introduced in the “Kinematics” part in Section 3.2.2.

The GUI integrates different modular programs into one single window which is written in Visual C++. In this incorporated environment, four control modules are involved and integrated in which the doctors or technicians could observe and manipulate the motion of the SP and the connecting mechanical frame.

a) Motion Control Window

In the motion control module, the spatial position and orientation of the end-effector of the SP and the lengths of the six legs are calculated using the forward and inverse kinematics. By inputting the six leg lengths, the orientation (roll, pitch and yaw) and coordinates (x-axis, y-axis and z-axis) of the end-effector are determined by applying the forward kinematics. By inputting the orientation and coordinates of the end-effector of the SP, the length of each individual of the six legs is calculated using inverse kinematics. The system can be also controlled by inputting the parameters of the extension or motion velocity of each individual actuator or by inputting the leg length of each individual leg. Furthermore, a real-time feedback section to control the position, velocity and acceleration of the actuators from the encoder of the actuators is also integrated. Figure 3.11 is the first version of the motion control user interface and Figure 3.12 is the second version of the control interface to view the velocity, spatial position, and acceleration of the actuators including the sequential operation steps to guide the user how to manipulate the SP.

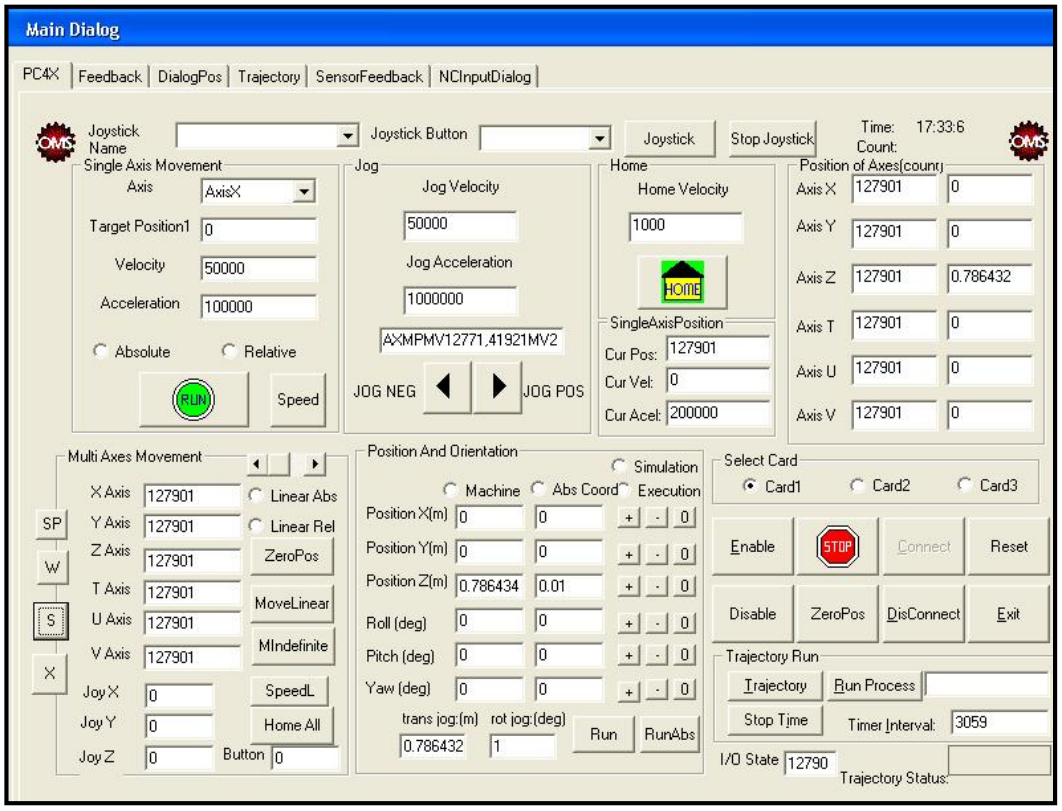

Figure 3.11 First version of the motion control user interface

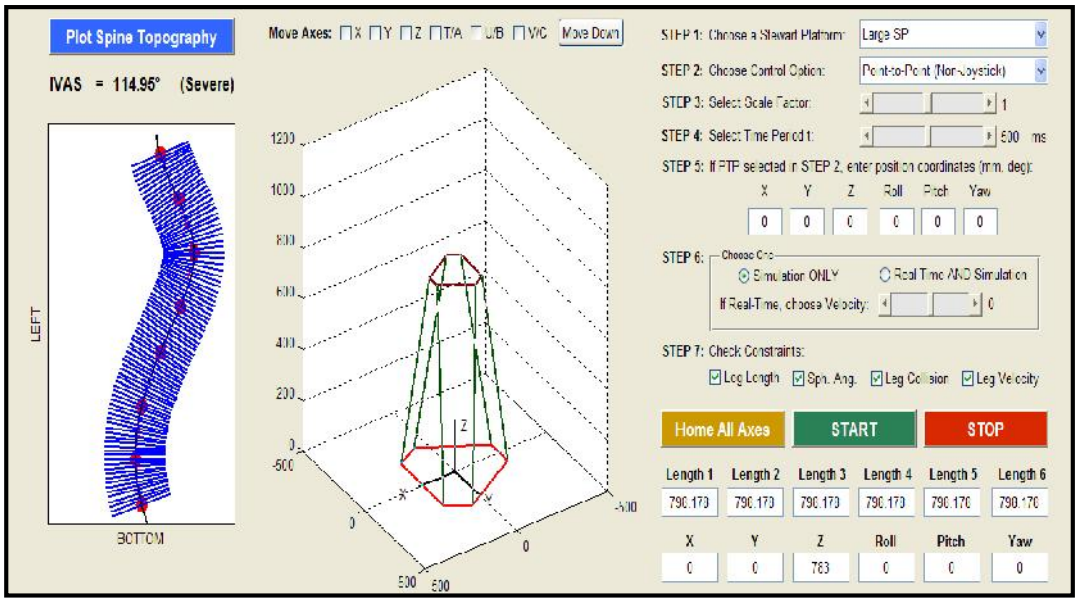

Figure 3.12 Second version of the motion control user interface in use

In the new version of the motion control user interface, the left column is the Spinal Deformity Interface to display the result of spinal deformity index and parameter as well as the shape and deformity of the scoliotic spine. The middle column of the control interface is the real-time display of the status of the SP. The right column of the interface is the control buttons and sequential steps to control the status of the SP. In Step 1, three SPs in the laboratory can be selected and for the purpose of human spinal deformity measurement, the largest SP is used. In Step 2, several control methods are provided in this program, such as joystick control, single point-to-point control, trajectory control, etc. The scale factor can be adjusted in Step 3. The moving period of time can be adjusted in Step 4 in order to control the velocity of the platform. Step 5 is used to input the x, y, z spatial coordinates and roll, pitch, yaw rotation parameters of the end-effector. Ay applying the inverse kinematics algorithm, the six leg lengths are determined. In Step 6, two control models are provided. The simulation model is designed to simulate the motion and posture of the SP and when this model is activating, only the virtual model of SP will move and the real SP does not move. The real-time and simulation model can control both the virtual SP model and the real SP. In Step 7, four types of constraints are selected and checked to ensure the security of the system, namely, the leg length should be in the motion range and does not damage the platform; The Sph. Ang. constraint means the angles of the movement of the legs should be in the motion range; leg collision means that in the movement of the platform, the legs should not collide with the other legs; leg velocity constraint is to limit the velocity of the legs in the acceptable range to avoid damaging the legs. The last two rows are the input parameters of leg lengths for each leg with the application of forward kinematics

and the spatial coordinates and rotation parameters for the plate with the application of inverse kinematics.

b) Sensor Control Interface

Figure 3.13 shows the sensor control interface which is designed for the exterior measurement sensor to be applied to the actuators of the SP. The exterior sensors are used to calibrate the platform and monitor the actual position and orientation of the mobile plate of the SP. After the real data of the position and orientation of the mobile plate has been obtained, the data can be presented and stored in this GUI.

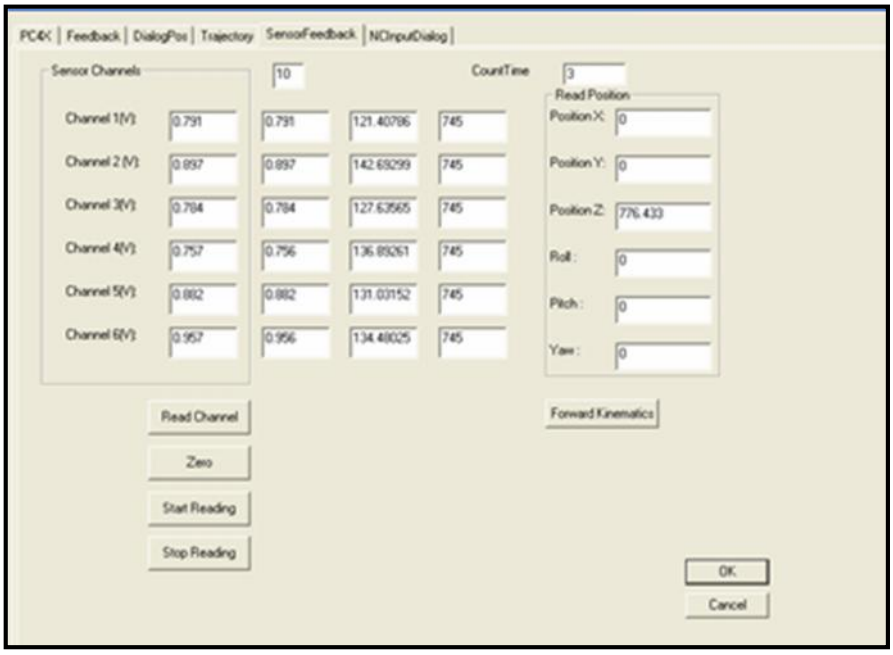

Figure 3.13 Exterior sensor control user interface

During the stroke of the actuator, the analog value of the wire extension of the wire sensor is switched to digital values calculated using the National

Instrument DAQ card. The digital value in the DAQ card is represented by voltage which is proportional to the length of the wire drawn from the wire sensors. The feedback values are used to balance and minimize the variance and error of the position and orientation of the mobile plate using forward kinematics.

c) Motion Control Feedback Window

The motion control feedback window is developed to read all the feedback values of the positions, velocities and accelerations of the encoder which is illustrated in Figure 3.14.

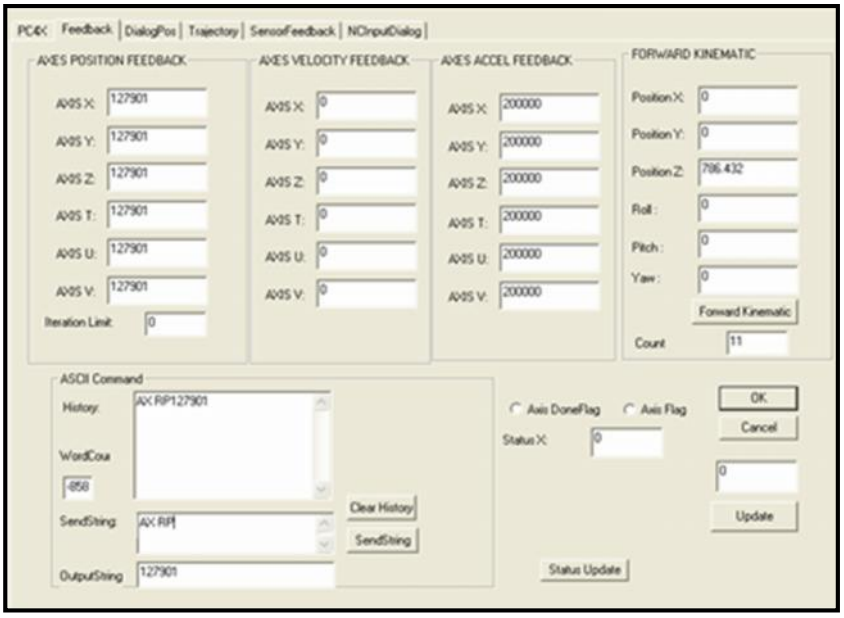

Figure 3.14 Interface of motion control feedback window

The ASCII dialog window is designed for the user to enter direct command codes to the SP which is efficient for the user to control the system when simple motion is required.

3.2.4 Assembly and Construction of the System

The SP is built with commercially available materials. Some of the mechanical components are fabricated in the Advanced Manufacturing Laboratory in the Department of Mechanical Engineering, National University of Singapore.

Figure 3.15 (a) shows the dimensions of the base plate of the SP and Figure 3.15 (b) shows the dimensions of the mobile plate. At the corners of the base plate, four handles are installed for easy lifting. The base is hollowed out at the centre to reduce its weight so as to increase the mobility of the platform. In the mobile plate, there are arrays of tapped holes on top of the platform, allowing accessories to be assembled for different applications.

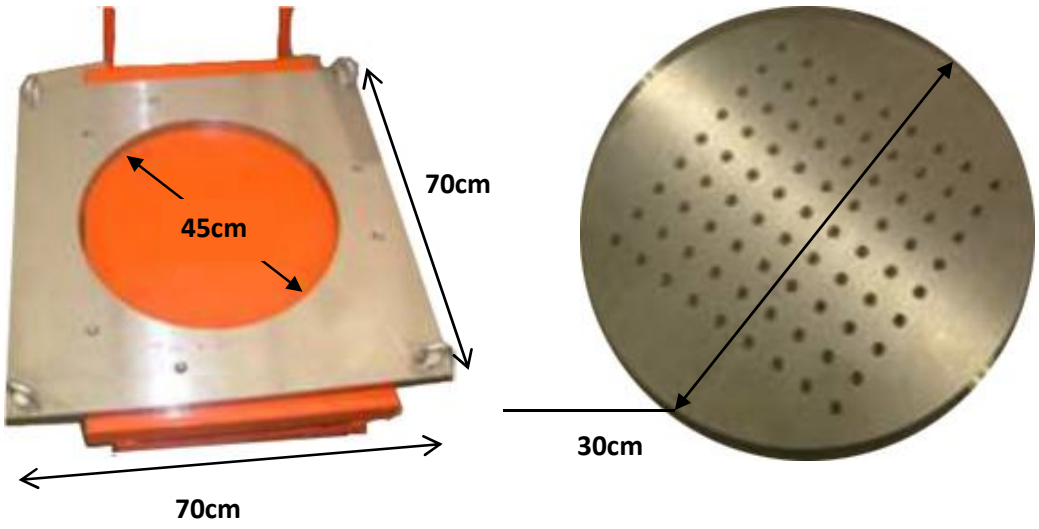

Figure 3.15 (a) Dimension of the base plate of the SP; (b) Dimension of the mobile plate of the SP

In the construction process of the SP, in order to ensure the safety of the SP, the force acting on each of the leg is evaluated. The force in each leg is 20.59N when a weight is applied. The force exerted on the legs increases to 83.89N when

a shear force is applied. Thus, when the platform reaches its maximum height, the force loading on the legs is 20.34N and 116.6N with respect to the vertical force and shear force.

On the base of the legs, linear actuators of UBA1 RV C400 with DC motors are fixed and mounted to control the legs movements. The linear actuator is the ball screw type with maximum dynamic and static loads of 1750N and 4000N respectively. Figure 3.16 shows the linear actuator with motor and Figure 3.17 shows the motor with drive. The motion systems stepper motor with drive MDMF2231-4 is selected to drive the actuator. The driving force is transmitted using belts running on the pulleys. The digital encoder of each motor also provides feedback for the position control.

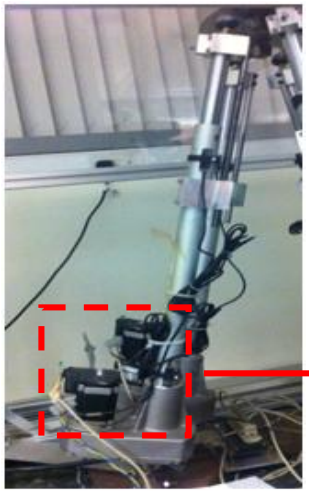

Figure 3.16 the linear actuator with motor

Figure 3.17 the motor with drive

The moveable mechanical frame is a detachable part assembled using several aluminum sections which the subject rests against. Figure 3.18 shows the

assembly of the mechanical frame. A foot step mark is attached at the front of the SP to indicate the position for the user to stand as shown in Figure 3.19.

Figure 3.18 Aluminum bar and the assemble of the mechanical moveable plate

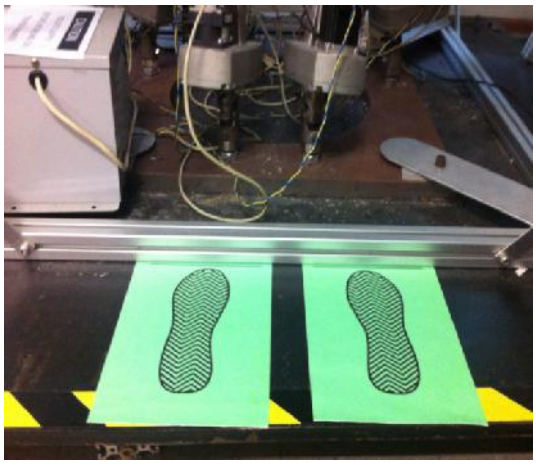

Figure 3.19 Sign of the foot step

Figure 3.20 shows the final construction of the platform and Figure 21 shows the final manufacture of the saddle-shape component used at the position of subject's waist. Figure 3.22 shows parts for constructing the moveable frame. It is a detachable part assembled using aluminum sections and two universal joints.

Figure 3.20 The components and final construction of the SP

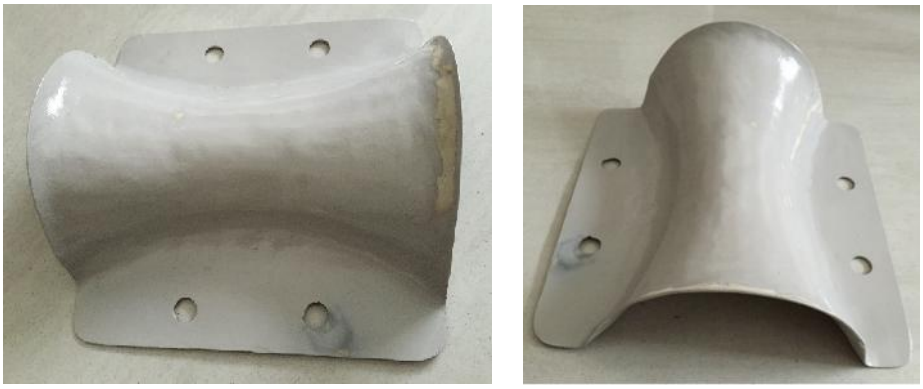

Figure 3.21 Manufacture of the Saddle-shape Component

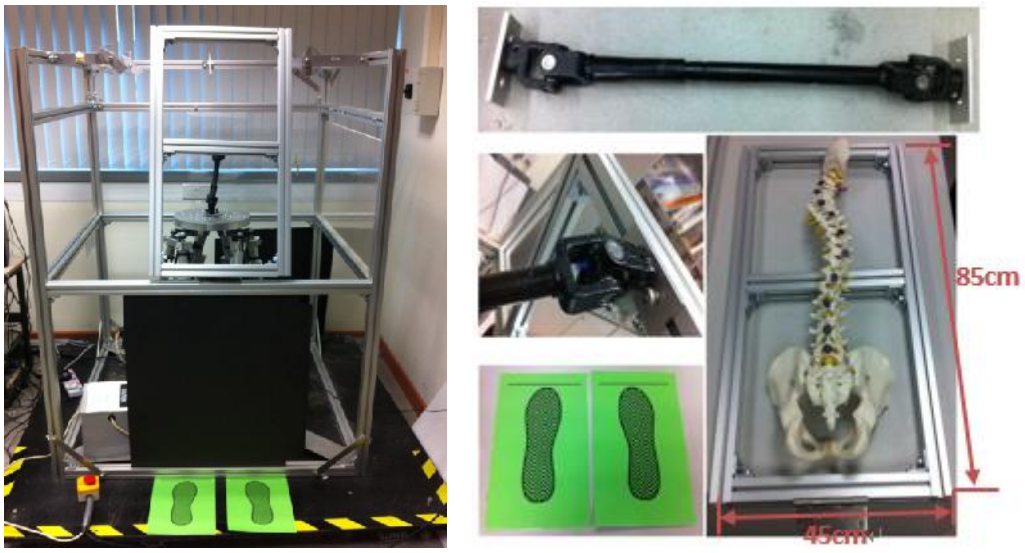

Figure 3.22 Construction of the moveable frame assembly using aluminum sections and the overall system

3.3 Stereo Vision Camera System and Bony Markers Arrangement

In the design of the human spinal deformity measurement system, the stereo vision camera system with reflective markers is used to provide and identify the 3D information of the position and orientation of each vertebra in order to generate the spinal shape by interpolating the vertebras.

Three OptiTrack V100:R2 motion capture cameras (Corvallis, OR, USA) are used in this system for patient's human back topology generation which can

offer integrated image capturing, data processing, and motion tracking in a powerful, compact package. The V100:R2 camera is capable of capturing fast moving objects, real-time streaming and customized user interface with its global shutter imager and 100 frames per second (FPS) capture speed. By maximizing its 640 × 480 VGA resolution through advanced image processing algorithms.

Figure 3.23 shows the configuration of the camera used in the system. By applying the OptiTrack camera system in the spinal distortion assessment research, desktop-friendly motion capture images and the spatial position and orientation information of the human back can be obtained. Table 3.1 lists the camera specifications.

Table 3.1 Specifications of the OptiTrack V100:R2 Camera Used in this Study

Specifications of the OptiTrack V100:R2 Camera			
Frame Rate	100 FPS (frame per second)	Resolution	640×480
Width	45.2 mm	Pixel Size	6×6 µm
Height	74.7 mm	Latency	10 ms
Depth	36.6 mm	Lens HFOV	45-60°
Weight	120 g	Ultra Bright	F# 1.6

Figure 3.23 Configuration of the OptiTrack stereo camera with 6-32 mounting holes on the back

Used together with the cameras, some specially designed markers are included in the process for human spine deformity measurement. The markers are standard one inch round balls which are made by reflective materials. Figure 3.24 shows the 7/16" diameter hard markers with mounting holes used in this study.

The software used in this research is the Tracking Tool motion tracking software. The free OptiTrack SDK provides complete access to the powerful capabilities of controlling OptiTrack V100:R2 camera. It is easy to use API and included sample applications to create customized tracking applications rapidly. The Tracking Tools software is used to achieve robust multi-camera 3D tracking in this research.

Another issue is the arrangement of these three cameras. The OptiTrack system is modular and it reduces the initial investment in motion tracking technology. The design of camera arrangement and Camera Installation and Data Obtain Process is shown in Figure 3.25.

Figure 3.24 7/16" diameter hard reflective markers with 6-32 mounting holes and the OptiWand calibration tool with three markers

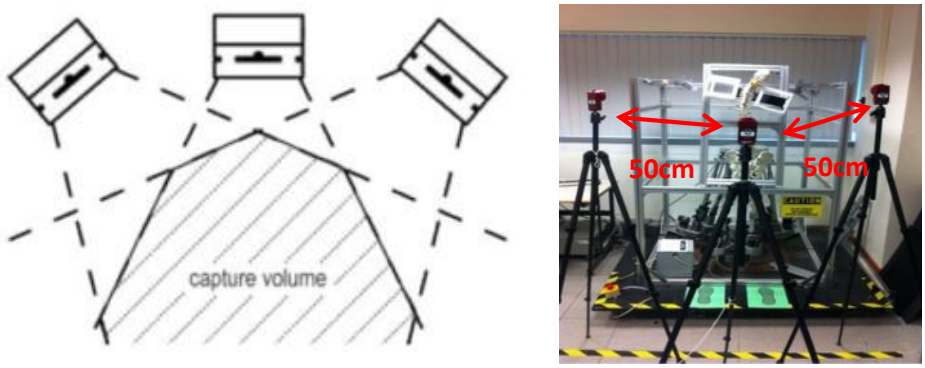

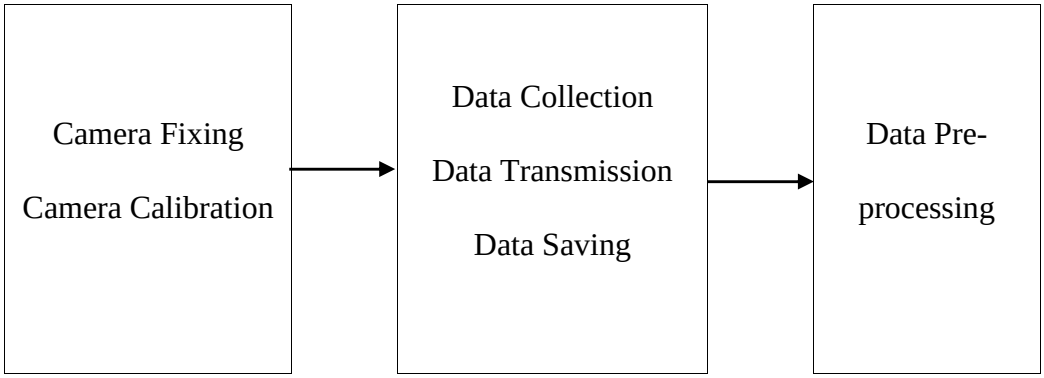

Figure 3.25 Camera arrangement and data acquisition process

Chapter 4 Surface Measurement Parameters and Indices for Adolescent Idiopathic Scoliosis Progression Assessment and Diagnosis

In order to describe the body shape acquired numerically from subjective visual assessment algorithms and surface topology apparatus (Inami et al. 1999; Suzuki et al. 1999), recent studies have highlighted the relationship between surface topology and the changes of the bony distortion using the scoliosis evaluation parameters and indices which are applied to define the cosmetic defect and to provide a non-invasive indicator for scoliosis progression.

4.1 Proposed Human Spinal Deformity Measurement Indices and Parameters

4.1.1 Spinal Visible Characteristics and Principles of Optimal Indices

In the early stage of the spinal deformity, the symptoms are not apparent in most cases. Until the underlying trunk curvature becomes significant, the pain starts to become severe. The very first signs or indications of the scoliosis are that the patient's clothes are not suitably fit, the pleats may hang unevenly or the patients may walk with abnormal gait.

The quantitative analysis for scoliosis requires more detailed physical examinations such as:

- The position of the head is not centered above the shoulders.
- The prominent points of the scapula are not symmetrical.
- One shoulder may be higher than the other.
- The spine and rib cage is deformed at "C" shape or "S" shape curves in the coronal plane.

- It appears that a longer distance between the elbow and trunk on one side of the body and a shorter distance between the elbow and trunk on the other side.
- The entire body leans to one side.
- The structure of muscles may change and uneven musculature may trend to one side of the spine.
- Asymmetric size and location of the breasts among females.
- The texture and looking of the skin overlying the spine area may changes.

Patias et al. (2010) provided a set of nine principles that should be followed to design an optimal index to evaluate the severity of a scoliosis curve. However, it is challenging to satisfy all these principles completely, and thus they can be used as guidelines instead. The nine principles are:

a. Indices should be measured with maximum achievable accuracy and in a direct manner. For instance, the coordinates and angles are direct measurements whereas the areas and volumes are calculated indirectly from other direct measurements. Therefore, indices based on direct measurements are more accurate and preferred.
b. Indices should be independent of the measurement techniques of the trunk deformities; else they cannot be used universally and will be highly dependent on the measurement methodology used.
c. Indices should be based on robust procedures and automatic processing techniques, eliminating as far as possible human intervention, human induced errors and objectivity.

d. Indices should be based on automatically detectable and uniquely identifiable anatomical landmarks. Landmarks used and the measured points on the back surface should be positioned unambiguously so that they can be detected automatically and easily.

e. Indices should require simple measuring protocols. Complicated protocols (e.g., patient position relative to the sensor, lighting conditions, etc.) are sources of errors.

f. Indices should be normalized in order to be comparable among patients, and should not depend on the trunk size, width of waist or length of arms. In this respect, they should be united or in the form of percentages.

g. Indices should provide a stable datum for progress monitoring over time. This means that they should either be coordinate-system-free or refer to a coordinate system that is stable over time.

h. Indices should be able to distinguish between different types of surface deformities (i.e., Coronal/Transverse/Sagittal, Left/Right semi-trunk, Single/Double curves Thoracic/Thoraco-Lumbar/Lumbar).

i. Indices should provide a clear and safe difference in magnitude between normality and pathology, so that pathology can be safely distinguished and diagnosed. This actually means increased sensitivity and specificity, and there is minimal error relative to the smallest detectable change.

4.1.2 The Inter-Vertebra Angular Separation (IVAS)

The human spine composes 33 vertebrae, from which the upper 24 vertebrae are connected when evaluating the severity of scoliosis in this research. These form

the cervical (top), thoracic (middle) and lumbar (bottom) regions of the spinal column. Each vertebra is separated by the upper and lower inter-vertebral discs that allow slight movement of the vertebrae and act as a ligament to hold the vertebrae together. Figure 4.6 shows an X-ray of a normal human spine, in which the horizontal and flat inter-vertebral discs between adjacent vertebrae can be clearly observed.

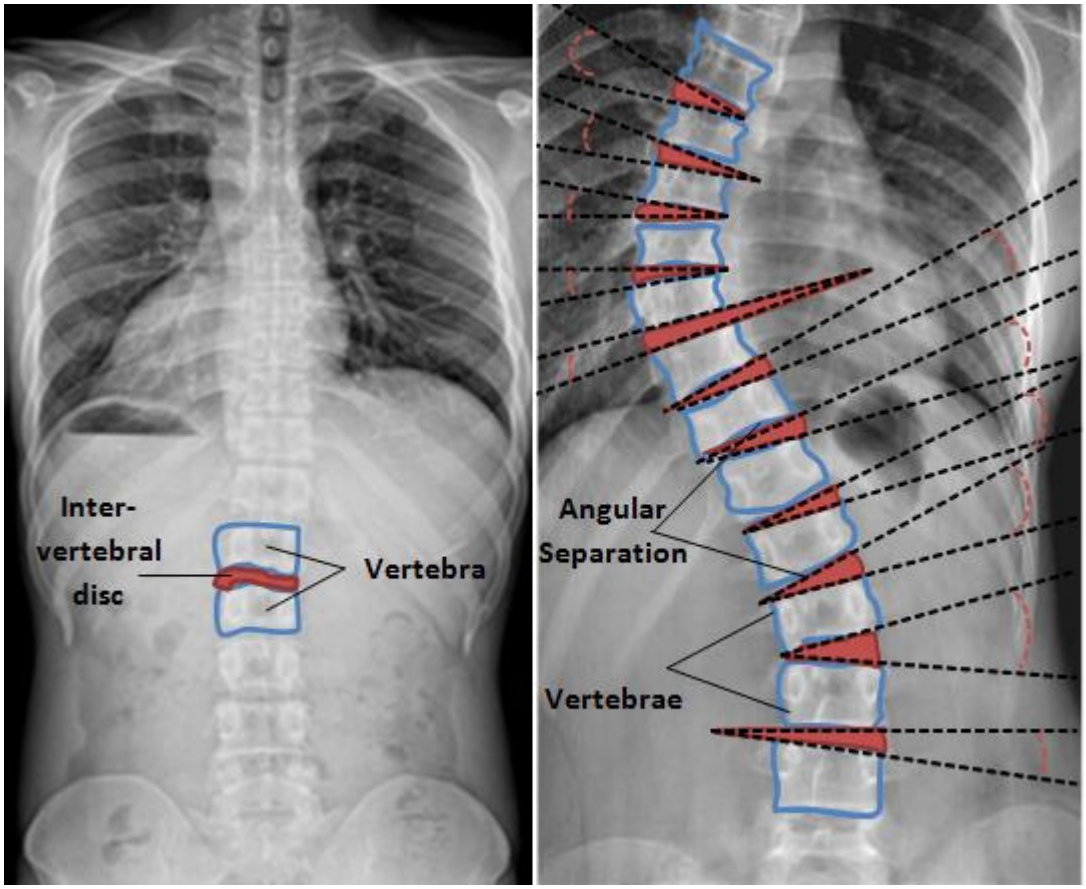

Figure 4.1 X-ray images of normal and scoliosis spines

(Source: http://commons.wikimedia.org/wiki/File:Scoliosis_(15-year-old).jpg)

However, for a scoliotic spine, not all the inter-vertebral discs are horizontal and flat. Figure 4.1 also shows an X-ray image of a scoliotic spine with a typical

'C-shape' curve in the thoracic region due to the curvature of the spinal column. The vertebrae are observed to deviate most from a vertical plumb line near the cervical-to-thoracic and thoracic-to-lumbar transition regions. At these specified regions, the inter-vertebral discs are found to rotate on the coronal plane, hence forming an angular separation between the pair of adjacent vertebrae.

Since these angular separations reflect a curvature in the spine, they can be summed up along the entire spinal column to provide an index that can be compared with the Cobb angle. The larger the total angles of separation, the more severe is the deformity. A proportional relationship between IVAS and the Cobb angle is sought in order to establish the IVAS method as a complementary tool to support the Cobb angle. This means that the severity of the scoliosis can be evaluated accurately using IVAS before the need for intrusive X-rays for the calculation of the Cobb angle.

The formulation of the proposed index of IVAS is follows:

$$\text{IVAS} = \sum_{i=1}^{n}(\text{angle between the } ith \text{ and } (i+1)th \text{ vertebrae}) \qquad (5)$$

For evaluating the feasibility of the IVAS index, 30 X-ray images of scoliotic spine (The source of the x-ray images sample is *http://www.pinterest.com/spinecor/scoliosis-x-ray/)* were used. The Cobb angle and the IVAS index for each of the 30 scoliotic spine subject were calculated. The correlation between the Cobb angle and the IVAS index were established in this research, which has shown the potentially high usefulness of the IVAS index.

In the 30 X-ray samples which were sourced for analysis, a breakdown is shown in Table 4.1. The mix of 'C'-shape and 'S'-shape scoliotic curves and a range

of mild, moderate and severe curves will allow for a more rigorous evaluation of the comprehensibility and versatility of the IVAS method in evaluating different types of curves.

Table 4.1 Breakdown of X-ray samples

Breakdown	**No. of Samples**	**Total**
'C'-shape	22	30
'S'-shape	8	
Mild (<20^o)	4	30
Moderate (20^o-70^o)	23	
Severe (>70^o)	3	

(In the table, the definition of "Mild" scoliosis means that the Cobb angle of the spine is less than 20^o deviation, "Moderate" scoliosis means that the Cobb angle of the spine is larger than 20^o and less than 70^o and "Severe" scoliosis is larger than 70^o.)

The type of curves, the lateral flexion values and the degree of vertebral rotation were analyzed from the posterior-anterior rachis radiograph taken while the patient was standing. The maximum value and minimum value of the Cobb angle of the scoliosis spine sample are 95.5° and 12° respectively. The mean Cobb angle of the scoliosis spine sample is 44.75° with standard deviation of 19.34°. The classes of curves are established following the Ponseti classification (Negrini and Negrini 2007) as shown in the Figure 4.2. The lateral flexion is decided by the Cobb angle and the subjects are classified into five classes (the Cobb angle larger than 50°, between 30° and 40°, between 20° and 30°, and between 10° and 20°).

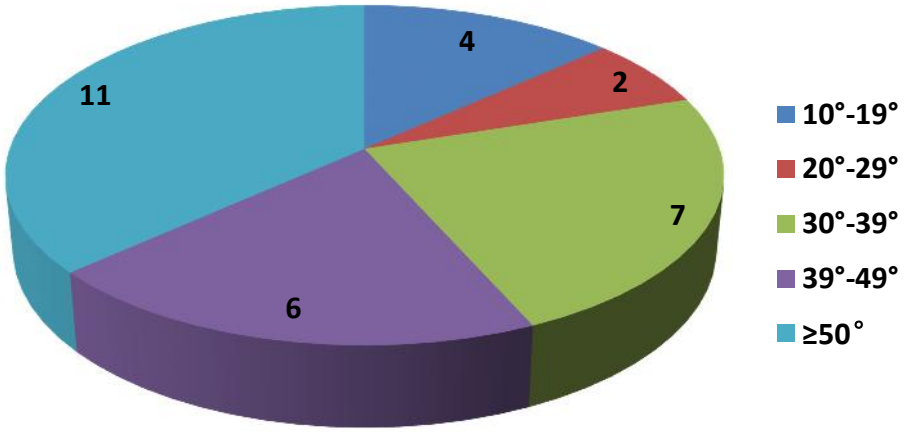

Figure 4.2 Radiographic Parameters of the Cobb Angles of the 30 Subjects

In order to quantify the asymmetry in the axial plane, the new IVAS index is devised and basically consists of the angular differences between each pair of adjacent vertebrae. Using the same 30 data sample of X-ray images of the scoliosis spine, the IVAS index is calculated using the following procedures:

1) Project the chosen X-ray sample onto a standard grid to obtain a preliminary estimate of the 2-D coordinates governing the shape of the spinal curve.
2) Determine the inter-vertebra disc area and the upper and lower edges of the vertebrae from the X-ray samples.
3) Apply the IVAS index method on radiographic images to obtain corresponding total angular separation (TAS_i) between each pair of adjacent vertebrae.
4) Repeat measurement with the IVAS method for the 30 selected X-ray samples.

5) Plot the Cobb angle and the IVAS index on the same set of axes to visualize their relationship.
6) Plot the Cobb angle against the IVAS index to obtain the best-fit trend-line.
7) Finally, using the Correl function in Microsoft Excel to obtain the correlation coefficient for these two sets of data.

4. 1.3 Modified Inter-Vertebra Angular Separation (MIVAS)

The IVAS index is a parameter designed for the human spinal deformity assessment to complement the Cobb angle and the computed results are shown in the next section. However, it is not easy to recognize the upper and lower edges of the vertebrae in the X-ray images due to the fuzzy color in the bone and muscle parts, and this limits the automatic computation potential in clinical applications. Thus, a modified IVAS is proposed in this section.

The MIVAS index is devised based on the nature of the interpolated curves, where the vertebrae and hence the inter-vertebrae discs, are not necessarily visible along the curves. Hence, the previous IVAS method has been modified for use on a line curve, without altering the governing principle of the evaluation method (i.e., to obtain the angular separation between two lines at landmarks along the spine). Similar to IVAS, the modified IVAS is calculated as the summation of the angles formed between the perpendicular lines through each pair of the adjacent vertebra.

In this case, the modified IVAS method consists of first drawing lines that are perpendicular to the curve at estimated fixed intervals, of which the feature points between the intervals are selected on the spinal curve. The positions of the subject's vertebra are selected as feature points. Next, the curve fitting algorithm of

the ‘Spline’ algorithm is applied in the MatLab to outline the spinal curve. Through each of the feature points, a normal line which is perpendicular to the tangent direction is drawn along the spine curve. Thereafter, the angular separation between each pair of lines is measured and summed up along the entire curve to obtain $MIVAS_i$ – a representation of the total angular separation measured using the modified IVAS method. Figure 4.3 shows an example of a scoliotic spine from an X-ray image and interpolation of the spinal curve.

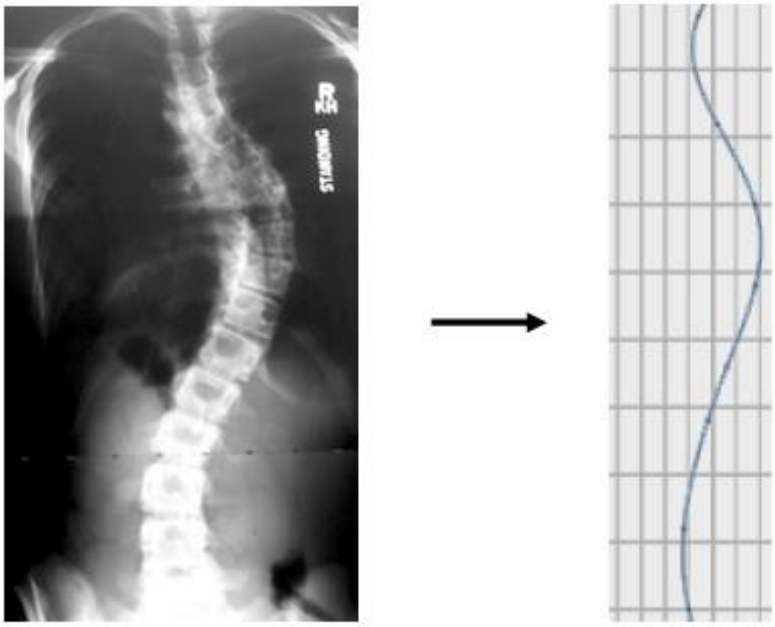

(a) (b)

Figure 4.3 Example of a scoliotic spine and curve fitting algorithm applied to the spinal curve

The MIVAS does not consider the inter-vertebra disc. The steps of calculating the MIVAS include:

1) Project the chosen X-ray sample onto a standard grid to obtain a preliminary estimate of the 2D coordinates governing the shape of the spinal curve.
2) Obtain the positions and coordinates of the vertebras of the subject's spine image.
3) Interpolate the points of the vertebra to form the spinal curve to simulate the shape of the scoliotic spine.
4) Through each position of the vertebra point on the curve, draw a perpendicular line to the curve.
5) Calculate the angles between the pair of adjacent perpendicular lines.
6) The modified index of MIVAS is defined as the average of the angles between the pair of the perpendicular lines.
7) Plot the Cobb angle against the modified MIVAS measurements to obtain the best-fit trend-line.
8) Finally, using the Correl function to obtain the correlation coefficient for these two sets of data.

With the input of the preliminary coordinates, Figure 4.3(b) shows the interpolated curve of one of the X-ray samples obtained using the "Interpolant (Cubic)" algorithm in MatLab; this curve is determined to be able to represent a scoliosis spine shape most accurately. The curve is observed to resemble closely the actual spinal curve shown in the X-ray in Figure 4.3(a).

The next step involves applying the modified method of MIVAS to the interpolated curve. Figure 4.4 shows a visual representation of the entire measurement process along the length of the curve, where eight lines are drawn at

an estimated fixed distance apart with each line being perpendicular to the curve at that vertebra point. Since in a scoliotic spine, the drawn lines along the normal direction are observed to be unparallel with each other, there is an angle between each pair of adjacent lines that can be measured and summed up along the entire length of the spine to obtain $MTAS_i$.

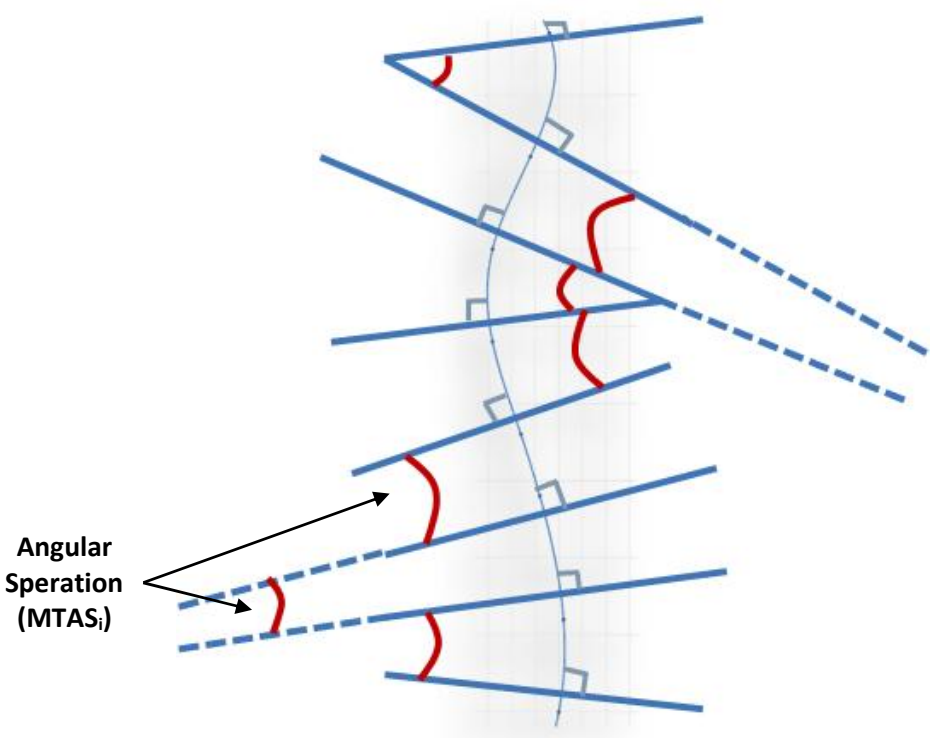

Figure 4.4 Modified MIVAS method applied on interpolated curve of an X-ray image

The formulation of the modified index of MIVAS is follows:

$$\text{MIVAS} = \sum_{i=1}^{n}(\text{angle between the } ith \text{ and } (i+1)th \text{ normal lines}) \quad (6)$$

For evaluating the feasibility of the MIVAS, the same data sample of 30 X-ray radiographic images are used to find the correlation between the Cobb angle

and the MIVAS, and the comparison shows a high correlation coefficient between the two indices.

4.2 Calculation Results of the Newly Proposed Spinal Deformity Indices

4.2.1 Calculation of the New-Proposed Index of IVAS

For the 30 scoliosis spinal data, the IVAS values obtained are 45.23°±19.19° and the Cobb angles obtained are 44.75°±19.34° (in μ±σ format).

Table 4.2 lists the measurements, in ascending order, on the 30 interpolated curves of the X-ray samples using the original IVAS index. The Cobb angles used were measured directly from the X-ray samples instead so as to provide a means of comparison of the feasibility with the IVAS index. Likewise, the larger the Cobb angle was used as the measured angle for 'S'-shaped curves as it represents greater severity of the scoliosis.

From Table 4.2, it can be seen that when the Cobb angle becomes larger, the IVAS index also becomes larger. A linear correlation exists between the Cobb angle and the IVAS index. The Cobb angle and the $IVAS_i$ values in Table 4.2 are plotted in an ascending order on the same axes, as shown in Figure 4.5. Although the absolute values of both methods are slightly different, as the Cobb angle increases, the $IVAS_i$ index also increases. This positive correlation is further analyzed using the linear regression algorithm based on the least square approach. By inputting the Cobb angles as 'y-axis' and the $IVAS_i$ values as 'x-axis', the computed correlation coefficient is $R^2 = 0.8619$ and $R = \sqrt{0.8619} = 0.9284$. Figure 4.10 shows the plot of the IVAS index against the Cobb angle. When the

Cobb angles are plotted against the IVAS*i* values, as shown in Figure 4.6, a gradient of 0.6537 of the linear trend-line further affirms the positive correlation.

Table 4.2 Measured Cobb angles and IVAS index using the same data sample

Sample Number	**Spinal Shape Type**	**Severity**	**The Cobb Angle (º)**	**IVAS (º)**
16	C	Mild	12.0	12.5
14	C		16.0	20
23	S		18.0	25
7	C		18.5	18
12	C	Moderate	23.0	22
8	C		27.0	25
5	C		30.0	33
3	S		34.0	25.5
4	C		35.0	21.5
21	C		35.0	40
30	S		37.0	43
17	C		38.0	34
9	C		39.0	35
15	C		42.0	60
20	S		42.5	48
1	S		45.0	51
25	C		47.0	59.5
13	S		48.0	46
19	C		49.0	51
10	C		51.0	48
18	S		53.5	59
22	C		54.5	53
28	C		54.5	53.5
2	S		55.5	50
6	C		56.0	52
27	C		60.5	63
29	C		62.0	58.5
24	C	Severe	79.5	85
26	C		84.0	90.5
11	C		95.5	74.5

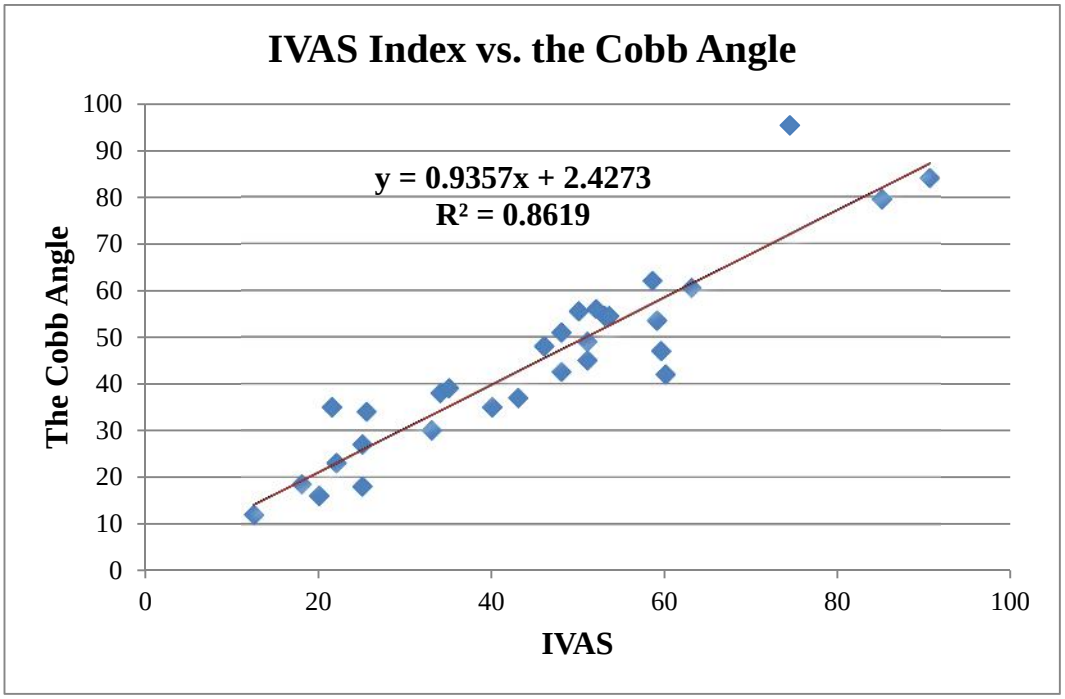

Figure 4.5 Plot of the IVAS index against the Cobb angle with R^2=0.8619

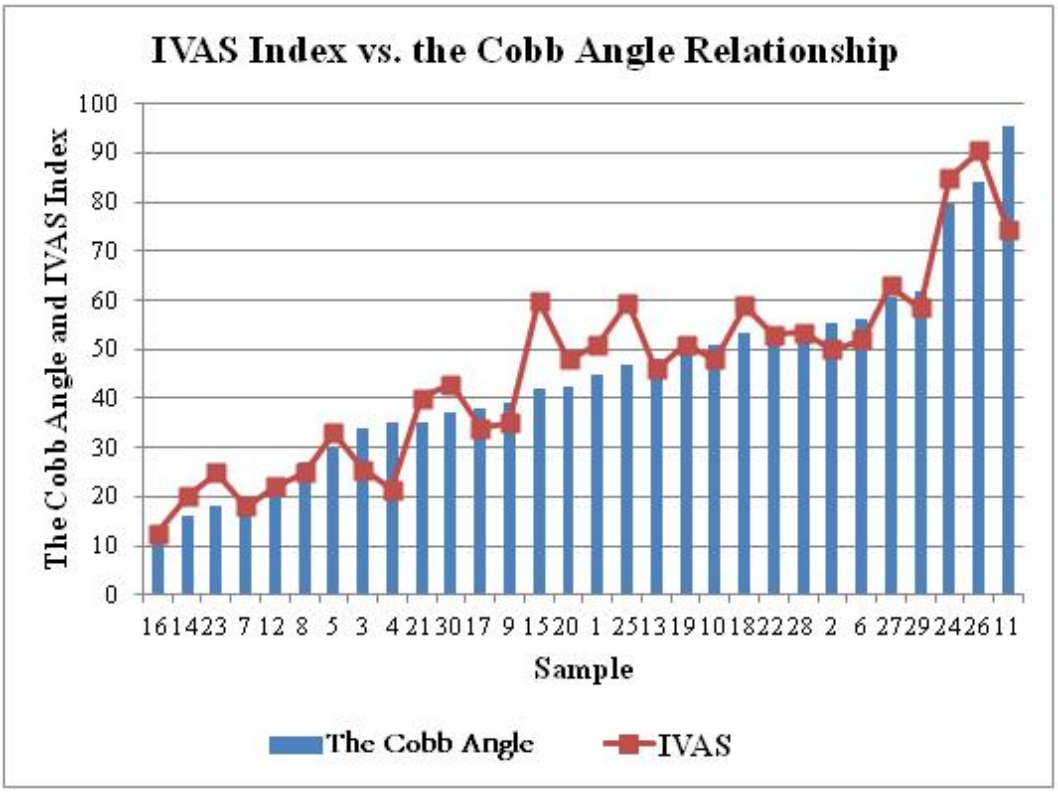

Figure 4.6 Bar chart of the IVAS index against the Cobb Angle

The high positive correlation between the Cobb angle and the IVAS index method is highlighted in Figure 4.6 with the regression equation of $y = 0.9357x + 2.4273$, where the line graph representing IVAS increases in tandem with the bar chart representing the Cobb angle measured. The computed correlation coefficient of 0.9284 is very close to the value of 1, thus implying a strong positive correlation between these two indices. This shows that the proposed index of IVAS has potentially high usefulness and feasibility.

4.2.2 Calculation of the Modified Newly Proposed Index of MIVAS

The same data sample of 30 X-ray images of the scoliosis spine are used in the calculation of the modified index of MIVAS. The calculation shows the MIVAS value of 117.69°±45.09° and the Cobb angle of 44.75°±19.34° (also in $\mu \pm \sigma$ format).

Table 4.3 shows the results, in ascending order, for the 30 interpolated curves of the X-ray samples using the modified index of MIVAS. The Cobb angles are measured directly from the X-ray samples, and the larger Cobb angle is taken to be the angle for 'S'-shape curves as it represents greater severity of the scoliosis. The MIVAS index is calculated using the feature point interpolation algorithm and the results are shown in Table 4.3.

Table 4.3 shows that the MIVAS index is quite different from the original IVAS. The MIVAS index is usually nearly three times as large as IVAS index. When the value of the Cobb angle increases, the MIVAS index increases.

Table 4.3 The Cobb angles and MIVAS index based on same data sample

Sample Number	Spinal Shape Type	Severity	Cobb Angle (º)	MIVAS (º)
16	C	Mild	12.0	29.31
14	C		16.0	70.75
23	S		18.0	66.8
7	C		18.5	52.55
12	C	Moderate	23.0	74.01
8	C		27.0	91.57
5	C		30.0	83.37
3	S		34.0	99.67
4	C		35.0	110
21	C		35.0	91.81
30	S		37.0	119.93
17	C		38.0	81.55
9	C		39.0	104.52
15	C		42.0	133.66
20	S		42.5	116.59
1	S		45.0	148.51
25	C		47.0	116.49
13	S		48.0	117.01
19	C		49.0	108.13
10	C		51.0	121.96
18	S		53.5	120.46
22	C		54.5	148.91
28	C		54.5	111.9
2	S		55.5	111.2
6	C		56.0	168.98
27	C		60.5	167.95
29	C		62.0	118.19
24	C	Severe	79.5	180.24
26	C		84.0	239.28
11	C		95.5	225.39

Similar to the correlation between the Cobb angle and the IVAS index, there is a linear correlation between the Cobb angle and the MIVAS index. The Cobb angle and the $MIVAS_i$ values in Table 4.3 are plotted in an ascending order on the same axes, as shown in Figure 4.7. The value of the $MIVAS_i$ is much larger than the Cobb angle and the original $IVAS_i$ index value. It can be seen that the absolute

values of both methods are quite distinct, and as the measured Cobb angle increases, the $MIVAS_i$ measured also increases. Similarly, the linear regression algorithm was applied and analyzed in the comparison of the MIVAS index and the Cobb angle and a positive correlation was found. The MIVAS is set as the 'x' value and the Cobb angle index as the 'y' value in Figure 4.7. The computed correlation coefficient between MIVAS and the Cobb angle is $R^2 = 0.8418$ and $R = \sqrt{0.8418} = 0.9175$. Figure 4.7 shows the scatter plot of the MIVAS index against the Cobb angle.

When the Cobb angle values are plotted against the $MIVAS_i$ values, as shown in Figure 4.8, a gradient of 0.3935 of the linear-trend line further affirms the positive correlation.

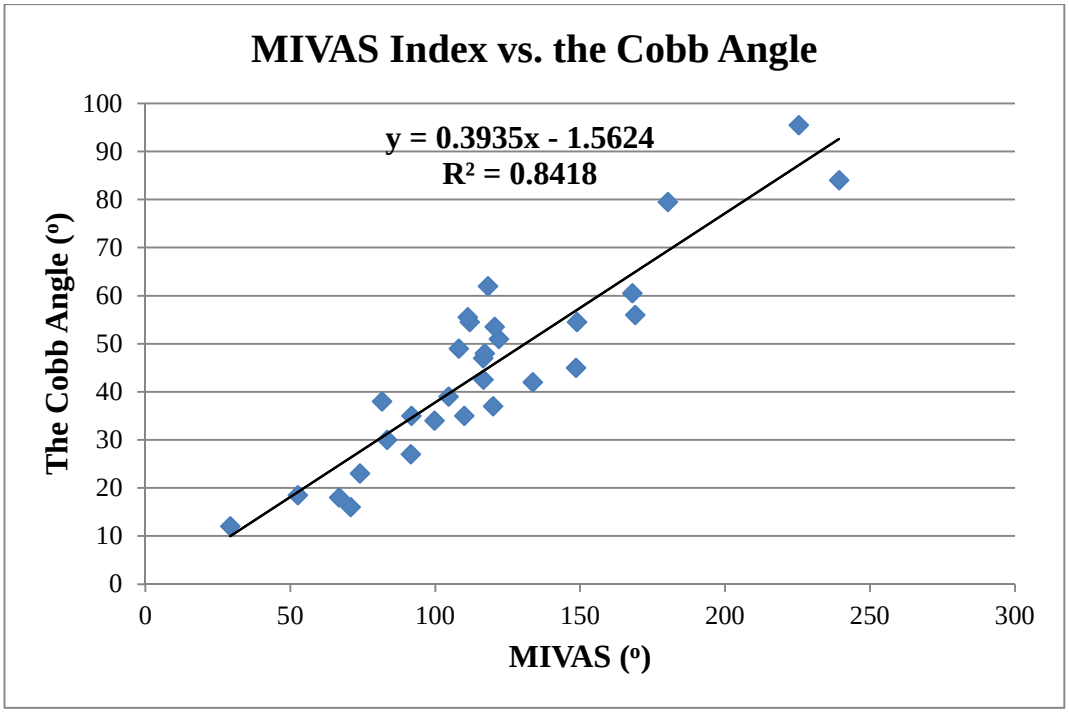

Figure 4.7 Plot of the MIVAS index against Cobb angle with R^2=0.8418

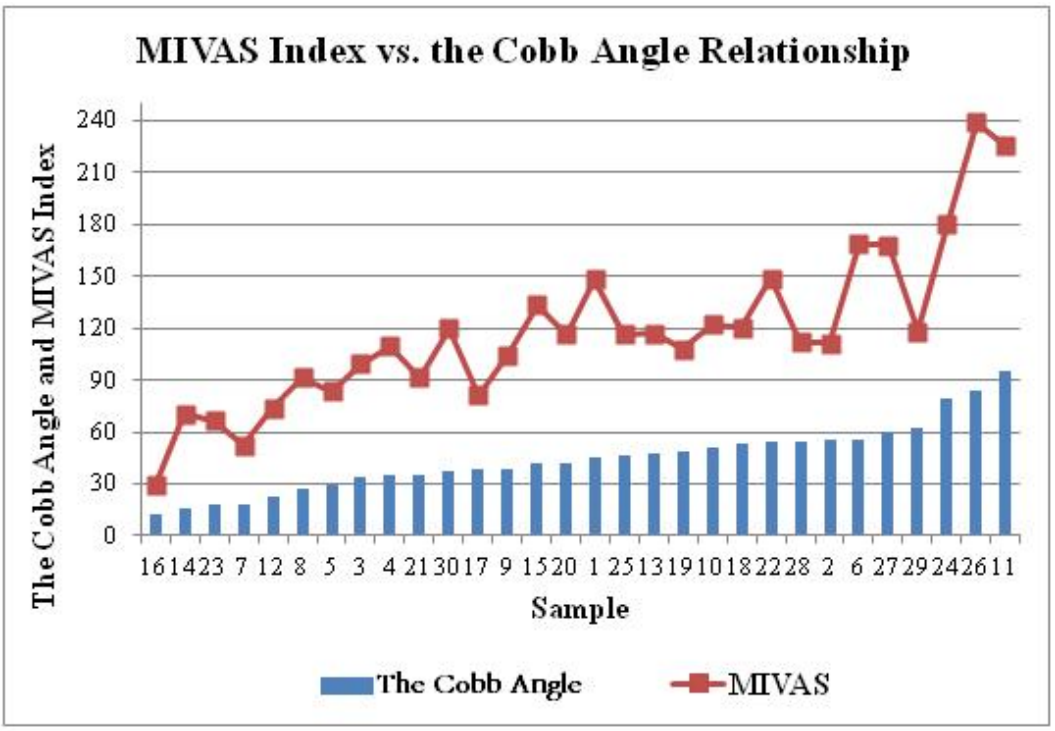

Figure 4.8 Bar chart of the MIVAS index against the Cobb angle

The positive correlation between the Cobb angle and the MIVAS index method is quite high (>0.9) which is shown in Figure 4.8 with the regression equation of $y = 0.3935x-1.5624$, where the line graph representing MIVAS increases in tandem with the bar chart representing the measured Cobb angle. The new correlation coefficient for MIVAS against the Cobb angle of 0.9175 is quite close to 1, i.e., there is a strong positive correlation between these two indices. This suggests the modified index of MIVAS is potentially useful.

4.3 Calculation of 3DIVAS Index for Measuring Spinal Deformity

4.3.1 3D Inter-vertebra Angular Separation Index (3DIVAS Index)

The 3DIVAS is designed based on the IVAS index and MIVAS index.

As a predictor for the risk of sustaining incident vertebral deformity, the spinal deformity index is a convenient tool to quantify the number and the severity of prevalent vertebral fractures. However, most of the indices are calculated or estimated based upon X-ray images, such as Cobb's angle, IVAS or MIVAS. Since this quantification must be taken into account to improve management of patients, the regular actions of taking X-ray images may potentially bring harmful to the patients.

This 3DIVAS is designed as a three-dimensional and radiation-free parameter to assess the severity of spinal deformity. The basic idea of calculating 3DIVAS is similar to the idea of calculating IVAS and MIVAS, which is based on inter-vertebra angular separation. Comparing to the two-dimensional indices of IVAS and MIAVS, 3DIVAS is a three-dimensional index.

The steps of calculating the 3DIVAS are:

1. Pre-processing and preparation. The patients need to expose bare back to the nurse or orthopedist and necessary equipment, such as reflective markers, camera system, computers etc., need to be set up and calibrated.
2. Vertebra center-point estimation. Using the markers to highlight the spinal vertebras centerline. Attaching the reflective markers onto the prominent points of the spine.
3. Obtaining the coordinates of the vertebra points (marker points) using the camera system.
4. Spinal centerline extraction. Using Interpolan (Cubic) curve fitting algorithm (general equation: $f(x) = piecewise\ polynomial$), the vertebra points are interpolated into 3D curve.

5. Through each vertebra point, the plane which is perpendicular to the curve is generated. The angular separation between the adjacent pair of planes are calculated and summed up.
6. The 3DIVAS is calculated as:

$$\text{3DIVAS} = \sum_{i=1}^{n} (\text{angle between the } ith \text{ and } (i+1)th \text{ normal planes})$$

Figure 4.9 shows an overview of the proposed method for measuring the three-dimensional and radiation-free index of 3DIVAS.

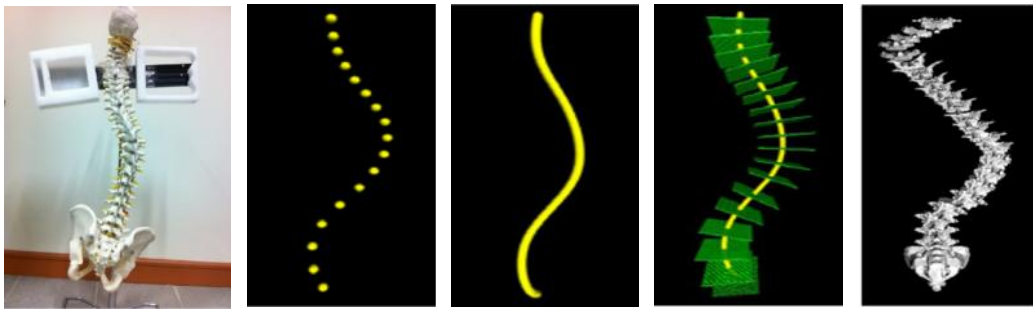

(1) (2) (3) (4) (5)

Figure 4.9 an overview of the proposed method to calculate the index of 3DIVAS. (1) Pre-processing, preparation and an example of attaching the markers onto the patient's back; (2) Vertebra centre-point estimation; (3) Spinal centerline extraction using the coordinates of the markers; (4) 3D Inter-vertebra angular separation measurement; (5) a visual sketch of the shape based on the 3DIVAS

In order to estimate the feasibility and reliability, the previous data set is used. The data set includes totally 30 spinal data samples in which there is 22 samples from C-shape scoliotic spines and 8 samples from S-shape scoliotic patients.

In the data set, the coordinates of the vertebras are calculated based on the profile paper and thus are 2D coordinates. Lacking of the 3D data sets for the experiment and calculation, a column of z-axis coordinates are arbitrarily added to the 2D data and transform it into 3D data. In the thoracic part of the spinal data sample, a positive number of the z-axis value is added to data set. And in the lumbar part of the spinal data sample, positive or negative number of z-axis value is added to the data set.

4.3.2 Calculation Results of the Newly Proposed 3D Spinal Deformity Indices

Similar to the calculation of IVAS and MIVAS, for the 30 scoliosis spinal data, the 3DIVAS values obtained are $128.59° \pm 43.72°$, while the Cobb angle of $44.74° \pm 19.34°$ (in $\mu \pm \sigma$ format) which is the same as in IVAS and MIVAS calculation. Table 4.4 shows the calculation results, in descending order, for the 30 interpolated 3D curves of the samples using the three-dimensional 3DIVAS. The Cobb angles are measured directly from the data set and the Cobb angles become larger as the severity of the scoliosis become greater.

From the table 4.4, it shows that 3DIVAS is different from the IVAS index and similar to the MIVAS index. The 3DIVAS is usually several times more than IVAS and similar to MIVAS.

Table 4.4 Measured Cobb angles and 3DIVAS index using the same data sample

Sample Number	**Spinal Shape Type**	**Severity**	**Cobb Angle (º)**	**3DMIVAS (º)**

16	C	Mild	12.0	43.006
14	C		16.0	88.964
23	S		18.0	89.974
7	C		18.5	79.530
12	C	Moderate	23.0	89.363
8	C		27.0	109.095
5	C		30.0	98.8418
3	S		34.0	123.250
4	C		35.0	137.420
21	C		35.0	117.240
30	S		37.0	142.088
17	C		38.0	99.991
9	C		39.0	127.483
15	C		42.0	180.660
20	S		42.5	139.705
1	S		45.0	157.694
25	C		47.0	139.843
13	S		48.0	155.260
19	C		49.0	129.723
10	C		51.0	146.079
18	S		53.5	164.842
22	C		54.5	178.521
28	C		54.5	154.598
2	S		55.5	133.431
6	C		56.0	191.975
27	C		60.5	200.798
29	C		62.0	221.671
24	C	Severe	79.5	195.578
26	C		84.0	284.415
11	C		95.5	238.143

Similar to the IVAS and MIVAS, the 3DIVAS index is compared to the Cobb angle and there is a linear correlation between the Cobb angle and the 3DIVAS index. As shown in Figure4.10, the values of the Cobb angle and the 3DINVAS index in Table 4.4 are plotted according to an ascending order on the same axes. From the figure, it can be seen that, for the same subject, as the measured Cobb angle increases, the calculated 3DIVAS also increases.

Using the calculated results, the linear regression algorithm was applied and analyzed in the comparison of the Cobb angle and 3DIVAS index in which a positive correlation was discovered. The 3DIVAS index is set as the 'x' value and the Cobb angle index is set as the 'y' value in Figure 4.10. The computed correlation coefficient between the 3DIVAS index and the Cobb angle is $R^2 = 0.8311$ and $R = \sqrt{0.8311} = 0.9116$. Figure 4.10 depicts the scatter plot of the 3DIVAS index and the Cobb angle.

When the 3DIVAS index values are plotted against the Cobb angle values, as shown in figure 4.11, a gradient of 000000 of the linear-trend line further proves the positive correlation.

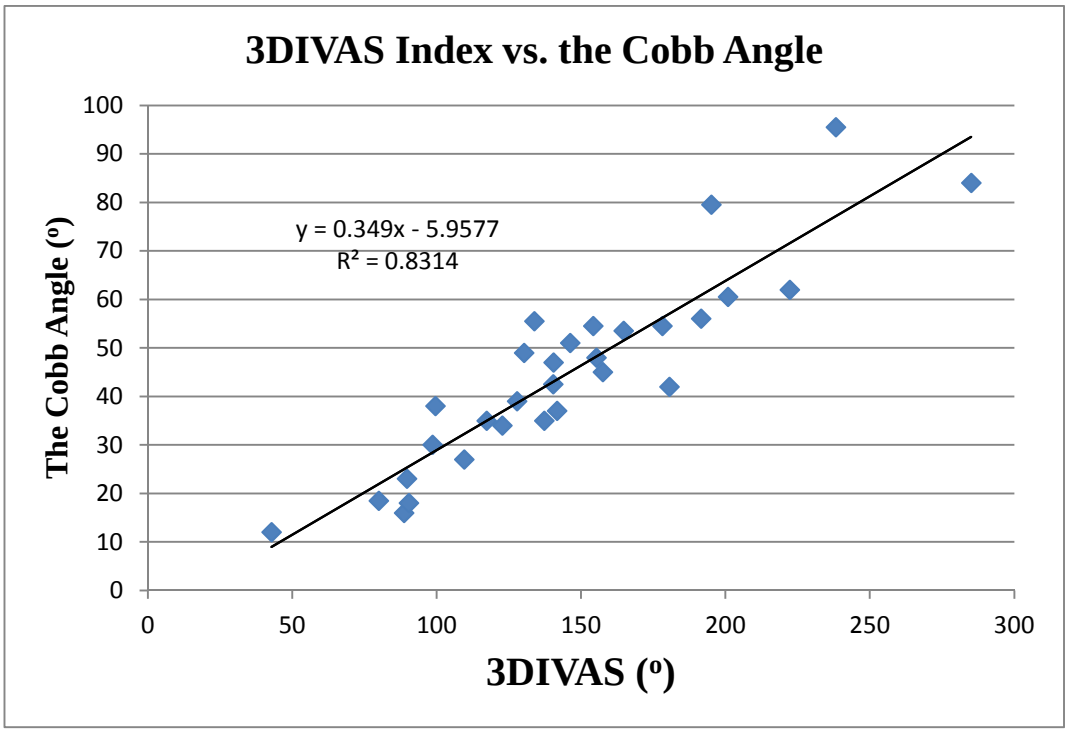

Figure 4.10 Plot of the 3DIVAS index against Cobb angle with R^2=0.8331

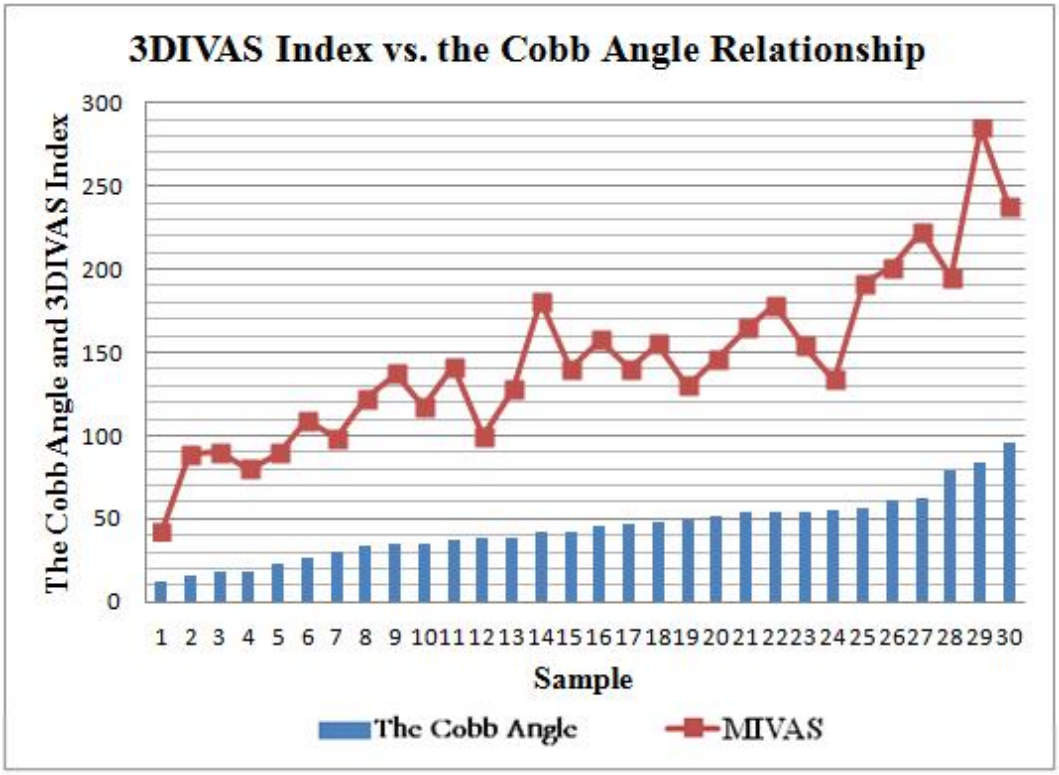

Figure 4.11 Bar chart of the 3DIVAS index against the Cobb angle

The positive correlation between the Cobb angle and the 3DIVAS index is high R=0.9116 (>0.9) shown in Figure 4.10, but is lower than MIVAS (R=0.9175). The regression equation is shown in Figure 4.10 of $y = 0.349x - 5.9577$, where the line graph representing the calculated 3DIVAS index increases in tandem with the bar chart representing the measured Cobb angles. As the coefficient is high with R=0.9116, it is supported that the 3D index of 3DIVAS is potentially feasible.

The benefits of using the 3DIVAS index are that this index is a radiation-free parameter that can avoid the harmful exposure to the X-rays and this index is calculated based on the 3D information of the scoliotic spinal curvature.

4.4 Conclusion about the New-Proposed Spinal Deformity Indices

The main factors that have been considered as the foundation for quantifying and assessing the scoliosis deformity are the severity of left-to-right asymmetry and the degree of spinal rotation. On the other hand, the degree of left-to-right unbalance and asymmetry is also quite critical for scoliosis evaluation. This research has proposed three new indices based on the angular separation between the pair of adjacent vertebra, which is potentially useful for the subject's body and spinal deformity evaluation in the coronal plane.

The IVAS, MIVAS and 3DIVAS are calculated and compared with Cobb angle. The calculation of the IVAS index and MIVAS need to be derived from the subject's X-ray images which are 2D images. And the 3DIVAS is designed based on the 3D information of the spinal curvature and a radiation-free index. They are used as complementary methods supporting the Cobb angle.

A comparison between the Cobb angle and IVAS, the Cobb angle and MIVAS and the Cobb angle and 3DIVAS has been conducted in this thesis. The correlation coefficient between IVAS and the Cobb angle is 0.9284, the correlation coefficient between MIVAS and the Cobb angle is 0.9175 and the correlation coefficient between 3DIVAS and the Cobb angle is 0.9116. The high correlation found between the clinical variable (Cobb angle) and topographic variables (IVAS, MIVAS and 3DIVAS) shows that although they use different calculation methods for different deformities, variations in the spinal column appear as variations of the topographic pattern. In this thesis, it has been shown that the newly proposed indices of IVAS, MIVAS and 3DIVAS have the potential to be used as tools for supporting the traditional scoliosis measurement methods.

Furthermore, a computer program has been developed using MatLab programming that can automatically determine the new indices (IVAS and MIVAS), and this simplifies the process of calculating these two indices.

In the future research, more data sets such as X-ray images, CT scan images or data from 3D camera system could be included in the calculation of the new-proposed indices for more experiments and tests.

4.5 Discussion of the New-Proposed Spinal Deformity Indices

While the positive gradient of the linear-trend line plotted in Figure 4.12 underlines linear proportionality between the two methods, its value of 0.3935 (i.e., large deviation from the value 1) implies that the magnitudes of the measured Cobb angles are on average, 0.3935 times the magnitude of the MIVAS.

Nevertheless, the relationship between the IVAS and the Cobb angle, between MIVAS and the Cobb angle and between 3DIVAS and the Cobb angle do not affect the feasibility of IVAS, MIVAS and 3DIVAS, since in comparing the indices, the value of importance is the correlation coefficient instead of the absolute measured angles. The proposed evaluation indices would only need to assist in evaluating the severity of the scoliotic spine by suggesting the same severity as in the measured Cobb angle. Therefore, in this case, it can be proposed that the absolute value of IVAS and MIVAS will be significantly larger than the Cobb angle for the same severity of scoliosis.

For next step, more data sample of scoliosis spine images will be used to determine the feasibility of the IVAS, MIVAS and 3DIVAS indices.

Chapter 5 Measurements with a Physical Spinal Model and Preliminary Experiment Results and Spinal Model Construction

5.1 Physical Spinal Model Preparation for the Imaging Process

In this preliminary experiment, a physical spinal model was used for a preliminary experiment. . The camera placement, capturing area and participant's direction is shown in Figure 5.1.

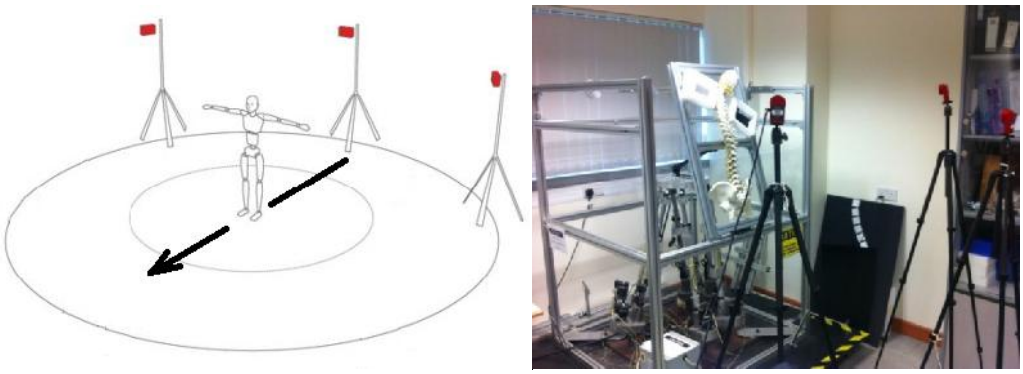

Figure 5.1 Camera placement, capturing area and participant's bending direction (depicted with dotted line)

During the measurement, the spinal model is labeled with round reflective markers as shown in Figure 5.2. These markers are attached at several prominent positions of the back corresponding to the locations of the vertebras according to the following anthropometric points: superior spinous processes of T1, T3, T6, T9, L1, L3 and L5 and both posterior superior iliac spines (PSIS) (T=thoracic and L=lumbar).

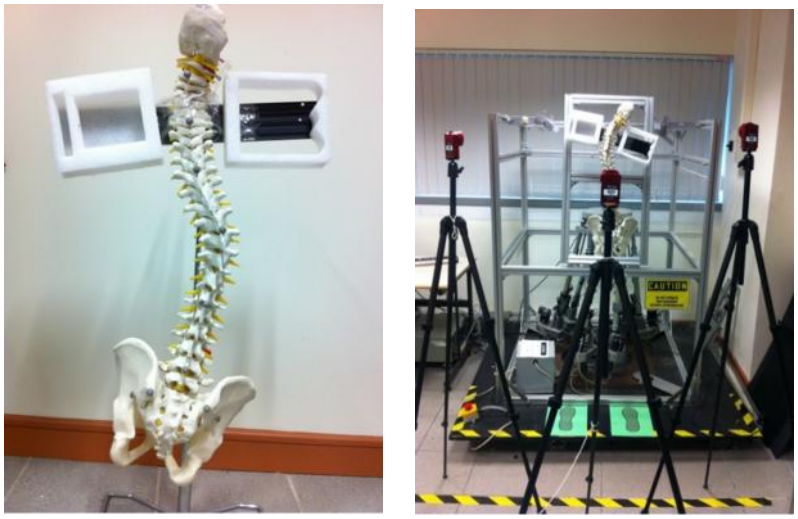

Figure 5.2 Mechanical frame and anthropometric marking position on the physical spinal model

The markers which are coated with retro-reflective material (3M#7610) are placed using hypoallergenic tape that reflect incident light directly back to the infrared cameras (IR). In this system, three IR cameras are used for data capture. The optical motion capturing system is selected for the main advantages of high update rates, low latency and scalable to fairly large areas (Medved 2002). The surrounding environment is designed carefully to reduce ambient noise e.g., brighter lights and exclusion of shiny background objects.

As reported, the average error of the OptiTrack optical motion capture cameras is less than 0.4 mm (Bethke et al. 2008) while the resolution of the OptiTrack camera is 640×480 and the lens HFOV is 45~60°.

A stationary laboratory coordinate system is defined by a vertically oriented Z-axis, an X-axis placed forward in the participant's facing direction, and a Y-axis perpendicular to the first two and pointing the direction according to the right-handed coordinates rules. The image capturing volume is set to be 2.50m, 2.50m

and 2.20m. For higher precision in marker capturing, a spinal skeleton model is used first and the tracking rate is of 100 FPS (frame per seconds) for the V100:R2 cameras used in the presented study.

5. 2 Calibration of the 3D Camera System

The SP and the imaging system are assembled using modular aluminum sections, universal joints and linkages. Three cameras are set up two meters away from the apparatus in a triangular layout.

Before the measurement process was conducted, the calibration stage and camera parameter setting was performed. In the view of the cameras, the virtual camera was aligned in a line and the objects cannot be detected. The OptiWand kit (with Calibration Square) and the self-calibration function in the software were used for the system calibration. The OptiWand kit is an improved three-reflective-marker camera calibration tool. Figure 5.3 (a) shows the three-marker calibration tool kit used in the system and Figure 5.3 (b) shows the calibration square used in the calibration process.

After placing and swinging the OptiWand kit in the overlapping view of the three cameras, the tool was made to move back and forth for several times. The three 3D cameras can track the trajectories of the OptiWand to identify the real position of the cameras. The camera can recognize the position and orientation of the markers on the OptiWand. Figure 5.4 shows the process of the calibration in the camera control program. In the picture, the pink, green and red lines were the trajectory of the OptiWand kit captured by the three cameras.

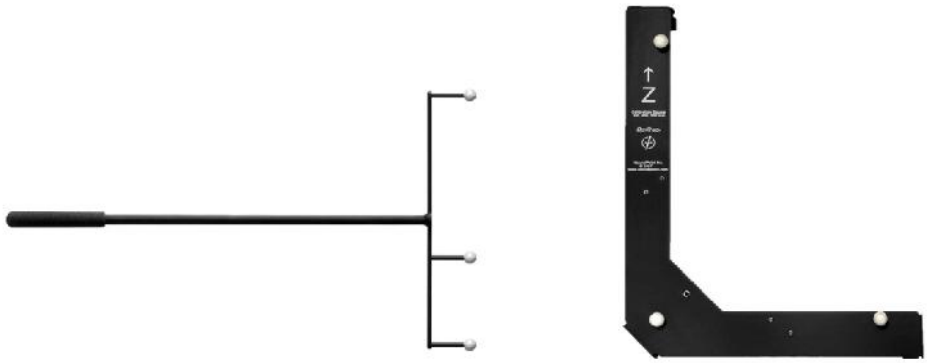

(a) (b)

Figure 5.3 (a) The three-marker OptiWand kit calibration tool; (b) the calibration square with three 5/8” hard markers

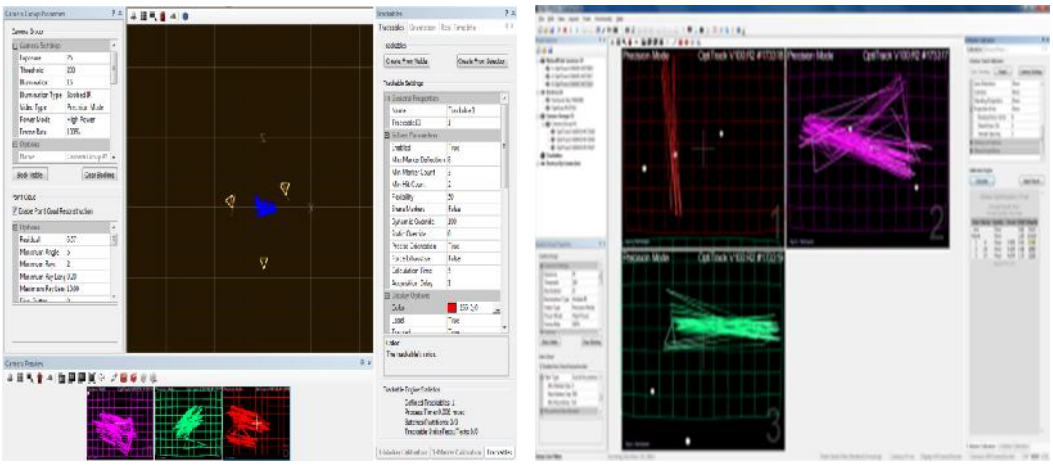

(a) (b)

Figure 5.4 (a) The calibration process in top view; (b) the calibration from the individual cameras.

Figure 5.5 is the setting and mode of the parameters in the calibration process. The “**Calibration Accuracy”** is to set the complexity of the calibration solver calculations, in which lower complexity will result in a lower quality calibration, but a significantly faster solution. Valid options are Low (Default),

Medium, High, Very High. The "**Wanding Time"** is used to select the amount of time in seconds allotted for wanding and 10 seconds is used here. The "**Approximate Volume"** selects the size of the captured volume that is being wanded. This option does not restrict the volume size, but is used to constrain the solver, and should be set as close to the real volume size as possible. The valid options are: 1 Cubic Meter, 3 Cubic Meters (default) and 6 Cubic Meters. 3 cubic meters mode is selected here. The "**Min Camera Coverage"** is designed to select the minimum number of cameras that must "see" a marker for it to be considered valid to take a sample. The valid range is set to be 3 to the number of cameras being calibrating in this study. The "**Selection**" option means how samples are selected from the wanding data. The "**Camera Group**" selects the camera group to be calibrated. The valid options are all currently assigned camera groups.

Calibration Options	
Calibration Accuracy	Low (Fast)
Wanding Time (Secon	10
Approximate Volume	3 Cubic Meters
Min Camera Coverage	3
Selection	Distributed
Camera Group	Camera Group #1

Figure 5.5 The setting of the parameters and mode in the calibration process

However, the images become more distorted as experiment continues as shown in Figure 5.6. As shown, the large circle spots with white color are the noisy data from the environment. The positions of the markers also become inaccurate. Until more calibration data are included, the calibration process is completed and

the cameras can identify the position of the markers to form a line using the three markers.

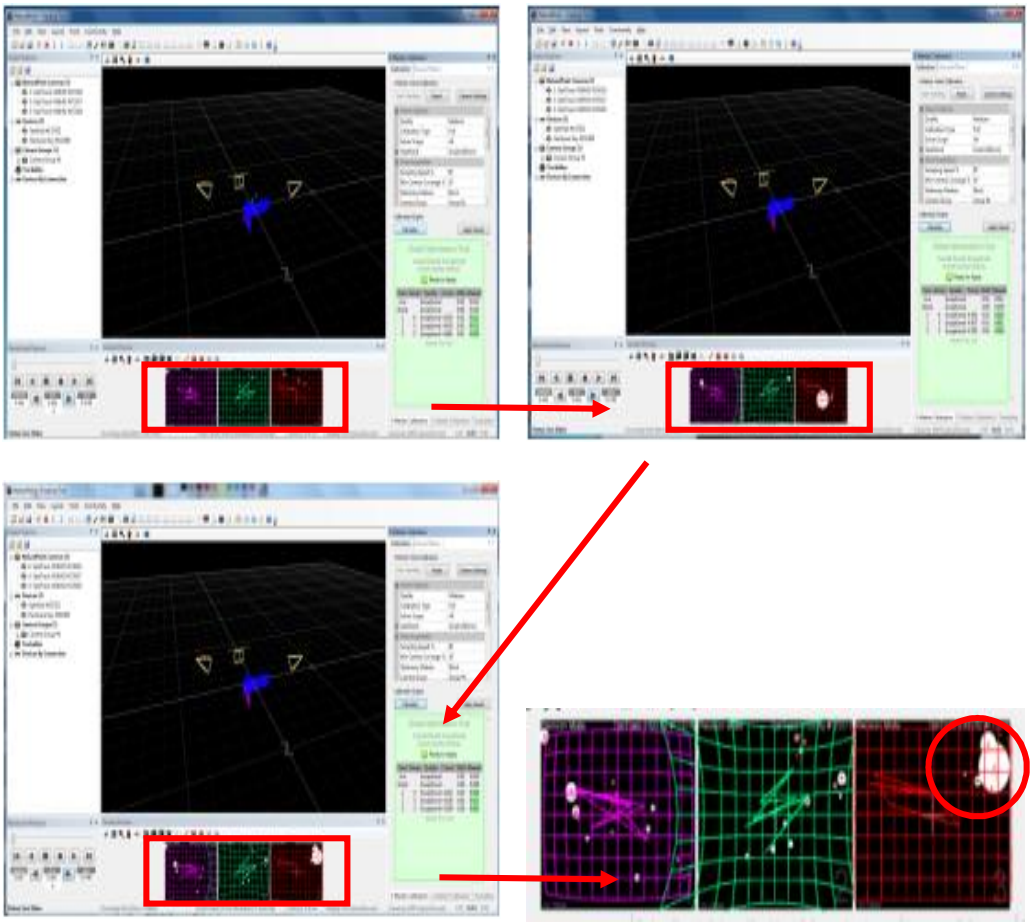

Figure 5.6 The calibration process when noisy data is present from the environment

If there are shining articles or noise points in the field of view (like the white circle spot), the calibration results will be also affected. The quality of image needs to be improved in order to track the trajectory of the markers and the coordinates of the feature points better. When the feature points and markers move in the field of the camera's view, the coordinates of the markers can also be extracted.

During wanding, the wand is moved slowly across the entire captured volume, covering as much space as possible for sufficient sampling. In order to obtain better results, the volume is wanded evenly and comprehensively throughout the space. Figure 5.7 (a) shows an example of proper wanding for a large motion capture volume. The volume may differ depending on camera setup and aiming in each session of the experiments. After wanding has been completed, examine the calibration panel for feedback on the number of samples collected. The window will show a “sufficiency rating” which defines whether sufficient samples have been recorded to meet the minimum requirements for low, medium, high, or very high quality. The rating only takes into account minimum samples, so a higher sample quantity should be used for larger volumes. In this three-camera system, the cameras are calibrated properly with an average of more than 1000 samples for each camera. In the calibration process, the number of sample data captured by each camera is 1696 for Camera 1, 1437 for Camera 2 and 1856 for Camera 3 which is shown in Figure 5.7 (b).

After the calibration process, the system can adjust the virtual camera positions according to the real camera positions by tracking the position of the markers. The view of the direction and orientation can also be changed to top view, side view, etc. The trajectory and position of the markers can be detected by the system accurately. Also, the mean error and standard deviation of the error of each camera are given by the system.

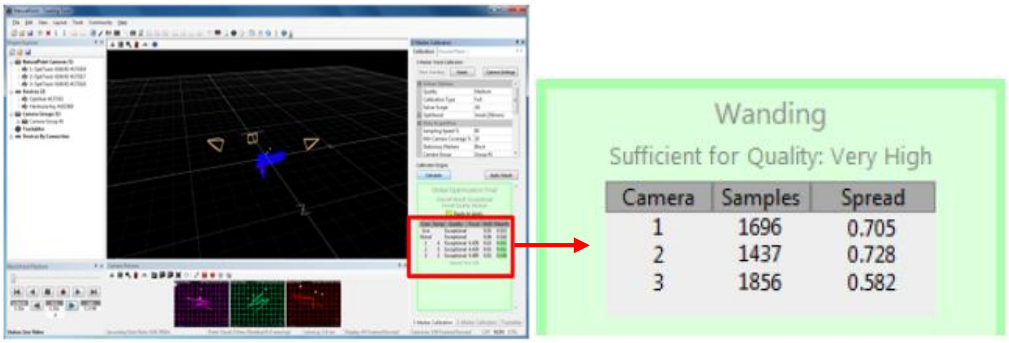

(a) (b)

Figure 5.7 (a) The wanding process using the OptiWand kit for calibration of the three cameras; (b) the number of data sample captured by each camera

5.3 Test of Proof of Concept

The OptiTrack camera system were designed to obtain the three dimensional location of markers within a measurement volume. A preliminary experiment is designed to test the accuracy of the system before it is applied to real subject. Figure 5.8 depicts the test wedge used in the experiment to determine accuracy of the system using the method of reconstruction distance between marker centers. Eleven 7/16" (11.11mm) diameter markers on bases are placed onto the hypotenuse face of the sample and the relative positions measured within the tolerances of the caliper. And figure 5.9 shows the sketch used in the preliminary test and table 5.1 lists the relative actual distances between the centers of the markers. Above the wedge, the markers are ensuring to tightly attach together to the wedge and the markers have 3mm drilled hole. Thus, the physical height of the maker centers above the surface of the test wedge is estimated of half of the diameter, which is 5.55mm.

Figure 5.8 the round markers and the test wedge

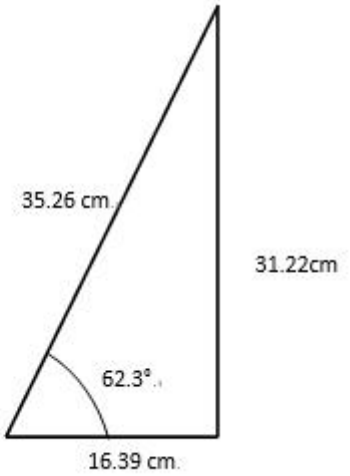

Figure 5.9 the dimensions of the wedge

Figure 5.10 shows the position and numbering of the markers, from marker 1 (M1) to marker 11 (M11), which are applied on the hypotenuse surface of the wedge.

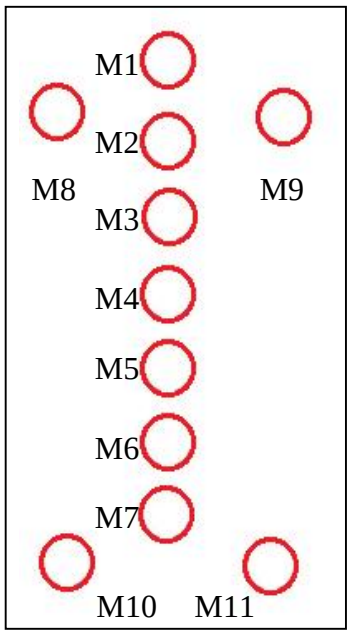

Figure 5.10 the sketch of the position and numbering of the markers

Table 5.1 The distance between the markers on the wedge

Marker Identification	Distances between the markers (mm)
M1-M2	50.24
M2-M3	50.77
M3-M4	49.68
M4-M5	50.27
M5-M6	49.97
M6-M7	50.33
M1-M8	71.10
M1-M9	70.83
M2-M8	68.67
M2-M9	68.54
M7-M10	62.30
M7-M11	62.24
M10-M11	84.04

Table 5.2 shows the actual diameters of the markers and the heights above the surface of the wedge.

Table 5.2 the marker Diameter and center heights

Marker Label	Marker Diameter (mm)	Marker Heights (including fixing tape) (mm)
M1	11.1125	11.44
M2	11.1125	11.76
M3	11.1125	11.31
M4	11.1125	11.40

M5	11.1125	11.24
M6	11.1125	11.25
M7	11.1125	11.67
M8	11.1125	11.83
M9	11.1125	11.59
M10	11.1125	11.37
M11	11.1125	11.29
Mean	11.1125	11.47
Standard Deviation	0	0.2105

Optitrack system assumes that the calculation of coordinates of the markers is based on the capture of spherical objects. Following routine calibration, the cameras capture serial images, sequential images every 20 seconds of the test object with the hypotenuse surface which is normal to the cameras. Calculations are then made. Table 5.3 shows the actual distances between the markers and measured distances between the markers which is captured by the cameras.

Table 5.3 Actual and measured distances (by cameras) between the markers

Marker Label	Actual Distances (mm)	Measured Distance (mm)	Difference of Actual and Measured Data (mm)
M1-M2	50.24	50.43	-0.19
M2-M3	50.77	50.32	0.45
M3-M4	49.68	49.87	-0.19
M4-M5	50.27	49.70	0.57
M5-M6	49.97	50.26	-0.29
M6-M7	50.33	49.60	0.73

M1-M8	71.10	70.69	0.41
M1-M9	70.83	70.33	0.5
M2-M8	68.67	68.29	0.38
M2-M9	68.54	69.03	-0.49
M7-M10	62.30	62.74	-0.44
M7-M11	62.24	61.83	0.41
M10-M11	84.04	84.30	-0.26
		Mean Error	0.122
		Standard Deviation	0.433

From the experience of body measurements using optical motion capture systems, it is considered clinically acceptable if the accuracy of marker reconstruction is less than 1mm. This tolerance is considered that it influents the accuracy less than the magnitude of palpation and the skin sway and movement (Robert S. Wainner, et al. 2003).

5.4 Imaging Process with the Physical Spinal Model

During the process of imaging, the physical spinal model is located in front of the moveable plate of the apparatus as close as possible to the frame to establish the necessary reference. Figure 5.11 shows the custom-built aluminum apparatus and the position of the spinal model during the process of measurement.

The spinal model is located upright at the beginning and is made to lean onto the moveable plate frame, as shown in Figure 5.12.

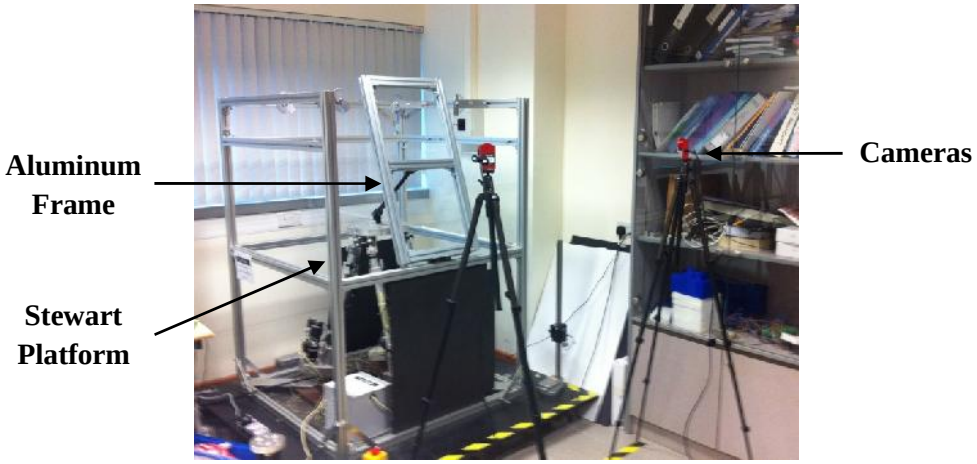

Figure 5.11 The setup of the custom-built aluminum spinal deformity measurement apparatus

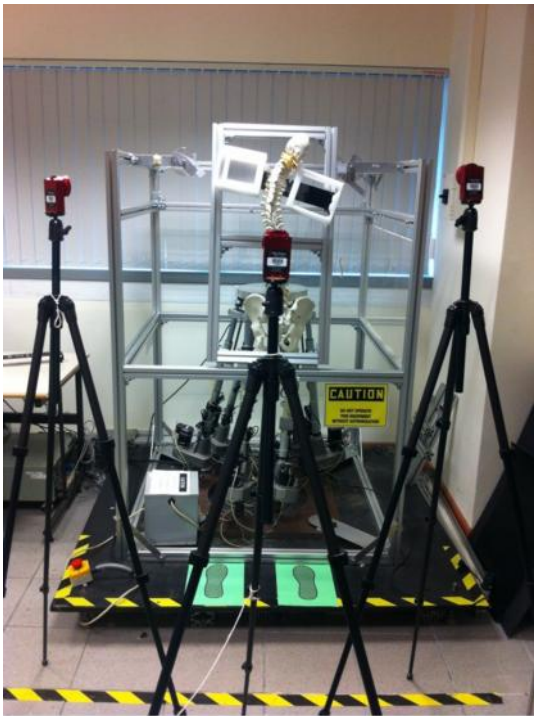

Figure 5.12 The position of the spinal model in the process of spinal deformity measurement and assessment

The six leg lengths of the SP are controlled using a MatLab program to achieve the horizontal movement of the SP. The custom-built moveable plate can

bend from 0 degree to 90 degrees. Figure 5.13 shows the schematic movement of the apparatus to make the model bend in a series of angles.

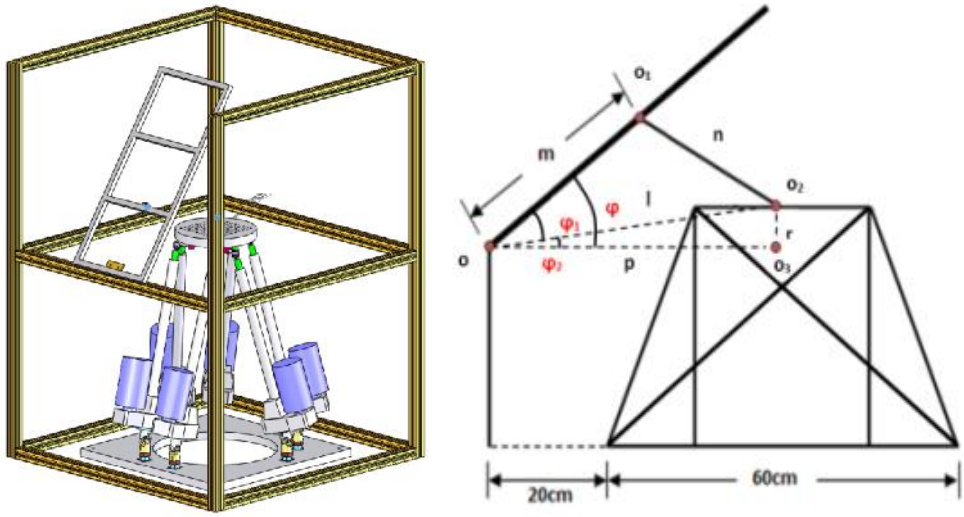

Figure 5.13 A schematic relationship of the mechanical apparatus

The objective is to find the value of parameter p and the six leg lengths to make φ equals to 0˚, 30˚, 45˚, 60˚ and 90˚. From the geometrical relationship, it is known that

$$\varphi = \varphi_1 + \varphi_2$$

In $\Delta o o_1 o_2$, $n^2 = m^2 + l^2 - 2m \cdot l \cdot \cos\varphi_1$

$$\Longrightarrow \varphi_1 = \cos^{-1}\frac{m^2 + l^2 - n^2}{2m \cdot l}$$

In $\Delta o o_2 o_3$, $\tan\varphi_2 = \frac{r}{p}$

$$\Longrightarrow \varphi_2 = \tan^{-1}\frac{r}{p}$$

In $\Delta o o_2 o_3$, $l^2 = r^2 + p^2$

In sum, $\varphi_1 = \cos^{-1}\frac{m^2 + l^2 - n^2}{2m \cdot l} = \cos^{-1}\frac{m^2 + r^2 + p^2 - n^2}{2m \cdot \sqrt{r^2 + p^2}}$

$$\varphi_2 = \tan^{-1}\frac{r}{p}$$

$$\varphi = \varphi_1 + \varphi_2 = \cos^{-1}\frac{m^2+r^2+p^2-n^2}{2\cdot\sqrt{r^2+p^2}} + \tan^{-1}\frac{r}{p}$$

In the design of the SP,

$m = 45\text{cm}$; $n = 40\text{cm}$; and $r = 20\text{cm}$;

$$\varphi = \varphi_1 + \varphi_2 = \cos^{-1}\frac{2025 + 400 + p^2 - 1600}{90\cdot\sqrt{400+p^2}} + \tan^{-1}\frac{r}{p}$$

$$= \cos^{-1}\frac{825 + p^2}{90\cdot\sqrt{400+p^2}} + \tan^{-1}\frac{20}{p}$$

Thus, the relationship between the value of ϕ and p can be obtained. By knowing the bending angle and the p value, the relationship between the six leg lengths of the SP and the bending angle of the frame is calculated using inverse kinematics, which is shown in Table 5.4.

By manipulating the SP, the model is controlled to bend into 0˚, 30˚, 45˚, 60˚ and 90˚ and to exhibit the model to the camera. For each bending angle, an image of the spinal model with the reflective markers is captured. The results and images are shown in the next section.

Table 5.4 The relationship between the six leg lengths and the bending angle

		Six Leg Length (mm)					
ϕ	Value of p	Leg 1	Leg 2	Leg 3	Leg 4	Leg 5	Leg 6
0°	82.61cm	914.818	790.375	801.306	864.981	844.626	905.259
30°	78.89cm	895.884	784.982	794.658	851.286	833.138	877.313

45°	70.03cm	855.628	779.171	785.720	824.531	812.007	849.618
60°	57.72cm	812.523	787.744	789.805	802.258	798.195	810.520
90°	31.23cm	779.899	867.310	860.477	817.575	831.890	787.431

5.5 Preliminary Experimental Results and Spinal Shape Construction

The rigid bodies in the interface are indicated by the collection of markers. These markers can be selected in the program and are created as trackable objects. The markers on the prominent points of the spinal model in this arrangement are considered as a rigid body representing the shape of the spine. The real benefit of establishing a rigid body using the collection of markers is that the program can provide the position and orientation of the rigid body. Therefore, the spine shape and trunk deformity can be expressed by the position and orientation of the markers. Figure 5.14 shows the interface of the imaging program and the position and orientation of the rigid body of the spinal model. The default point clouds of the markers are circles in white color.

During the imaging process, when some of the markers are missing or cannot be detected in the view of the cameras, the program will attempt to assume the positions of those markers. Thus, the program can still track the rigid body of the model even when some of the markers are missing. Figure 5.15 shows the results and images from each of the camera separately.

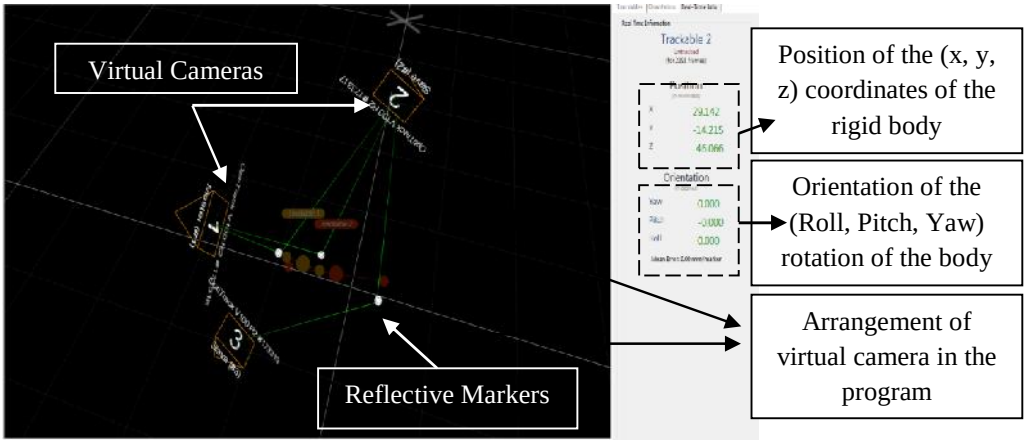

Figure 5.14 The interface of the imaging program and the position and orientation of the markers

As shown in Figure 5.15, the group of markers is tracked by each of the stereo OptiTrack cameras separately. By compiling the images from each camera, the entire rigid body of the spine can be established.

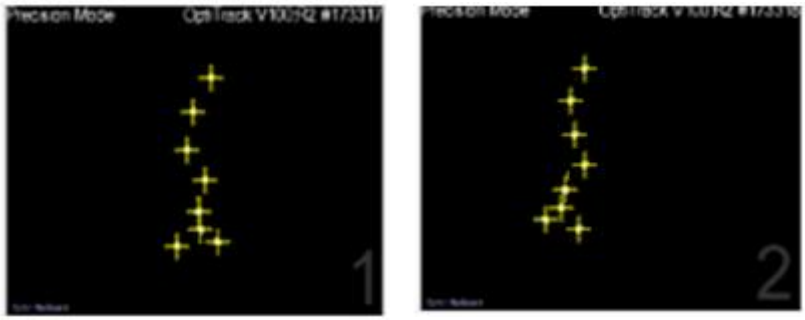

Figure 5.15 Tracking results and images obtained from camera 1 and camera 2

The program is designed to perform semi-automated offline measurements from convergent digital images. The x, y and z coordinates and roll, pitch, yaw rotation matrix of the object points of interest can be obtained. Figure 5.16 (a) shows the results of the digitizing process of the markers. In the system, the coordinates of the markers are generated automatically. The distance between every two markers is also calculated which is shown in Figure 5.16 (b).

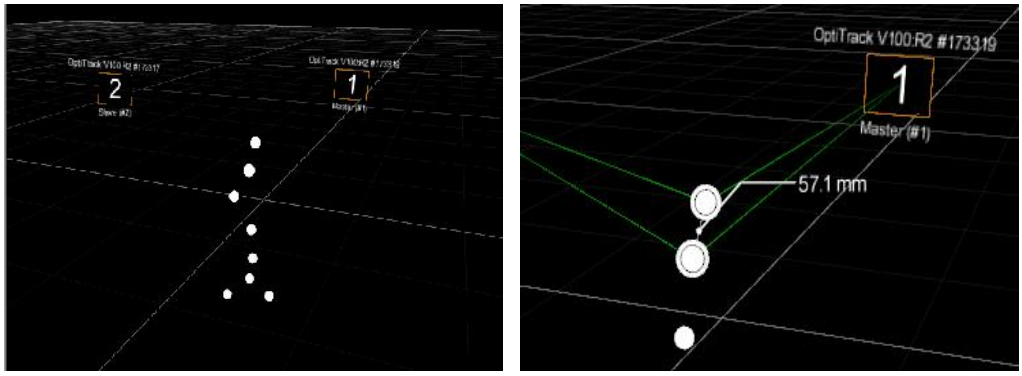

Figure 5.16 (a) Result of digitizing process of the markers; (b) the calculation of the distance between every two markers

Table 5.5 presents the coordinates of each marker obtained automatically from the program, and Table 5.6 shows the calculated distance between every two markers. The results are usable with occasional noisy data points from the background. The rigid body of the spinal model is represented by the collection of markers and the spinal shape can be observed clearly from the sets of cameras. The coordinates of each marker and the distance between each two markers are collected. This preliminary experiment proves that in the current laboratory environment, the spinal deformity evaluation system is usable and reliable for trunk distortion assessment.

Table 5.5 Results of the coordinates of the each marker

	X	Y	z
Marker 1	-0.145008	-0.236902	0.117362
Marker 2	-0.126229	-0.224495	0.130079
Marker 3	-0.140872	-0.182758	0.136821
Marker 4	-0.167695	-0.162210	0.143276
Marker 5	-0.155306	-0.139213	0.148242
Marker 6	-0.159935	-0.154273	0.153394

Marker 7	-0.142007	-0.142556	0.160575
Marker 8	-0.156304	-0.161728	0.161369

Table 5.6 Calculated distances between every two markers

Distance between the two markers	Marker1 and Marker2	75.85mm
	Marker2 and Marker3	94.74mm
	Marker3 and Marker4	84.40mm
	Marker4 and Marker5	76.59mm
	Marker5 and Marker6	66.58mm
	Marker6 and Marker7	72.59mm
	Marker6 and Marker8	73.93mm
	Marker7 and Marker8	61.50mm

In the next section, besides the construction and setting up of the mechanical apparatus and the stereo vision cameras system, more sets of experiments will be conducted using the physical spinal model and take the images for each bending angle.

Chapter 6 System Calibration and Evaluation Process Optimization

Manufacturing and assembly tolerance can cause an inherent problem where the system parameters, such as the leg lengths of the SP are not exactly equal to the theoretical values in the kinematic simulation. Thus, the system calibration process is designed to ensure the precision of the system. Generally, kinematic calibration is a process of recognizing the practical values of the kinematic parameters in the simulation model. Therefore, by iterating the kinematic parameters, the inverse kinematic computation of the required actuator length and joint angles could generate more accurate bending angles.

The calibration process generally consists of four fundamental stages, namely, (a) design and development of a kinematic model that includes a collection of parameters that could be used to determine the correlation between the activated actuator leg lengths and spatial position; (b) measurement of the manipulator poses and coordinates; (c) capturing the practical position and pose using stereo vision cameras and comparing the two results between the theoretical and practical poses; (d) error minimization through searching for the optimum kinematic model parameters of the manipulator from the pose measurements and manipulator activated actuators; and (e) correction for the geometric parameter errors in the manipulator kinematic model.

The kinematics formula is crucial for controlling the pose of the SP to its pre-set desired location. The main purpose of the calibration is to find the actual kinematic parameters that have deviated from their nominal values due to the defective assembly and manufacturing tolerance.

One of the most important steps of the calibration process is error modelling which is designed for sketching geometric factors that lead to motion inaccuracy of the platform. The errors considered in the calibration process are geometric deviations and are treated as static values or constants.

The configuration of the SP can be fully described with 42 kinematic parameters. There are seven kinematic parameters for each leg of the Stewart platform, which are the leg length offset L_i (one parameter for each leg), locations of the spherical joints a_i (three parameters for each leg) and locations of the universal joints b_i (three parameters for each leg). Since there are six legs for the Stewart platform, there are totally $6 \times 7 = 42$ parameters to control the SP.

The local coordinate system is defined arbitrarily located at the base of the Stewart platform denoted by $\{P\}$ and kinematic parameters can be solved in the kinematic calibration process. The location of the origins of $\{P\}$ has no effect on the error calculation and system calibration. The algorithm of the calibration process is shown in Figure 6.1.

The six leg lengths of the Stewart platform are set arbitrarily at the beginning for original input. The theoretical position and coordinates of the mobile plate of the SP is calculated using the forward kinematic algorithm. Due to manufacturing and assembly inaccuracy, the real or practical position of the platform will be different from the theoretical position in the simulation program. Measurement data are taken from the OptiTrack digital cameras. These cameras provide additional depth information and 3D coordinates of the feature points which are used to calibrate the SP. The stereo cameras are installed in front of the platform with reference to the global coordinate system. There is no specific constraint on

the position of the cameras; however, they must be located where the angle of view can cover the platform.

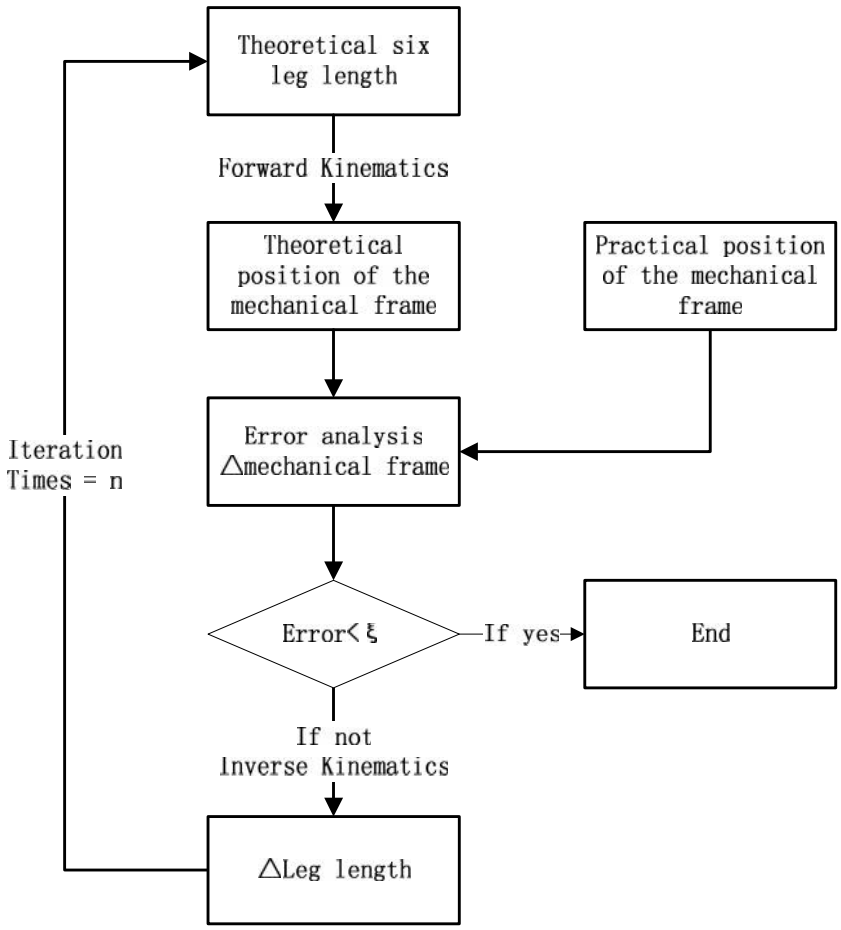

Figure 6.1 The algorithm and architecture of the calibration process

An array of reflective markers is used and attached directly onto the platform and mechanical frame of the system. In the calibration process, nine markers are used where six markers are attached on the left and right side of the frame, two markers are attached on the top and bottom side and one marker is attached on the center which is shown in Figure 6.2.

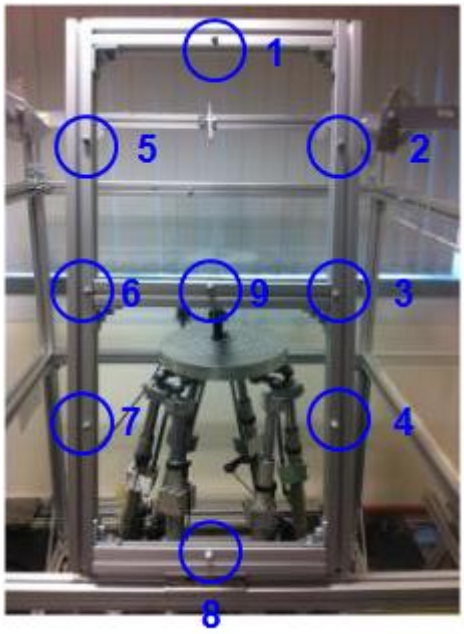

Figure 6.2 Preparations of the markers and apparatus for the calibration

The global coordinates system {*W*} is set and attached on the floor where the cameras are installed as the reference for the measurement. The comparison (D-value) between the theoretical and practical positions of the platform is defined as the errors. Using inverse kinematic algorithms, an iterated set of six leg lengths is calculated based on the D-value. The process of iteration ensures the error or D-value can be reduced. When the D-value becomes sufficiently small, which is less than δ (set value based on a specific application), the final coordinates and position of the platform can be accepted. Table 6.1 is the original six leg lengths of the Stewart platform.

The procedure of conducting the calibration process is as follows:

1) Bending the mobile plate into a series of angles (30 ˚, 45 ˚, 60 ˚and 90˚).

2) Calculate the theoretical position of physical bone and markers p_i^{φ}.

3) Identify the practical position of the markers through OptiTrack q_i^{φ}.

4) Evaluate the errors between the theoretical and real value using the formula.

Table 6.1 The original six leg lengths of the SP

	Six Leg Lengths of the SP (mm)					
ϕ	**Length 1**	**Length 2**	**Length 3**	**Length 4**	**Length 5**	**Length 6**
0˚	914.818	790.375	801.306	864.981	844.626	905.259
30˚	895.884	784.982	794.658	851.286	833.138	877.313
45˚	855.628	779.171	785.720	824.531	812.007	849.618
60˚	812.523	787.744	789.805	802.258	798.195	810.520
90˚	779.899	867.310	860.477	817.575	831.890	787.431

For each bending angle, the residual or the error is calculated as:

$$\text{Residual}_i = \sqrt{(x_1 - x_2)^2 + (y_1 - y_2)^2 + (z_1 - z_2)^2}$$

$$= \sqrt{(\Delta x_i)^2 + (\Delta y_i)^2 + (\Delta z_i)^2}$$

$$\text{Residual} = \frac{1}{n}\sum_{i=1}^{n} \text{Residual}_i$$

Tables 6.2 to 6.5 show the results of the calibration in one iteration. In Table 6.2, the first three rows show the original input of leg lengths to bend the frame into 30˚. The theoretical coordinates of the nine markers are calculated in the simulation using forward kinematic algorithm, and are shown in the second section of Table 6.2. The actual positions of the markers are captured by the cameras and the distance (D-value) between the theoretical and actual values is computed. The residual is calculated as the average of the D-value, which is shown in the last row in Table 6.2. Tables 6.3 to 6.5 show the calibration results when the frame is bent into 45˚, 60˚ and 90˚.

Table 6.2 Result of calibration for bending the frame into 30˚

	Six Leg Length (mm)					
Angle	**Leg 1**	**Leg 2**	**Leg 3**	**Leg 4**	**Leg 5**	**Leg 6**
30˚	895.884	784.982	794.658	851.286	833.138	877.313
Theoretical Position and Coordinates of the Markers						
	Marker 1	**Marker 2**	**Marker 3**	**Marker 4**	**Marker 5**	**Marker 6**
x-axis	1.7	22.4	21.7	22.0	-23.0	-22.7
y-axis	5.5	4.9	4.3	3.7	4.9	4.3
z-axis	160.8	141.3	121.8	102.1	141.9	122.0
	Marker 7	**Marker 8**	**Marker 9**			
x-axis	-22.0	2.3	2.0			
y-axis	3.7	3.0	4.3			
z-axis	102.8	82.7	121.8			
Practical Position and Coordinates of the Markers Captured by Cameras						
	Marker 1	**Marker 2**	**Marker 3**	**Marker 4**	**Marker 5**	**Marker 6**
x-axis	1.1	22.1	22.0	21.6	-22.8	-21.9
y-axis	5.8	5.0	4.4	3.5	4.3	4.1
z-axis	160.1	140.9	120.9	103.7	143.7	122.3
	Marker 7	**Marker 8**	**Marker 9**			
x-axis	-22.3	4.0	2.5			
y-axis	3.7	3.5	4.2			
z-axis	102.4	81.5	120.8			
Distance between the Theoretical Position and Practical Position of Marker 1 to 9						
	Marker 1	**Marker 2**	**Marker 3**	**Marker 4**	**Marker 5**	**Marker 6**
Distance	1.0	0.5	0.9	1.6	1.9	0.8
	Marker 7	**Marker 8**	**Marker 9**			
Distance	0.6	2.1	1.1			
Residual	1.155					

Table 6.3 Result of calibration for bending the frame into 45˚

	Six Leg Length (mm)					
Angle	**Leg 1**	**Leg 2**	**Leg 3**	**Leg 4**	**Leg 5**	**Leg 6**
45˚	855.6	779.2	785.7	824.5	812.0	849.6
Theoretical Position and Coordinates of the Markers						
	Marker 1	**Marker 2**	**Marker 3**	**Marker 4**	**Marker 5**	**Marker 6**
x-axis	1.6	22.1	22.9	21.7	-23.4	-23.2
y-axis	6.7	6.2	5.6	5.0	5.8	5.3
z-axis	158.4	138.9	119.5	99.99	137.7	119.8
	Marker 7	**Marker 8**	**Marker 9**			
x-axis	-23.0	2.7	2.2			
y-axis	4.8	4.4	5.6			
z-axis	100.8	80.5	119.5			
Practical Position and Coordinates of the Markers Captured by Cameras						
	Marker 1	**Marker 2**	**Marker 3**	**Marker 4**	**Marker 5**	**Marker 6**
x-axis	1.6	21.1	22.0	20.1	-23.9	-23.2
y-axis	6.6	7.0	5.1	5.3	5.1	5.2
z-axis	157.3	140.0	120.7	100.9	138.8	118.8
	Marker 7	**Marker 8**	**Marker 9**			
x-axis	-23.1	2.4	2.0			
y-axis	4.2	4.6	5.7			
z-axis	101.1	81.6	120.8			
Distance between the Theoretical Position and Practical Position of Marker 1 to 9						
	Marker 1	**Marker 2**	**Marker 3**	**Marker 4**	**Marker 5**	**Marker 6**
Distance	1.1	1.7	1.6	1.9	1.4	1.0
	Marker 7	**Marker 8**	**Marker 9**			
Distance	0.6	1.2	1.4			
Residual	1.313					

Table 6.4 Result of calibration for bending the frame into 60˚

	Six Leg Length (mm)					
Angle	**Leg 1**	**Leg 2**	**Leg 3**	**Leg 4**	**Leg 5**	**Leg 6**
60˚	812.5	787.7	789.8	802.3	798.2	810.5
Theoretical Position and Coordinates of the Markers						
	Marker 1	**Marker 2**	**Marker 3**	**Marker 4**	**Marker 5**	**Marker 6**
x-axis	1.57	21.3	21.8	22.4	-21.8	-21.5
y-axis	7.8	7.2	6.5	5.8	7.5	6.0
z-axis	156.8	137.3	117.7	98.2	137.3	117.2
	Marker 7	**Marker 8**	**Marker 9**			
x-axis	-21.9	2.2	1.9			
y-axis	5.4	5.2	6.3			
z-axis	99.6	78.7	117.5			
Practical Position and Coordinates of the Markers Captured by Cameras						
	Marker 1	**Marker 2**	**Marker 3**	**Marker 4**	**Marker 5**	**Marker 6**
x-axis	1.8	21.6	21.3	21.7	-22.6	-21.3
y-axis	7.0	6.5	7.2	6.8	7.1	6.5
z-axis	156.6	138.0	117.0	99.0	137.9	116.4
	Marker 7	**Marker 8**	**Marker 9**			
x-axis	-22.6	1.1	1.5			
y-axis	6.2	5.4	6.6			
z-axis	98.1	78.1	116.3			
Distance between the Theoretical Position and Practical Position of Marker 1 to 9						
	Marker 1	**Marker 2**	**Marker 3**	**Marker 4**	**Marker 5**	**Marker 6**
Distance	0.9	1.0	1.2	1.4	1.1	0.9
	Marker 7	**Marker 8**	**Marker 9**			
Distance	1.9	1.2	1.3			
Residual	1.192					

Table 6.5 Result of calibration for bending the frame into 90˚

	Six Leg Length (mm)					
Angle	**Leg 1**	**Leg 2**	**Leg 3**	**Leg 4**	**Leg 5**	**Leg 6**
90˚	779.9	867.3	860.5	817.6	831.9	787.4
Theoretical Position and Coordinates of the Markers						
	Marker 1	**Marker 2**	**Marker 3**	**Marker 4**	**Marker 5**	**Marker 6**
x-axis	1.6	22.2	22.4	22.6	-21.8	-21.9
y-axis	8.0	7.6	7.2	6.7	8.0	7.7
z-axis	154.3	135.9	115.5	96.1	135.3	115.4
	Marker 7	**Marker 8**	**Marker 9**			
x-axis	-22.2	2.4	2.0			
y-axis	6.8	6.3	7.4			
z-axis	96.4	76.6	115.4			
Practical Position and Coordinates of the Markers Captured by Cameras						
	Marker 1	**Marker 2**	**Marker 3**	**Marker 4**	**Marker 5**	**Marker 6**
x-axis	2.3	22.1	22.8	21.5	-21.9	-21.0
y-axis	8.0	8.8	7.9	6.1	7.1	7.1
z-axis	155.2	135.9	115.3	96.6	135.7	116.4
	Marker 7	**Marker 8**	**Marker 9**			
x-axis	-22.7	2.7	1.2			
y-axis	6.1	6.4	7.2			
z-axis	97.9	77.5	116.8			
Distance between the Theoretical Position and Practical Position of Marker 1 to 9						
	Marker 1	**Marker 2**	**Marker 3**	**Marker 4**	**Marker 5**	**Marker 6**
Distance	1.1	1.3	0.9	1.4	1.0	1.5
	Marker 7	**Marker 8**	**Marker 9**			
Distance	1.7	1.0	1.6			
Residual	1.226					

After one iteration, the new input of the six leg lengths of the SP has been changed and updated. A comparison of the residuals of the markers positions among different bending angles is shown in Figure 6.3.

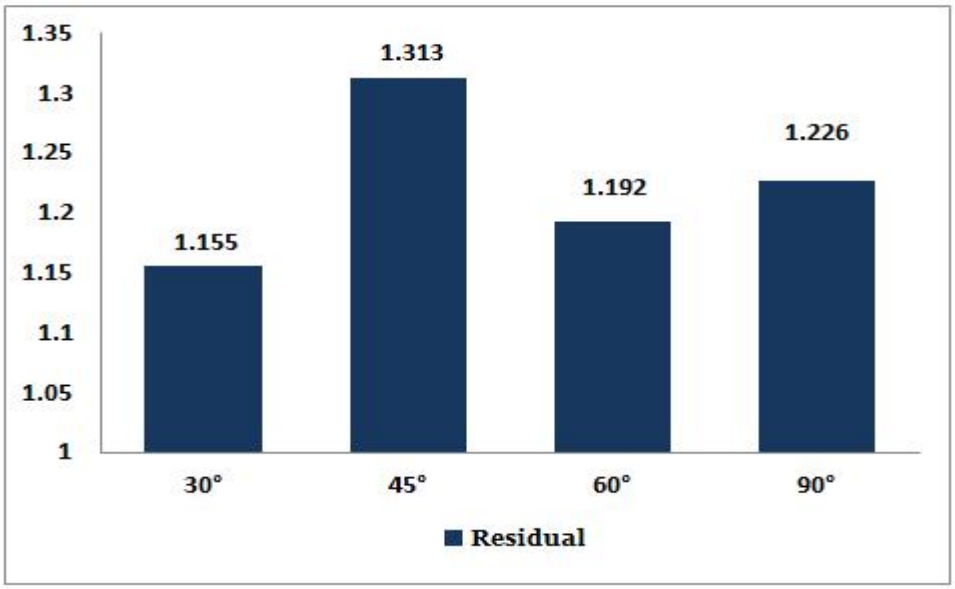

Figure 6.3 Comparison of residuals of the markers positions for different bending angles

After five rounds of iterations using the algorithm, the new input of the six leg lengths of the SP is obtained to reduce the residuals, which are shown in Table 6.6. Using this input, the actual position of the platform can be located precisely to ensure accurate bending angles of the frame.

Table 6.6 New inputs of six leg lengths of the SP after one round of iteration

	Six Leg Length of the SP (mm)					
ϕ	**Length 1**	**Length 2**	**Length 3**	**Length 4**	**Length 5**	**Length 6**
0˚	927.361	793.753	815.060	869.133	842.267	909.379
30˚	892.848	786.214	826.333	878.061	829.387	874.502
45˚	868.004	779.271	838.650	889.426	822.030	844.273
60˚	804.287	788.360	849.005	895.277	834.050	808.308
90˚	782.356	782.553	860.714	917.762	833.907	779.903

Calibration of a Stewart platform to eliminate its static error is not a simple task. The calibration of PKMs (Parallel Kinematics Mechanisms) has principally been evaluated in terms of analysis using forward and inverse kinematic models. Essentially, the errors are from imperfect manufacturing and assembly. Some problematic error sources that are difficult to solve include localized heat generation in the joints and other mechanical parts, nonlinear kinematic mapping or axis aligning errors. Meanwhile, the calibration issue also affects controller development and stiffness analysis and these issues also relate to the system accuracy.

Chapter 7 Implementation of the Spinal Deformity Evaluation System and Case Study

For many scoliotic patients, the motivation of receiving treatment is to improve their physical posture than to correct or stabilize the trunk curvature, thus psychological effects and cosmetic concerns are some of the most important reasons for which the treatment methods have been decided. Correspondingly, the emphasis has been clinically changed to quantifying body asymmetry with the objective of producing medical treatment plans and assessing the outcome. Recently, most of the clinicians' decisions are built on either qualitative evaluation tools such as Adam's forward bending test, the Walter Reed Visual Assessment scale, etc. The development of this dedicated apparatus provides the opportunity to obtain multiple samples of the landmark locations and positions from a skeletal mature subject in order to construct baseline levels and acquire an insight into the variability of values observed from a range of standard morphological measures. The aim of the experiment in this chapter is to quantify the impact of the changes in stance and bending postures during and in between measurements. Another aim is to test the potential usefulness of the apparatus using the physical spinal model.

7.1 Physical Spinal Model Preparation for the Imaging

In the measurement experiments, different "types" of scoliosis spines are tested according to scoliosis classification system. Scoliosis classifications are used to facilitate the objective assessment of a disease for different examiners, thus making the results as uniform and comparable as possible. King classification

system is used in defining the idiopathic scoliosis in this experiment (J. S. Smith, 2008).

King scoliosis classification defies 5 types of idiopathic scoliosis which is shown in Figure 7.1, whereby the severity of a case is determined based on the following parameters:

- Cobb angle of scoliosis 2D image
- Determination of flexibility index based on bending radiographs

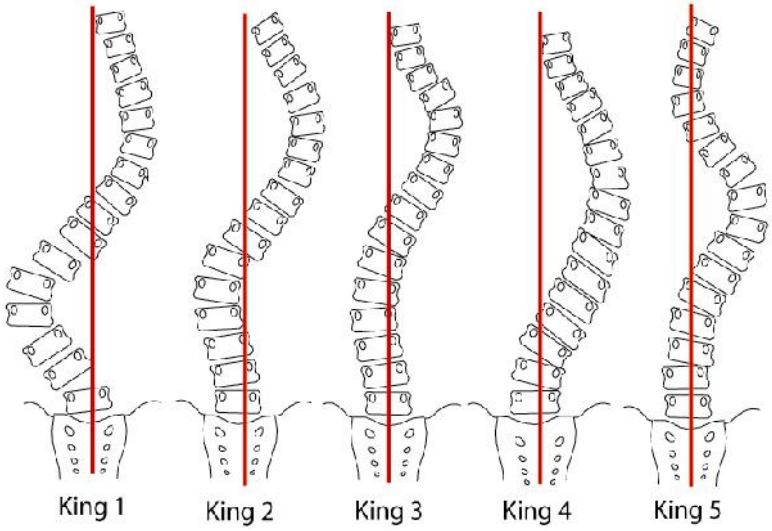

Figure 7.1 King classification of idiopathic scoliosis

In Figure 7.1, the different types of scoliosis are described as:

• King type I: Shows an S-shaped curve crossing the midline of the thoracic and lumbar curves. The lumbar curve is largerand more rigid than the thoracic curve. The flexibility index in the bending radiographs is negative.

• King type II: Shows an S-shaped curve where both the thoracic major curve and the lumbar minor curve cross over the midline. The thoracic curve is larger.

• King type III: Shows a thoracic curve where the lumbar curve does not cross the midline.

• King type IV: Shows a long thoracic curve where the 5th lumbar vertebra is centered over the sacrum, but the 4th lumbar vertebra is already angled in the direction of the curve.

• King type V: Shows a thoracic double curve where the 1st thoracic vertebra (T1) angles into the convexity of the upper curve.

The spinal model is made to bend into the five types of scoliosis according to the King system. For each King type scoliosis, the physical spinal model is attached to the mechanical frame and bends into serial bending angles of 0°, 30°, 45° and 60°. For each bending angle, the 3D coordinates of the markers are obtained by the cameras. The MIVAS index is calculated based on the 3D coordinates provided by the stereo cameras.

As the Cobb's angle is calculated based on 2D image and the stereo vision cameras can only provide 3D image, the z-axis values of the marker coordinates are set 0, which makes the 3D image into 2D image in x-y plane. And then the Cobb's angles are calculated.

Before the measurement, the spinal model is labeled with round reflective markers as shown in Figure 7.2, which is a King type I scoliosis. These markers are attached at several prominent positions of the back corresponding to the locations of the vertebras according to the following anthropometric points, namely, superior spinous processes of T1, T4, T8, L1, L3 and L5 and both posterior superior iliac spines (PSIS).

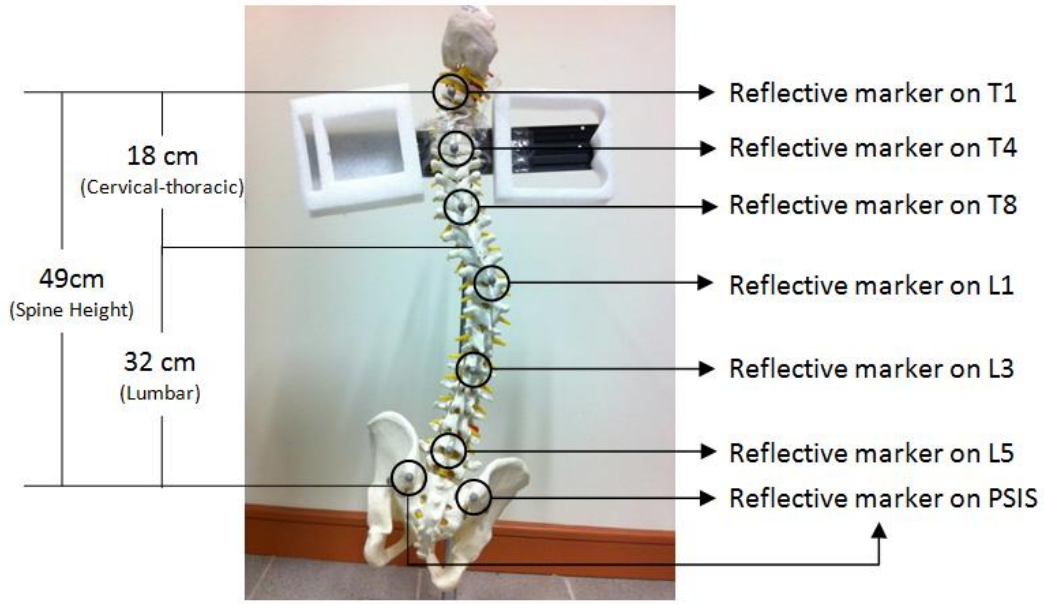

Figure 7.2 Marking positions of anthropometric markers on vertebrae and images captured from the cameras

King type I King type II King type III King type IV King type V

Figure 7.3 shows the physical spinal models used in the experiments according to the King classification system.

7.2 Calibration of the 3D Camera System

The SP and the imaging system are assembled using modular aluminum sections, universal joints and linkages. Three cameras are set up two meters away from the measurement area in a triangular layout. Before the measurement,

calibration is performed. The OptiWand and the self-calibration function in the program are used for the system calibration. The OptiWand is moved back and forth several times in the overlapped region of the three cameras. The three 3D cameras can track the trajectories of the OptiWand to identify the real position of the cameras.

After calibration, the position of the system can be adjusted based on the virtual camera position by tracking the position of the markers. The direction and orientation of the virtual cameras can also be changed to top and side views to observe the model. The trajectory and position of the markers can be detected accurately.

7.3 Imaging Process with the Physical Spinal Model

During the imaging process, the spinal model is located in front of and as close as possible to the frame to establish the necessary reference. Figure 7.4 shows the setup of the custom-built aluminum frame and the position of the cameras.

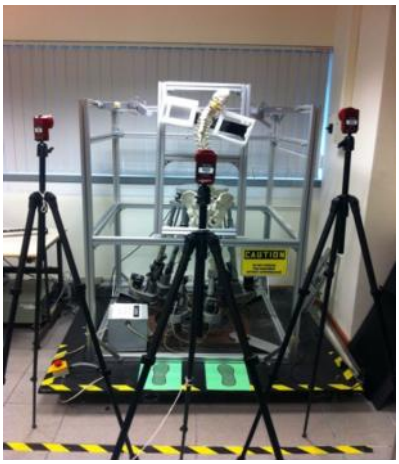

Figure 7.4 The setup of the aluminum frame and the position of the spinal model during measurement

The markers can be selected in the program and are created as trackable objects. The markers on the prominent points on the skeletal model in this arrangement are considered as a rigid body presenting the shape of the spine. The benefit of establishing a rigid body using the collection of markers is that the program can provide the position and orientation of the rigid body. Therefore, the spine shape and trunk deformity can be expressed by the position and orientation of the markers.

During the measurement process, the bottom of the model is fixed which cannot move and the upper part of the model is attached to the moveable frame. Thus, when the SP and the moveable frame moves, the model bends accordingly.

When the model bends, the location of the reflective markers change and the spinal shape of the model also changes. The coordinates of the markers are obtained by capturing the image of the model by the stereo cameras.

7.4 Result Analysis and Discussion

7.4.1 King Type I Scoliosis

King Type I is S-shape scoliosis that the lumbar curve is larger than the thoracic curve which is shown in Figure 7.5.

Figure 7.5 Physical spinal model of King type I scoliosis

As the frame is bent forward, the spinal model bends following its movement. The coordinates and orientation of each marker are obtained by the image capturing process using the three cameras.

- **Bending 0°**. Figure 7.6 (a) shows the measurement process when the spinal model is upright (bends 0°) and figure 7.6 (b), the spine shape on the right. Table 7.1 presents the coordinates of each marker obtained from the program.

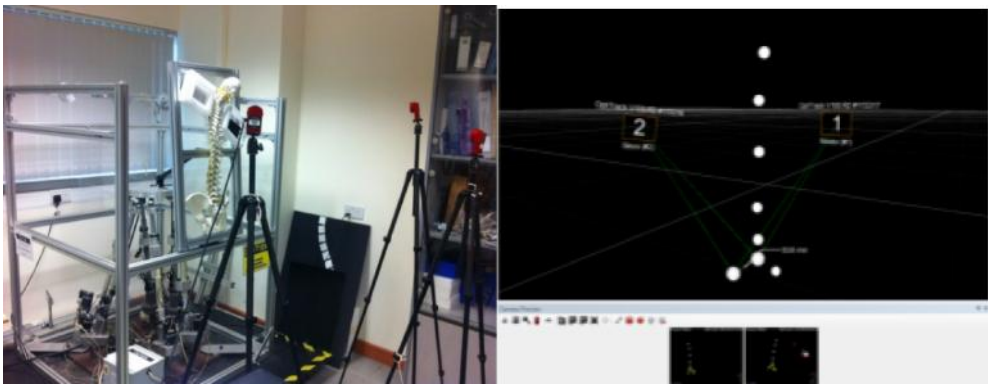

(a) (b)

Figure 7.6 (a) Process of the measurement when the physical spinal model is unbent, i.e., 0°; (b) the spinal shape aligned and calculated by the camera

Table 7.1 Coordinates of each marker for bending the model 0° (no bending)

(unit: meter)

Bending 0°	X	Y	Z
Marker 1	0.0949	0.4214	0.0092
Marker 2	0.0954	0.2941	0.0601
Marker 3	0.0900	0.1749	0.0916
Marker 4	0.0800	0.0545	0.0909
Marker 5	0.0740	-0.0696	0.0793
Marker 6	0.0637	-0.1687	0.0839
Marker 7	0.1666	-0.2631	0.1071
Marker 8	-0.0381	-0.2490	0.1138

- **Bending 30°.** Figure 7.7 (a) shows the process of the measurement when the spinal model is bent 30° and Figure 7.7 (b), the spine shape on the right. Table 7.2 presents the coordinates of markers obtained from the program when the model is bent into 30°.

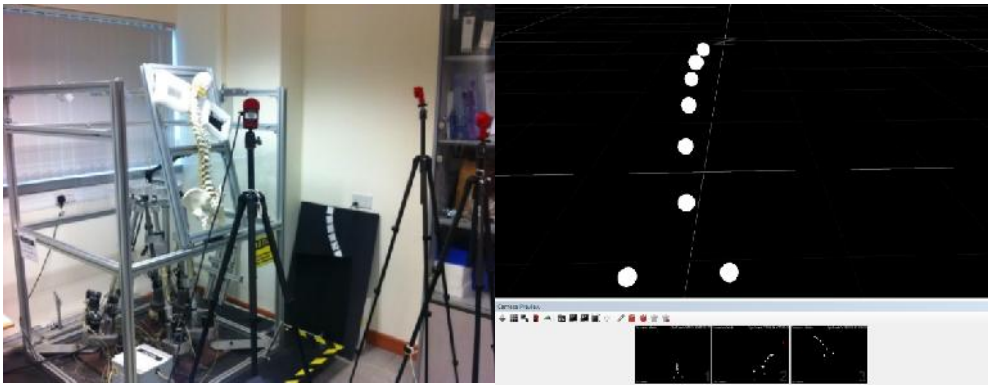

(a) (b)

Figure 7.7 (a) Process of the measurement when the physical spinal model is bent 30°; (b) the spinal shape aligned and calculated by the camera

Table 7.2 Results of the coordinates of each marker for bending the model into 30° (unit: meter)

Bending 30°	X	Y	Z
Marker 1	0.0684	0.1618	-0.6016
Marker 2	0.0747	0.1087	-0.4843
Marker 3	0.0802	0.0617	-0.3817
Marker 4	0.0805	0.0042	-0.2924
Marker 5	0.0875	-0.0605	-0.1791
Marker 6	0.0805	-0.1434	-0.0801
Marker 7	0.1938	-0.2436	0.0111
Marker 8	-0.0138	-0.2233	0.0240

- **Bending 45°.** Figure 7.8 (a) shows the process of the measurement when the spinal model is bent 45° and Figure 7.8 (b) the spine shape on the right. Table 7.3 presents the coordinates of markers obtained from the program when the model is bent into 45°.

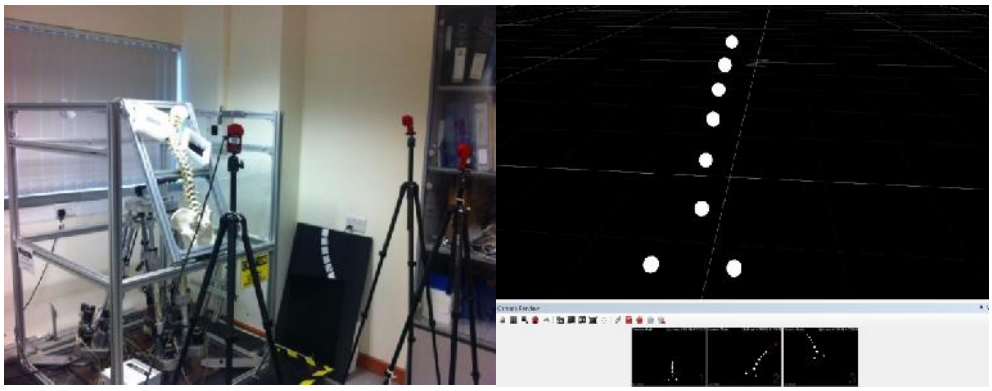

(a) (b)

Figure 7.8 (a) Process of the measurement when the physical spinal model is bent 45°; (b) the spinal shape aligned and calculated by the camera

Table 7.3 Results of the coordinates of each marker for bending the model 45°

(unit: meter)

Bending 45°	X	Y	Z
Marker 1	0.1270	0.3200	-0.3365
Marker 2	0.1008	0.2474	-0.2570
Marker 3	0.0966	0.1530	-0.1841
Marker 4	0.0866	0.0546	-0.1288
Marker 5	0.0849	-0.0593	-0.0786
Marker 6	0.0793	-0.1513	-0.0288
Marker 7	0.1893	-0.2538	0.0356
Marker 8	-0.0165	-0.2361	0.0470

- **Bending 60°.** Figure 7.9 (a) shows the process of the measurement when the spinal model is bent into 60° and Figure 7.9 (b) the spine shape on the right. Table 7.4 presents the coordinates of markers obtained from the program when the model is bent into 60°.

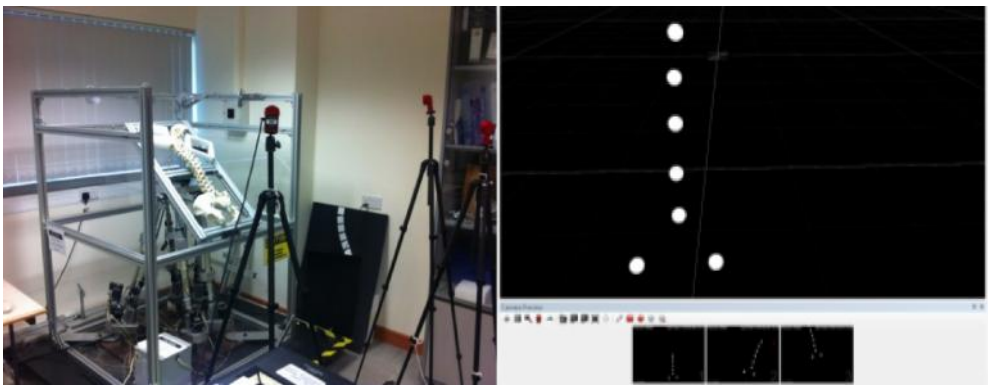

(a) (b)

Figure 7.9 (a) Process of the measurement when the physical spinal model bends 60°; (b) the spinal shape aligned and calculated by the camera

Table 7.4 Results of the coordinates of each marker for bending the model into 60° (unit: meter)

Bending 60°	X	Y	Z
Marker 1	0.0577	0.0489	-0.6993
Marker 2	0.0737	0.0369	-0.5751
Marker 3	0.0771	0.0167	-0.4584
Marker 4	0.0752	-0.0198	-0.3494
Marker 5	0.0772	-0.0762	-0.2252
Marker 6	0.0597	-0.1418	-0.0993
Marker 7	0.1739	-0.2419	0.0083
Marker 8	-0.0376	-0.2251	0.0168

The rigid body of the physical spinal model represented by the collection of markers and the spinal shape can be observed clearly. The coordinates of each marker and the distance between every pair of adjacent markers are collected. This experiment proves that in the current laboratory environment, the human spine deformity system is usable and reliable for trunk distortion assessment.

7.4.2 King Type II Scoliosis

King type II scoliosis presents an S-shape curve where the lumbar curve is less than the thoracic curve which is shown in Figure 7.10.

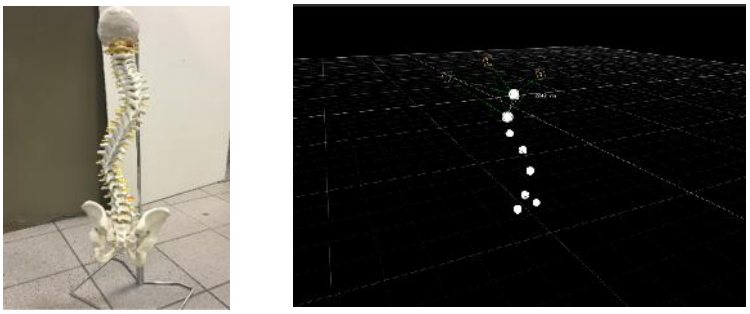

Figure 7.10 Physical spinal model of King type II scoliosis

The measurement results of bending the King type II scoliosis model (bending angles are 0°, 30°, 45°, 60°) are compiled and shown in Table 7.5.

Table 7.5 Marker coordinates on the King type II scoliosis model

Bending 0°	X	Y	Z
Marker 1	-0.0927	0.1541	0.996
Marker 2	-0.2268	-0.2118	1.0376
Marker 3	-0.1523	-0.0379	1.0051
Marker 4	-0.1936	-0.372	1.1278
Marker 5	-0.1120	-0.5026	1.2543
Marker 6	-0.1192	-0.6679	1.3457
Marker 7	-0.2030	-0.7659	1.3379
Marker 8	-0.0472	-0.7665	1.4128
Bending 30°	X	Y	Z
Marker 1	-0.2751	-0.1138	1.1496
Marker 2	-0.2646	0.2772	1.1662
Marker 3	-0.2694	0.0862	1.1469
Marker 4	-0.3755	0.4283	1.1690
Marker 5	-0.1036	-0.4094	1.3761
Marker 6	-0.1141	-0.5655	1.4835
Marker 7	-0.1895	-0.6697	1.4733
Marker 8	-0.0439	-0.6541	1.5642
Bending 45°	X	Y	Z
Marker 1	-0.3107	0.0453	1.2472
Marker 2	-0.3639	0.4135	1.3683
Marker 3	-0.3382	0.2377	1.2972
Marker 4	-0.4983	0.5368	1.4130

Marker 5	-0.1071	-0.2767	1.4263
Marker 6	-0.0937	-0.4453	1.5129
Marker 7	-0.1463	-0.5596	1.4825
Marker 8	-0.0117	-0.5300	1.5859
Bending 60°	X	Y	Z
Marker 1	-0.2420	-0.0581	1.1494
Marker 2	-0.4365	0.2695	1.2125
Marker 3	-0.3740	0.1062	1.1433
Marker 4	-0.4755	0.4169	1.3018
Marker 5	-0.0955	-0.3048	1.2607
Marker 6	-0.0996	-0.4361	1.3983
Marker 7	-0.1537	-0.5524	1.3999
Marker 8	-0.0313	-0.4915	1.5056

7.4.3 King Type III Scoliosis

King type III scoliosis presents a C-shape curve where the lumbar curve does not cross the midline which is shown in Figure 7.11.

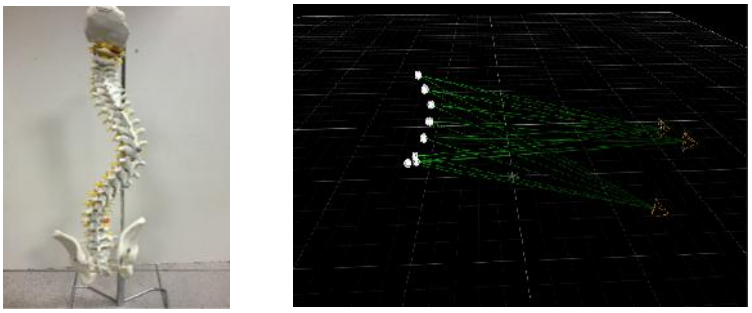

Figure 7.11 Physical spinal model of King type III scoliosis

The measurement results of bending the King type III scoliosis model (bending angles are 0°, 30°, 45°, 60°) are compiled and shown in Table 7.6.

Table 7.6 Marker coordinates on the King type III scoliosis model

Bending 0°	X	Y	Z
Marker 1	-0.4539	0.1510	0.9078
Marker 2	-0.5058	0.0270	0.9184
Marker 3	-0.4676	-0.1941	1.0198
Marker 4	-0.4024	-0.3406	1.1271
Marker 5	-0.4161	-0.5105	1.2415
Marker 6	-0.4605	-0.6505	1.2716
Marker 7	-0.5570	-0.7514	1.2454
Marker 8	-0.3757	-0.7317	1.2814
Bending 30°	X	Y	Z
Marker 1	-0.2848	-0.7577	1.1291
Marker 2	-0.3017	-0.6854	1.1655
Marker 3	-0.3034	-0.4728	1.1804
Marker 4	-0.3473	-0.2905	1.2039
Marker 5	-0.4271	-0.4085	1.2204
Marker 6	-0.4961	-0.5554	1.2573
Marker 7	-0.5423	-0.6728	1.2321
Marker 8	-0.4054	-0.6829	1.2821
Bending 45°	X	Y	Z
Marker 1	-0.0528	-0.2482	1.1408
Marker 2	-0.0551	-0.2927	1.1829
Marker 3	-0.0594	-0.3795	1.2108
Marker 4	-0.0654	-0.4072	1.2391
Marker 5	-0.0634	-0.4673	1.2465
Marker 6	-0.1451	-0.5880	1.2769
Marker 7	-0.2416	-0.6789	1.2270
Marker 8	-0.0939	-0.6781	1.3392

Bending 60°	X	Y	Z
Marker 1	-0.2239	-0.1580	1.1321
Marker 2	-0.4339	0.2673	1.2126
Marker 3	-0.3921	0.1032	1.2482
Marker 4	-0.2760	0.3159	1.3050
Marker 5	-0.1907	-0.3071	1.3553
Marker 6	-0.2909	-0.4366	1.3977
Marker 7	-0.1641	-0.5514	1.4060
Marker 8	-0.1327	-0.4915	1.5097

7.4.4 King Type IV Scoliosis

King type IV scoliosis presents a large C-shape curve that the thoracic curve is long where the 5th lumbar vertebra is centered over the sacrum, but the 4th lumbar vertebra is already angled in the direction of the curve which is shown in Figure 7.12.

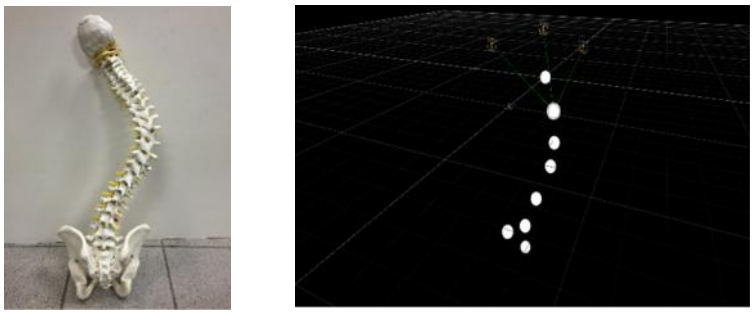

Figure 7.12 Physical spinal model of King type IV scoliosis

The measurement results of bending the King type IV scoliosis model (bending angles are 0°, 30°, 45°, 60°) are compiled and shown in Table 7.7.

Table 7.7 Marker coordinates on the King type IV scoliosis model

Bending 0°	X	Y	Z
Marker 1	-0.2962	-0.1049	1.3640
Marker 2	-0.2686	0.0656	1.2934
Marker 3	-0.2987	-0.2256	1.4141
Marker 4	-0.2159	0.2703	1.2561
Marker 5	-0.2295	-0.3949	1.5177
Marker 6	-0.3190	-0.7031	1.6060
Marker 7	-0.1586	-0.6611	1.6591
Marker 8	-0.2425	-0.5808	1.6137
Bending 30°	X	Y	Z
Marker 1	-0.4319	0.4346	1.4618
Marker 2	-0.4999	0.2436	1.4004
Marker 3	-0.5190	0.0531	1.3853
Marker 4	-0.4986	-0.0882	1.3862
Marker 5	-0.3984	-0.5119	1.5826
Marker 6	-0.4632	-0.6333	1.6042
Marker 7	-0.4149	-0.3040	1.4429
Marker 8	-0.3010	-0.5803	1.6469
Bending 45°	X	Y	Z
Marker 1	-0.3660	0.0292	1.4780
Marker 2	-0.5160	0.5382	1.5956
Marker 3	-0.4234	0.1637	1.4784
Marker 4	-0.4853	0.3410	1.5040
Marker 5	-0.2685	-0.1874	1.5556
Marker 6	-0.2548	-0.4114	1.6890
Marker 7	-0.1901	-0.4807	1.7867
Marker 8	-0.3169	-0.5406	1.6824

Bending 60°	X	Y	Z
Marker 1	-0.5879	0.6757	1.8290
Marker 2	-0.4685	0.3287	1.6507
Marker 3	-0.4063	0.2081	1.6238
Marker 4	-0.5343	0.4948	1.7037
Marker 5	-0.3031	-0.0098	1.6442
Marker 6	-0.2092	-0.3442	1.8194
Marker 7	-0.3495	-0.3985	1.7309
Marker 8	-0.2822	-0.2741	1.7417

7.4.5 King Type V Scoliosis

King type V scoliosis presents a double curve in thoracic part where the 1st thoracic vertebra (T1) angles into the convexity of the upper curve which is shown in Figure 7.13.

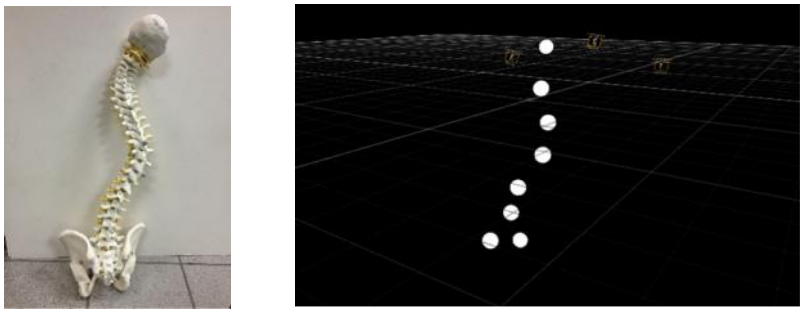

Figure 7.13 Physical spinal model of King type V scoliosis

The measurement results of bending the King type V scoliosis model (bending angles are 0°, 30°, 45°, 60°) are compiled and shown in Table 7.8.

Table 7.8 Marker coordinates on the King type V scoliosis model

Bending 0°	X	Y	Z
Marker 1	-0.3130	0.3596	1.3992
Marker 2	-0.3126	0.1514	1.4442

Marker 3	-0.3695	-0.0222	1.4398
Marker 4	-0.3866	-0.1758	1.4952
Marker 5	-0.3583	-0.3344	1.6500
Marker 6	-0.3617	-0.4476	1.7196
Marker 7	-0.3083	-0.5694	1.8348
Marker 8	-0.4160	-0.6033	1.7058
Bending 30°	X	Y	Z
Marker 1	-0.4411	0.4935	1.5590
Marker 2	-0.3964	0.3012	1.5214
Marker 3	-0.3506	-0.0382	1.5025
Marker 4	-0.3980	0.1260	1.4929
Marker 5	-0.2396	-0.4982	1.6613
Marker 6	-0.1014	-0.4757	1.7577
Marker 7	-0.2130	-0.2067	1.6080
Marker 8	-0.1853	-0.3456	1.6746
Bending 45°	X	Y	Z
Marker 1	-0.4570	0.3125	1.4877
Marker 2	-0.3974	-0.0335	1.4594
Marker 3	-0.4965	0.4972	1.5329
Marker 4	-0.4529	0.1353	1.4532
Marker 5	-0.2513	-0.2048	1.5556
Marker 6	-0.2218	-0.3415	1.6322
Marker 7	-0.1355	-0.4720	1.7203
Marker 8	-0.2844	-0.4935	1.6403
Bending 60°	X	Y	Z
Marker 1	-0.5078	0.4586	1.5487
Marker 2	-0.5911	0.6023	1.6462
Marker 3	-0.3918	0.1093	1.4747

Marker 4	-0.4704	0.2683	1.4826
Marker 5	-0.2051	-0.2017	1.6275
Marker 6	-0.2626	-0.3536	1.6133
Marker 7	-0.2359	-0.0596	1.5654
Marker 8	-0.1206	-0.3374	1.7050

7.5 Result Analysis and a Novel Evaluation Index for Spinal Deformity Progression Evaluation

In this section, a novel evaluation index for adolescent idiopathic scoliosis measurement and diagnosis is introduced to complement the existing assessment indices, such as the Cobb angle (Cobb 1948) etc. The new evaluation index is based on the phenomenon of the tilt and deviation of the vertebras in a scoliotic spine, which forms the tilt angles between each pair of adjacent vertebras.

Figure 7.14 shows an example of a scoliotic spine from the interpolation of positions of markers to form the spinal curve.

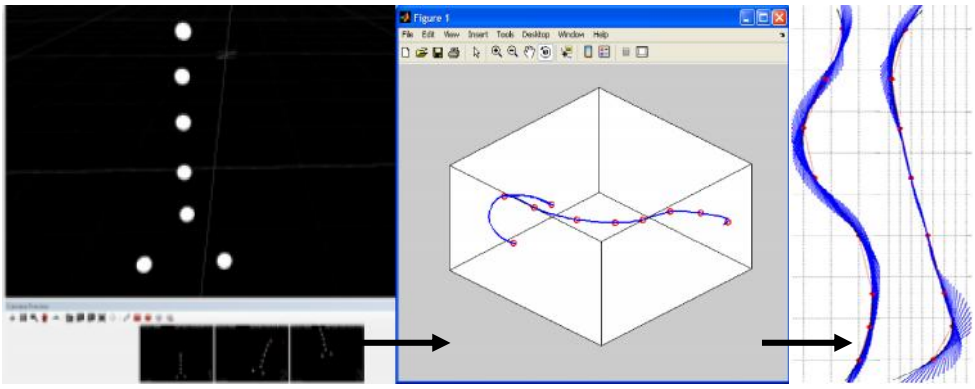

Figure 7.14 An example of curve fitting algorithm applied to the spinal curve and the calculation of the angle between the adjacent perpendicular lines

According to the experiment results, the scoliotic spinal shapes according to the King classification system are estimated. In the experiments, the coordinates

of the markers attached on the spine are captured and measured, which is used to establish the curvature of the spine. In conjunction of the SP and stereo vision system, the new-designed IVAS index and the standard Cobb angles are calculated and compared to estimate the severity of the trunk. Figure 7.15 shows a calculation example of the parameters.

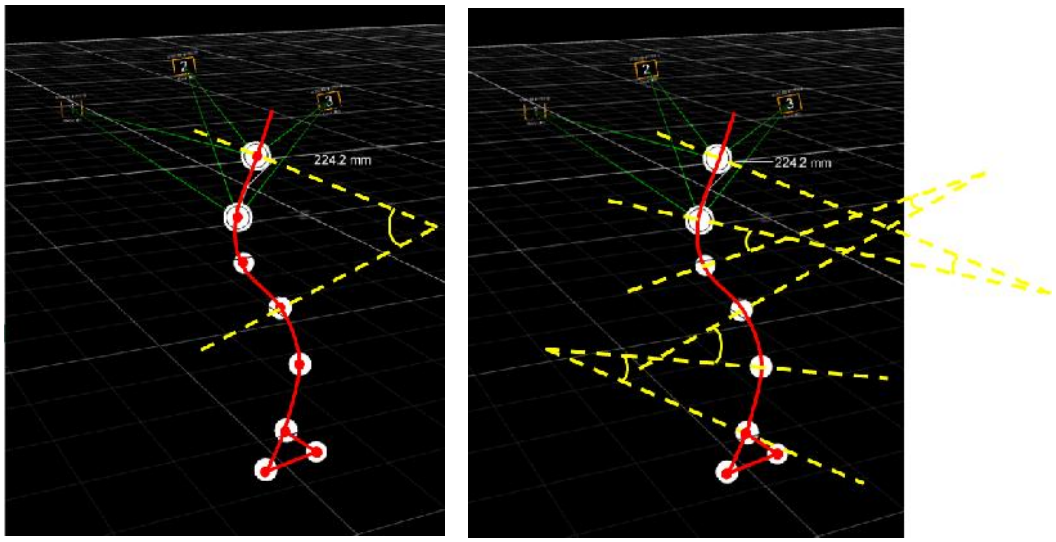

The Cobb Angle The IVAS Index

Figure 7.15 Calculation of the Cobb angle and IVAS index

In order to calculate and estimate the severity of the five types of King Classification of scoliosis, different types of spinal model with curvature according to King Classification method were tested using the system, for each type of spinal curvature, four tilting angles are tested. In order to compare the new-designed IVAS index and MIVAS index to the traditional Cobb angle, X-ray images for each type of King Classification scoliotic model were captured and the Cobb angles are calculated according to the X-ray images. Figure 7.16 shows the process of obtaining the Cobb angle and IVAS for each type of King Classification scoliosis.

Using the physical model in the system, the student managed to achieve the following tasks:

- The SP and mechanical frame can manipulate the model into different bending angles accurately. For each bending angle, the spinal shape are successfully simulated using the camera system and software.
- The Cobb angle for each type of King Classification scoliotic model is calculated using the X-ray image of the model.
- The innovative indices are calculated according to the experiment using the system to evaluate the severity of the spinal curvature and deformity.
- The Cobb angle and the IVAS index and MIVAS index are compared.

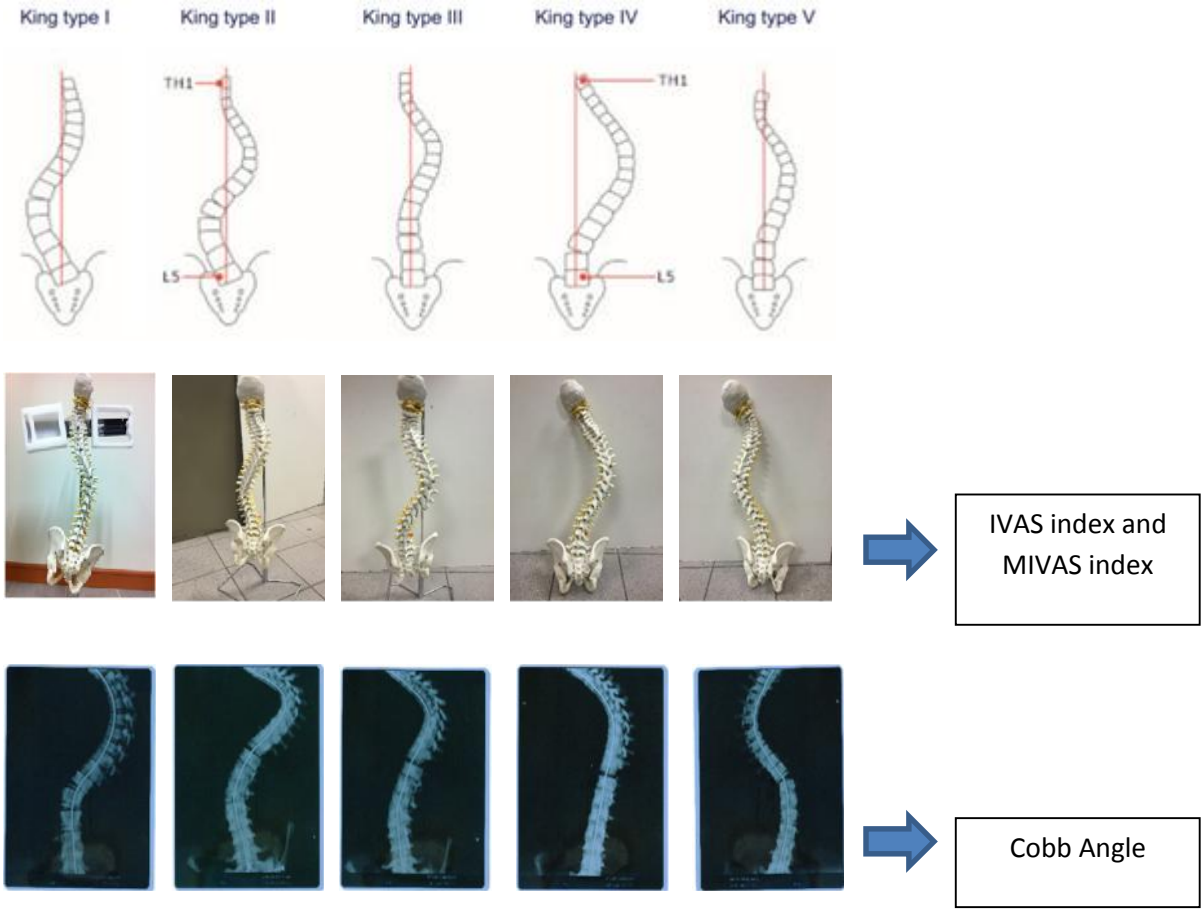

Figure 7.16 Obtaining the Cobb angle and IVAS for King Classification scoliosis

Table 7.9 lists the measurements, in ascending order of the four bending angles, on the interpolated curves of the image of the physical spinal model using the original IVAS index. The Cobb angles used were measured directly from the 2D interpolated curves by setting the y-coordinates as 0 in the data samples instead so as to provide a means of comparison of the feasibility with the IVAS index and the Stewart platform system.

Table 7.9 Measured Cobb angles and IVAS index using same data

Classification	Bending Angles (°)	Severity	Cobb Angle (°)	IVAS Index (°)
King Type I	0	Mild	10.5	8.5
	30	Mild	12.0	17.5
	45	Mild	14.5	23
	60	Mild	13.0	25.5
King Type II	0	Mild	19.5	26.5
	30	Moderate	21.5	30.5
	45	Moderate	30.5	31.5
	60	Moderate	32.0	36.5
King Type III	0	Mild	15.5	15.5
	30	Moderate	18.5	24.0
	45	Moderate	35.5	38.5
	60	Moderate	51.5	49.5
King Type IV	0	Moderate	21.5	21.5
	30	Moderate	28.0	34.5
	45	Moderate	36.5	38.5
	60	Moderate	49.0	49.0
King Type V	0	Mild	17.0	20.5

	30	Moderate	28.5	26.5
	45	Moderate	32.5	33.5
	60	Moderate	35.0	42.5

From Table 7.5, it can be found that when the bending angles of the spinal model become larger (from 0° to 60°), the Cobb angle and the IVAS index both become larger, which means the spinal curve is more distinct. As the IVAS index and the Cobb angle change in the same direction, a linear correlation exists between the IVAS index and the Cobb angle.

The Cobb angle and the IVAS Index values according to the King classification in Table 7.9 are plotted in ascending order on the same axes, as shown in Figure 7.17 to 7.21.

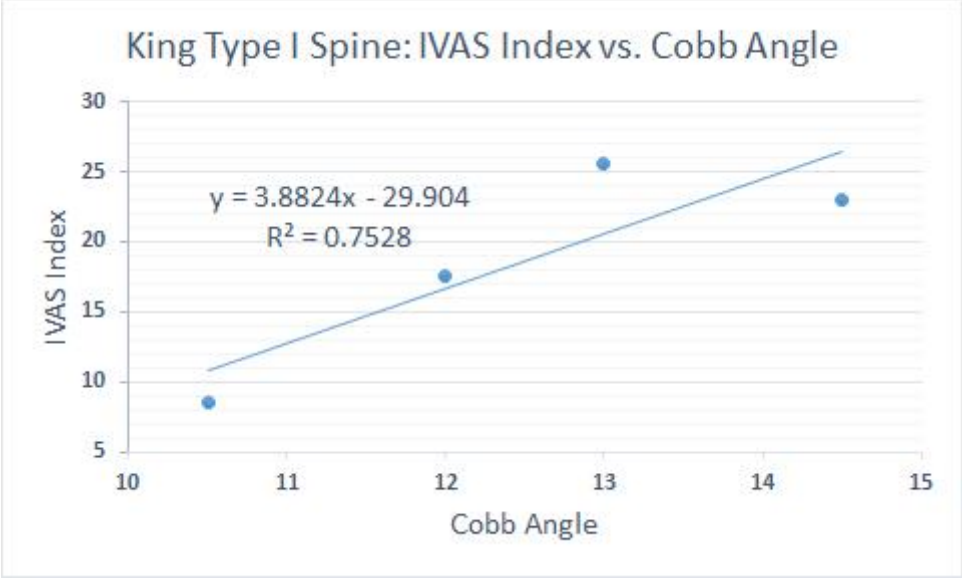

Figure 7.17 Plot of the IVAS index against the Cobb angle of King type I spine

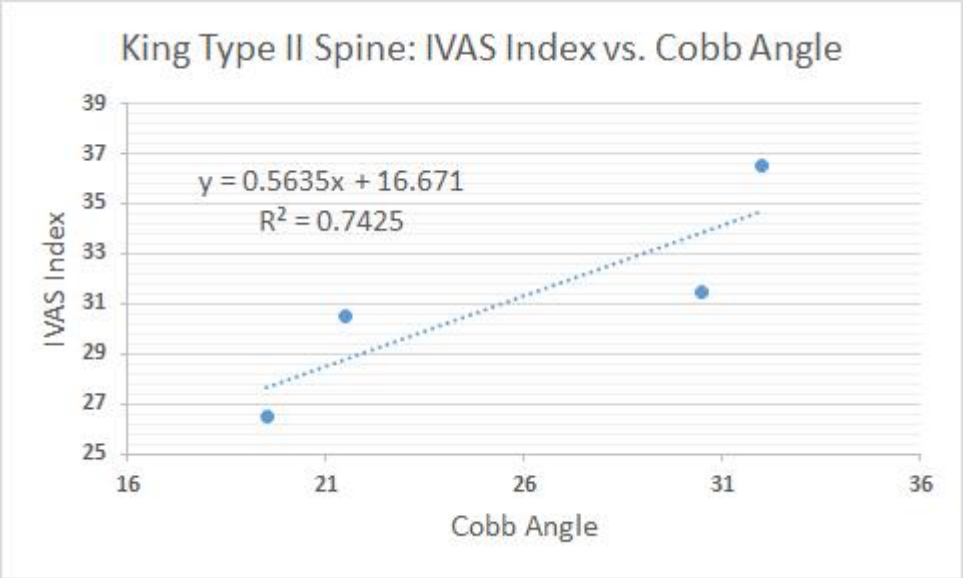

Figure 7.18 Plot of the IVAS index against the Cobb angle of King Type II spine

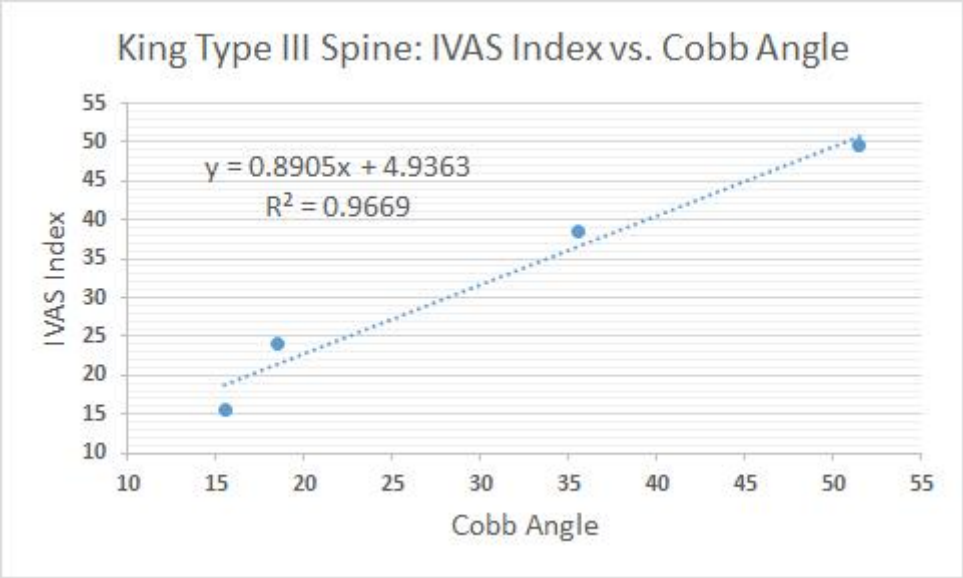

Figure 7.19 Plot of the IVAS index against the Cobb angle of King Type III spine

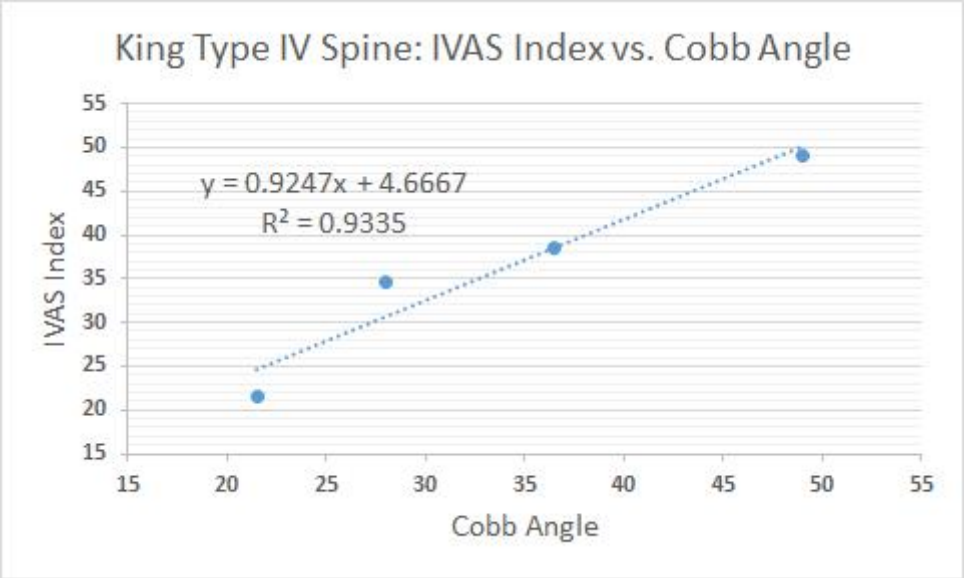

Figure 7.20 Plot of the IVAS index against the Cobb angle of King Type IV spine

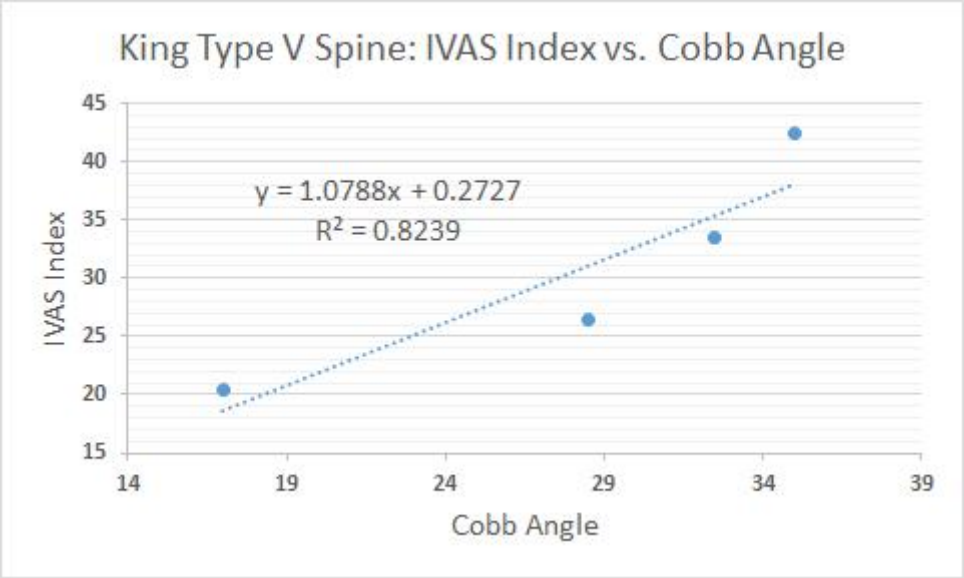

Figure 7.21 Plot of the IVAS index against the Cobb angle of King Type V spine

The high positive correlation between the Cobb angle and the IVAS index methods is highlighted in Figure 7.17 to 7.21, where the line graph representing IVAS and Cobb angle change in the same direction. The computed correlation

coefficients are close to the value of 1, thus implying a strong positive correlation between these two indices. This shows that the proposed index of IVAS has potentially high usefulness and feasibility.

In this case, from the measurement of the IVAS index and the Cobb angle, this spinal model presents mild and moderate spinal deformity based on the King classification system.

Chapter 8 Conclusions and Recommendations

The routine approach in evaluating and monitoring the progress of scoliosis in most orthopedic clinics is to take radiographs continuously of full spinal images. The traditional approach has a number of advantages. Aside from frequent exposure to X-ray radiation and its side effects, and the unreliable use of 2D images to represent 3D deformity, the measurement method cannot correlate effectively the spinal deformity evaluation index to the unbalance of the body shape. Much effort has been expended by many researchers to seek reliable methods to reduce radiation hazard and improve the reliability of the correlation between different types of spinal deformity and changes in the back surface shape. However, most of the proposed means have been found to be prone to deviation and errors and are not robust for different cases of scoliosis, thus restricting their acceptance in the practical environment as a useful alternative to radiography. In this thesis, a novel method to measure the skeletal deformity, monitor scoliosis progression and provide surgical outcomes has been developed via a mechanical apparatus and medical imaging techniques, such as a stereo vision camera systems.

8.1 Summary

The study of surface topography systems has been an epidemic research topic in recent years in quantifying body shapes and meeting patients' cosmetic concerns, physical impairment and quality of life that warrants a re-evaluation of the medical relevance of non-radiographic measurement techniques. Other surface measurement methodologies are based on observational devices, such as the Adams forward bending test, simple hand-held devices, and optical systems, such as

structured light patterns and Moiré fringe topography. However, most of the approaches have been criticized to be prone to deviations arising from the standing position, stance posture, breathing and sway. Currently, only limited studies (Denis et al. 2004; Duong et al. 2009) have been published that utilize multiple samples to measure the back shape asymmetry. This thesis reports on the application and design of an original apparatus and analytic programming with the objectives of developing a method to quantify the variation of topographical and morphological appearance and back surface shape measurement to explain and present clinical results, to quantify any improvements in the specificity of the current methods, and to integrate the facility to acquire trunk ranges of motion.

X-ray images from thirty adult subjects representing musculo-skeletal disorder are used to compare the results obtained from the system developed. The calculation of the novel indices for spinal deformity, IVAS, MIVAS and 3DIVAS, shows that this system is potentially useful for scoliosis diagnosis and further assessment. The results show that the proposed indices are clinically useful to quantify body symmetry and trunk unbalance. The future objective of the research is to apply the same methods to pre- and post-operative adolescent idiopathic scoliosis of individual patients and age-matched the subjects in next-step clinical studies.

8.2 Conclusions

In this thesis and study, the author has designed and established the application and performance of a new surface topography measurement apparatus integrating clinically valuable evaluation indices that are useful during the regular

examination of the presence and severity of spinal deformity when assessing psychosocial influence, treatment results and physical impairment among scoliotic subjects medical analyzed as adolescent idiopathic scoliosis.

In this research, an innovative and integrated system has been designed and constructed to accomplish an inherently safe, non-contact and reusable tool for the spinal deformity diagnosis and evaluation of scoliosis patients. This is an attempt to incorporate a Stewart platform, which is a parallel kinematic motion manipulator, a specially-designed mechanical apparatus and stereo vision techniques of OptiTrack 3D camera system. The availability of the inherently safe technique and apparatus focusing mainly on the body shape and spinal deformity establishes the opportunity to undertake deeper research. Comparing to the traditional methods, this system has the advantages of radiation-free, high repeatability and high efficiency, where is can be used in the hospitals and routine school lateral spinal examination.

In this study, in order to complement the traditional scoliosis evaluation index, i.e., the Cobb angle parameter, three new indices, IVAS index, MIVAS index and 3DIVAS index, have been proposed based on the angular separation between the pairs of adjacent vertebra. The calculation of the IVAS and MIVAS index is based on the subject's X-ray images. The index of 3DMIVAS is independent of the radiography images and this can reduce the radiation exposure to the subjects. On the basis of the calculation of the X-ray data sample, a comparison of the Cobb angle and the IVAS, and the Cobb angle and the MIVAS has been conducted. The correlation coefficient between IVAS and the Cobb angle is 0.9284, and the correlation coefficient between MIVAS and the Cobb angle is 0.9175. The high

correlation found between the clinical variable (Cobb angle) and the topographic variables (IVAS and MIVAS) shows that although they use different calculation methods for different deformities, variations in the spinal column appear as variations of the topographic patterns. In this study, it has been shown that the newly proposed IVAS and MIVAS indices have the potential to be used as tools for supporting the traditional scoliosis measurement methods.

Besides providing 3D measurements of the anthropometric markers for positioning the vertebras and 3D topology of the human back, the technique provides a user friendly interface and a detachable mechanical frame. A case study involving the trunk shape of a physical spinal model demonstrates the capability of the developed system to assess the spinal distortion and frontal angular parameter. The experiment involving the spinal model was conducted in which the postures and bending angles can be accurately controlled by the Stewart platform. For each of the bending angles, e.g., 0^{o}, 30^{o}, 45^{o}, 60^{o} and 90^{o}, the images of the model's back surface topography were captured for spinal deformity and trunk asymmetry analysis. By studying the experiment results, it is shown that the system is potentially useful to assist the doctors and orthopedists in their decision-making process.

8.3 Research Contributions

This research incorporates two fields of studies, namely, the design and development of robot-assisted apparatus consisting of a Stewart platform and stereo vision techniques, and the subject of spinal deformity evaluation index and parameters. Detailed investigations of the proposed integrated system have led to

some generally applicable concepts for the tasks that require accurate-controlling and radiation-free application.

The main contribution of this thesis consists of the experimental verification of the proof of concept of using the Stewart platform as the motion controlling tool, using stereo vision cameras to capture surface topography to generate spinal shape, and the proposed indices for complementing the existing evaluation parameters for trunk asymmetry assessment. The research achievements in this thesis are summarized as follows:

- Application of Stewart platform and stereo vision techniques for human back deformity and trunk imbalance measurement.
- Design and construction of a customized mechanical frame for controlling the bending postures securely and accurately.
- Implementation of the user interface to present the presence and severity of the spinal deformity and trunk unbalance.
- Three spinal deformity indices, IVAS, MIVAS and 3DIVAS, based on the angular separations are introduced and the usefulness of the indices has been examined.
- Virtual spinal shape building with accurate 3D positions of bony markers.
- Experimental case studies based on the King classification system of scoliosis involving physical spinal model to validate the system were conducted to show the potential usefulness of the system.

8.4 Future Research Work

The scope of this study sets the boundary for the research to demonstrate the validity of the mechanical apparatus with associated stereo vision camera system and the proposed spinal deformity evaluation indices from the analysis of data obtained from the collection of skeletally mature adult. Additional studies can be undertaken through the acquisition and investigation of information involving the adolescent idiopathic scoliosis patients and comparing age-matched subjects.

Future research can be focused on confirming the functionality of the application, efficacy and usefulness of the apparatus in adding to the knowledge of body sway, posture and movements. In addition, scoliosis is a 3D deformity of the spine. In conventional x-rays, the spinal surgeon measures the frontal plane (Cobb angle), the sagittal plane (kyphosis, lordosis), and the rotation of the vertebral bodies based on evaluation of the pedicle rotation (Mehta 1973). Frontal plane measurements of the scoliotic spine alone do not provide sufficient information for the management of scoliosis. The next-step research is to apply this approach to a 3D evaluation for the spinal shape construction.

Furthermore, the IVAS index and MIVAS index are designed in the coronal plane (frontal plane). However, frontal plane measurements of the scoliotic spine alone may not provide sufficient information for scoliosis management. This methodology of using angular separation to define and evaluate the severity of scoliosis can also be applied to the other two planes for further spinal deformity evaluation, namely, the sagittal plane (evaluating kyphosis and lordosis) and the transverse plane (evaluating rotation of vertebrae bodies and rotation of rib cage).

Last but not least, another key point for future research would be to compare the results obtained from pre-operative and post-operative scoliotic children and the comparing groups of healthy children to establish the impact of the disease and treatments on the cosmetic appearance. The hypothesis to be tested should be that before and after the operation of scoliosis, there would be significant improvement for the spinal deformity using the surface measurement techniques. Using the apparatus and method provided in this thesis, we can regularly examine the effects of the operation through the non-contact and radiation-free method.

The promise is that the acceptance of the non-contact surface topography method in the clinical and research communities will stimulate much more important research and become a useful approach to help improve the quality of life of many scoliotic adolescent pupils throughout the world.

References

A. Aliverti, G. Ferrigno, A. Pedotti, (1993), Surface analysis by laser beam scanning and stereophotogrammetry, Optical Tools for Manufacturing and Advanced Automation, International Society for Optics and Photonics, p.209-219

A. Aliverti, G. Ferrigno, A. Pedotti, (1995), Back Surface Analysis by Laser Beam Scanning and Stereo-Photogrammetry, Amsterdam, Netherlands: IOS Press.

F. Berryman (2004), Fourier transform profilometry for measuring back shape in scoliosis, University of Wolverhampton.

F. Berryman, P. Pynsent, J. Fairbank (2008), "Measuring the rib hump in scoliosis with ISIS2", Studies in Health Technology Informatics **140**, p.65-67.

F. Berryman, P. Pynsent, J. Fairbank, S. Disney (2008), "A new system for measuring three-dimensional back shape in scoliosis", European Spine Journal **17**(5), p.663-672.

I.V. Adair, W. MC. Van, G.W.D. Armstrong (1977), "Moiré topography in scoliosis screening." Clinical orthopedics and related research **129**, p.165-171.

J. Bago, J. M. Climent, S. Pineda, C. Gilperez (2007), "Further evaluation of the Walter Reed Visual Assessment Scale: correlation with curve pattern and radiological deformity", Scoliosis **2**(1), p.12.

L.M. Benneker, P. F. Heini, S.E. Anderson, M. Alini, K. Ito (2005), "Correlation of radiographic and MRI parameters to morphological and biochemical assessment of intervertebral disc degeneration", European Spine Journal **14**(1), p.27-35.

M.A. Asher, S. M. Lai, D.C. Burton, B. Manna (2004), "Maintenance of trunk deformity correction following posterior instrumentation and arthrodesis for idiopathic scoliosis", Spine **29**(16), p.1782-1788.

M.A. Asher, and D. C. Burton (2006), "Adolescent idiopathic scoliosis: natural history and long term treatment effects", Scoliosis **1**(1), p.2.

M.A. Bail, A. Eigensee, G. Haeusler, J.M. Herrmann, M.W. Lindner (1997), "3D imaging of human skin: optical in-vivo tomography and topology by short-coherence interferometry", BiOS'97, Part of Photonics West, International Society for Optics and Photonics, p.64-75.

M. Beauchamp, H. Labelle, G. Grimard, C. Stanciu, B. Poitras, J. Dansereau (1993), "Diurnal variation of Cobb angle measurement in adolescent idiopathic scoliosis", Spine **18**(12), p.1581-1583.

N. Andreff, P. Renaud, P. Martinet (2004), "Vision-based kinematic calibration of an H4 parallel mechanism: practical accuracies", Industrial Robot: An International Journal **31**(3), p.273-283.

N. Andreff, T. Dallej, P. Martinet (2007), "Image-based Visual Servoing of a Gough—Stewart Parallel Manipulator using Leg Observations", The International Journal of Robotics Research **26**(7), p.677-687.

P.O. Ajemba, N. G. Durdle, V.J. Raso (2007), "A torso-imaging system to quantify the deformity associated with scoliosis", Instrumentation and Measurement, IEEE Transactions on **56**(5), p.1520-1526.

P.O. Ajemba, N.G. Durdle, V.J. Raso (2008), "A novel visualization scheme for monitoring and tracking of torso deformities in scoliosis", Research Into Spinal Deformities 6, **140**, p363.

P.O. Ajemba, N. G. Durdle, V.J. Raso(2009), "Characterizing torso shape deformity in scoliosis using structured splines models", Biomedical Engineering, IEEE Transactions on **56**(6), p.1652-1662.

W.P. Bunnell (1984), "An objective criterion for scoliosis screening", The Journal of Bone and Joint Surgery, American volume **66**(9), p.1381-1387.

W.P. Bunnell (1993), "Outcome of spinal screening", Spine **18**(12), p.1572-1580.

P. Côté, B. G. Kreitz, J.D. Cassidy (1998), "A study of the diagnostic accuracy and reliability of the Scoliometer and Adam's forward bend test", Spine **23**(7), p.796-802.

M. Callegari, and A. Suardi (2003), "Hybrid kinematic machines for cooperative assembly tasks", Proceedings, International Workshop: Multiagent Robotic Systems: Trends and Industrial Applications, Robocup, p.68-78.

G. Carbone and M. Ceccarelli (2005), "A serial-parallel robotic architecture for surgical tasks", Robotica **23**(3), p.345-354.

D. Carman, R. Browne, J. Birch (1990), "Measurement of scoliosis and kyphosis radiographs: intraobserver and interobserver variation", Journal of Bone and Joint Surgery, American volume **72**(3), p.328-333.

A. Carr, R. Jefferson, A. Turner-Smith, A. Beavis (1991), "An analysis of normal back shape measured by ISIS scanning", Spine **16**(6), p.656-659.

K.S. Chai, K. and K. Young (2001), "Designing a Stewart Platform based Cooperative System for Large Component Assembly", Proceedings of IEEE International Conference on Methods and Models in Automation and Robotics, 2001.

H. Chanal, E. Duc, P. Ray (2007), "A new approach for the geometrical calibration of parallel kinematics machines tools based on the machining of a dedicated part", International Journal of Machine Tools and Manufacture **47**(7), p.1151-1163.

S.H. Chen and L.C. Fu (2006), "The Forward Kinematics of the 6-6 Stewart Platform Using Extra Sensors, Systems, Man and Cybernetics", SMC'06, IEEE International Conference, 2006.

K.C. Cheok, J. L. Overholt, R.R. Beck (1993), "Exact methods for determining the kinematics of a Stewart platform using additional displacement sensors", Journal of Robotic Systems **10**(5), p.689-707.

P. Chiacchio, F. Pierrot, L. Sciavicco, B. Siciliano (1993), "Robust design of independent joint controllers with experimentation on a high-speed parallel robot", Industrial Electronics, IEEE Transactions on **40**(4), p.393-403.

C. Chiang (1969), "Moiré patterns from the surface and their application in measuring topography", Journal of Physics D: Applied Physics **2**(2), p.287.

R. Clavel, P. Helmer, T. Niaritsiry, S. Rossopoulos (2005), "High precision parallel robots for Micro-Factory applications", Robotic Systems for Handling and Assembly: p.285-296.

J.R. Cobb (1948), "Outline for the study of scoliosis", Instructional Course Lecture **5**: p.261-275.

A. Codourey and E. Burdet (1997), "A body-oriented method for finding a linear form of the dynamic equation of fully parallel robots", Proceedings of 1997 IEEE International Conference on Robotics and Automation, IEEE, 1997.

J. Cortés and T. Siméon (2005), Sampling-based motion planning under kinematic loop-closure constraints, Algorithmic Foundations of Robotics VI, Springer**:** p.75-90.

J. Cortes and T. Simeon (2003), "Probabilistic motion planning for parallel mechanisms", Proceedings of ICRA'03 IEEE International Conference on Robotics and Automation, 2003, volume 3, p.4354-4359.

J.J. Craig (2004). "Introduction to robotics: mechanics and control" p.175

P. Curran and D. Groves (1990), "An accurate, fast and cost effective method for the measurement of body shape and the assessment of spinal deformity", Proceedings of the 6th International Symposium on Surface Topography and Spinal Deformity, p.24-30.

T. Dallej, N. Andreff, Y. Mezouar, P. Martinet (2006), "3D pose visual servoing relieves parallel robot control from joint sensing", proceedings of 2006 IEEE/RSJ International Conference on Intelligent Robots and Systems, IEEE, 2006.

T. Dallej, H. Hadj-Abdelkader, N. Andreff, P. Martinet (2006), "Kinematic calibration of a Gough-Stewart platform using an omnidirectional camera", proceedings of 2006 IEEE/RSJ International Conference on Intelligent Robots and Systems, IEEE, 2006.

D. Daney, N. Andreff, G. Chabert, Y. Papegay (2006), "Interval method for calibration of parallel robots: Vision-based experiments", Mechanism and Machine Theory **41**(8): p.929-944.

N. Daniell (2007), "A comparison of the accuracy of the Vitus Smart® and Hamamatsu Body Line® 3D whole-body scanners", Proceedings of the 10th

International Society for the Advancement of Kinanthropometry Conference, 2007, p.39-54.

J. Daruwalla and P. Balasubramaniam (1985), "Moiré topography in scoliosis. Its accuracy in detecting the site and size of the curve", Journal of Bone & Joint Surgery, British Volume **67**(2): p.211-213.

B. Dasgupta and P. Choudhury (1999), "A general strategy based on the Newton–Euler approach for the dynamic formulation of parallel manipulators", Mechanism and Machine Theory **34**(6): p.801-824.

S. Delorme, H. Labelle, C.E. Aubin (2002), "The Crankshaft Phenomenon: Is Cobb Angle Progression a Good Indicator in Adolescent Idiopathic Scoliosis?" Spine **27**(6): p. 145-151.

P. Dietmaier (1998), The Stewart-Gough platform of general geometry can have 40 real postures, Advances in Robot Kinematics: Analysis and Control, Springer**:** p.7-16.

M.B. Dobbs and S. L. Weinstein (1999), "Infantile and juvenile scoliosis", Orthopedic Clinics of North America **30**(3): p.331-341.

B. Drerup and E. Hierholzer (1987), "Automatic localization of anatomical landmarks on the back surface and construction of a body-fixed coordinate system", Journal of biomechanics **20**(10): p.961-970.

B. Drerup and E. Hierholzer (1994), "Back shape measurement using video rasterstereography and three-dimensional reconstruction of spinal shape", Clinical Biomechanics **9**(1): p.28-36.

N. Durdle, D. Hill, Z. Zhang, V.J. Raso (1995), "A Surface Modelling System for the Study of Scoliosis", Three Dimensional Analysis of Spinal Deformities, Volume 15, p.21-26.

J. Fairbank (2004), "Historical perspective: William Adams, the forward bending test, and the spine of Gideon Algernon Mantell", Spine **29**(17): p.1953-1955.

E.F. Fichter (1986), "A Stewart platform-based manipulator: general theory and practical construction", The International Journal of Robotics Research **5**(2): p.157-182.

W. Frobin and E. Hierholzer (1982), "Analysis of human back shape using surface curvatures", Journal of biomechanics **15**(5): p.379-390.

W. Frobin and E. Hierholzer (1991), "Video rasterstereography: a method for on-line measurement of body surfaces", Photogrammetric engineering and remote sensing **57**(10): p.1341-1345.

J. Gallardo, J. Rico, A. Frisoli, D. Checcacci, M. Bergamasco (2003), "Dynamics of parallel manipulators by means of screw theory", Mechanism and Machine Theory **38**(11): p.1113-1131.

Z. Geng and L. S. Haynes (1993), "Dynamic control of a parallel link manipulator using a CMAC neural network", Computers & electrical engineering **19**(4): p.265-276.

Z. Geng and L. S. Haynes (1994), "An effective kinematics calibration method for Stewart platform", Proceedings of Fifth International Symposium on Robotics and Manufacturing, 1994, p.87-92.

Z. Geng, L. S. Haynes, J.D. Lee, R.L. Carroll (1992), "On the dynamic model and kinematic analysis of a class of Stewart platforms", Robotics and Autonomous Systems **9**(4): p.237-254.

P.F. Giampietro, R. D. Blank, C.L. Raggio, S. Merchant, F.S. Jacobsen, T, Faciszewski, S.K. Shukla, A.R. Greenlee, C. Reynolds, D.B. Schowalter (2003), "Congenital and idiopathic scoliosis: clinical and genetic aspects", Clinical Medicine & Research **1**(2): p.125-136.

S. Goh, R. Price, P. Leedman, K. Singer (1999), "Rasterstereographic analysis of the thoracic sagittal curvature: a reliability study", Journal of Musculoskeletal Research **3**(02): p.137-142.

C. Goldberg, E. Fogarty, D. Moore, F. Dowling (1997), "Scoliosis imaging and the problem of postural sway", Studies in Health Technology and Informatics: p.297-300.

C. Goldberg, D. Moore, E. Fogerty, F. Dowling (1999), "Surface topography and Cobb angles in idiopathic scoliosis", Studies in Health Technology and Informatics: p.53-56.

C. Gosselin, and J. Angeles (1990), "Kinematic inversion of parallel manipulators in the presence of incompletely specified tasks", Journal of Mechanical Design 112: p.494.

V. Gough and S. Whitehall (1962), "Universal tyre testing machine", Proceedings of FISITA 9th International Technical Congress, 1962, p.117-137.

J.E. Gray, A. D. Hoffman, H.A. Peterson (1983), "Reduction of radiation exposure during radiography for scoliosis", Journal of Bone and Joint Surgery American **65**(1): p.5-12.

C. Griffiths, J. FitzGerald, R. Tweedie, M. Gibson, M. Leonard (1997), "Accuracy and repeatability of spinal asymmetry measurements using surface topography with and without upper body fixation", Studies in Health Technology and Informatics: p.301-304.

T. Grivas, V. Mouzakis, E. Vasiliadis, K. Mihas, V. Polyzois (2005), "Why the prevalence of AIS is different in various countries? Relation to geographic latitude and the possible role of the age at menarche", Proceedings of IMAST: 7–9 July, 2005, Banff.

H. Guo and H. Li (2006), "Dynamic analysis and simulation of a six degree of freedom Stewart platform manipulator", Proceedings of the Institution of Mechanical Engineers, Part C: Journal of Mechanical Engineering Science 220(1): p.61-72.

P. Poncet, S. Delorme, R. Dudley, J.L. Ronsky, J. Dansereau, J. Harder, R.D. Dewar, H. Labelle, P.H. GU, R.F. Zernicke (1999), "3D reconstructions of the external and internal geometries of the trunk using laser and stereo-radiographic imaging techniques", Research Into Spinal Deformities Two 2: p.21-24.

Y. Harada, Y. Takemitsu, M. Imai (1981), "The role of contour line photography using the light cutting method and Moire photography in school screening for scoliosis, Moire fringe topography and spinal deformity", Proceedings of an International Conference, 1981, p.113-121.

K. Harib, A. Sharif Ullah, A. Hammami (2007), "A hexapod-based machine tool with hybrid structure: Kinematic analysis and trajectory planning", International Journal of Machine Tools and Manufacture 47(9): p.1426-1432.

K. Harib and K. Srinivasan (2003), "Kinematic and dynamic analysis of Stewart platform-based machine tool structures", Robotica 21(5): p.541-554.

D. Harris (1995), "Parallel-linkage robot coordinate transformation through screw theory", 9th World Congress on the Theory of Machines and Mechanisms, 1995, p.1565-1568.

D.A. Hoffman, J. E. Lonstein, M.M. Morin, W. Visscher, B.S. Harris, J.D. Boice (1989), "Breast cancer in women with scoliosis exposed to multiple diagnostic x rays", Journal of the National Cancer Institute 81(17): p.1307-1312.

J.Y. Hong, S.W. Suh, H.N. Modi, J.H. Yang, S.Y. Park (2013), "Analysis of factors that affect shoulder balance after correction surgery in scoliosis: a global analysis of all the curvature types", European Spine Journal: p.1-13.

J.P. How, B. Bethke, A. Frank, D. Dale, J. Vian (2008), "Real-time indoor autonomous vehicle test environment", Control Systems, IEEE 28(2): p.51-64.

C.I. Huang, C.F. Chang, M.Y. Yu, L.C. Fu (2004), "Sliding-mode tracking control of the Stewart platform", proceedings of 5th IEEE Asian Control Conference, 2004, p.562-569

C.I. Huang and L.C. Fu (2004), "Adaptive backstepping tracking control of the Stewart platform", 43rd IEEE Conference on Decision and Control, 2004, p.5228-5233.

T. Huang, D. G. Chetwynd, D.J. Whitehouse, J. Wang (2005). "A general and novel approach for parameter identification of 6-DOF parallel kinematic machines", Mechanism and Machine Theory 40(2): p.219-239.

K.Inami, N. Suzuki, T. Ono, Y. Yamashita, K. Kohno, H. Morisue (1999). "Analysis of posterior trunk symmetry index (POTSI) in scoliosis", Research Into Spinal Deformity **2**(59): p.85-88.

C. Innocenti (2001), "Forward kinematics in polynomial form of the general Stewart platform", Journal of Mechanical Design 123: p.254.

D. Jakobovic and L. Jelenkovic (2002), "The forward and inverse kinematics problems for Stewart parallel mechanisms", Proceedings of the 8th International Science Conference on Production Engineering, Brijuni.

J. James (1954), "IDIOPATHIC SCOLIOSIS The prognosis, diagnosis, and operative indications related to curve patterns and the age at onset", Journal of Bone & Joint Surgery, British Volume 36(1): p.36-49.

W.J. KANE (1977), "Scoliosis prevalence: a call for a statement of terms", Clinical Orthopedics and Related Research 126: p.43-46.

S. Kim and S. Lee (1992), "Cartesian space dynamic model of serial-parallel manipulator systems and their dynamic performance evaluation", Proceedings of the 31st IEEE Conference on Decision and Control, IEEE, 1992, p.327-328.

H.A. King, J. H. Moe, D.S. Bradford, R.B. Winter (1983), "The selection of fusion levels in thoracic idiopathic scoliosis", Journal of Bone and Joint Surgery American 65(9): p.1302-1313.

S. Kleinberg (1922), "The operative treatment of scoliosis", Archives of Surgery 5(3): p.631-645.

S. Kock and W. Schumacher (2000), "A mixed elastic and rigid-body dynamic model of an actuation redundant parallel robot with high-reduction gears",

Proceedings of IEEE International Conference on in Robotics and Automation, 2000, p.1918-1923.

T. Kotwicki (2008), "Evaluation of scoliosis today: Examination, X-rays and beyond", Disability and Rehabilitation 30(10): p.742-751.

T. Kotwicki, E. Kinel, W. Stryla, A. Szulc (2007), "Discrepancy in clinical versus radiological parameters describing deformity due to brace treatment for moderate idiopathic scoliosis", Scoliosis 2(18): p.1748-7161.

J. Lallemand, A. Goudali, S. Zeghloul (1997), "The 6-dof 2-Delta parallel robot", Robotica 15(04): p.407-416.

T. Laulund, J. Søjbjerg, E. Hørlyck (1982), "Moire topography in school screening for structural scoliosis", Acta Orthopaedica 53(5): p.765-768.

R. LeBlanc, H. Labelle, C. Rivard, B. Poitras, J. Kratzenberg (1997), "Three-dimensional (3D) postural evaluation of normal human subjects", Studies in Health Technology and Informatics: p.293-296.

J. Legaye, W. Lokietek, C. Orban, N. Jacqumin (1992), "The ISIS optic scanner: its use in the evaluation and control of spinal deviations", Acta orthopaedica belgica 58: p.66.

M. Letts, A. Quanbury, G. Gouw, W. Kolsun, E. Letts (1988), "Computerized ultrasonic digitization in the measurement of spinal curvature", Spine **13**(10): p.1106-1110.

A.R. Levy, M. S. Goldberg, N.E. Mayo, J.A. Hanley, B. Poitras (1996), "Reducing the lifetime risk of cancer from spinal radiographs among people with adolescent idiopathic scoliosis", Spine 21(13): p.1540-1547.

C.G. Li, H.S. Ding, P.D. Wu (2003), "Application of mrac to a 6-DOF parallel machine tool", 2003 IEEE International Conference on Machine Learning and Cybernetics, p.2164-2167.

G. Liu, Y. Wu, X. Wu, Y. Kuen, Z. Li (2001), "Analysis and control of redundant parallel manipulators", Proceedings of 2001 ICRA IEEE International Conference on Robotics and Automation, IEEE, 2001, p.3748-3754.

K. Liu, F. Lewis, G. Lebret, D. Taylor (1993), "The singularities and dynamics of a Stewart platform manipulator", Journal of Intelligent and Robotic Systems 8(3): p.287-308.

X.C Liu, J. G. Thometz, R.M. Lyonn, J. Klein (2001), "Functional classification of patients with idiopathic scoliosis assessed by the Quantec system: a discriminant functional analysis to determine patient curve magnitude", Spine 26(11): p.1274-1279.

J. Lonstein (1994), "Adolescent idiopathic scoliosis", The Lancet 344(8934): p.1407-1412.

J.E. Lonstein and J. Carlson (1984), "The prediction of curve progression in untreated idiopathic scoliosis during growth", Journal of Bone and Joint Surgery American 66(7): p.1061-1071.

T.G. Lowe, M. Edgar, J.Y. Margulies, N.H. Miller, V.J. Raso, K.A. Reinker, C.H. Rivard (2000), "Etiology of Idiopathic Scoliosis: Current Trends in Research", The Journal of Bone and Joint Surgery 82(8): p.1157-1157.

M.F. Mínguez, M. Buendía, R.M. Cibrián, R. Salvador, M. Laguía, A. Martin, F. Gomar (2007), "Quantifier variables of the back surface deformity obtained with a

noninvasive structured light method: evaluation of their usefulness in idiopathic scoliosis diagnosis", European Spine Journal 16(1): p.73-82.

S. Mao, L. Xu, Z. Zhu, B. Qian, J. Qiao, L. Yi, Y. Qiu (2013), "Association between genetic determinants of peak height velocity during puberty and predisposition to adolescent idiopathic scoliosis", Spine 38(12): p.1034-1039.

F. Marquet, S. Krut, F. Pierrot (2001). "ARCHI: a new redundant parallel mechanism-modeling, control and first results", Proceedings of 2001 IEEE/RSJ International Conference on Intelligent Robots and Systems, IEEE, p.183-188.

F. Marquet, S. Krut, F. Pierrot (2002), "Enhancing parallel robots accuracy with redundant sensors", Proceedings of ICRA'02 IEEE International Conference on Robotics and Automation, IEEE, 2002, p.4114-4119.

O. Masory, J. Wang, H. Zhuang (1996), "Kinematic modeling and calibration of a Stewart platform", Advanced Robotics 11(5): p.519-539.

M.J. McMaster (1983), "Infantile idiopathic scoliosis: can it be prevented?" Journal of Bone & Joint Surgery, British Volume 65(5): p.612-617.

V. Medved (2002), Measurement of human locomotion, CRC press, p. 132-138.

J. Meng and Z. Li (2005), "A general approach for accuracy analysis of parallel manipulators with joint clearance", 2005 IEEE/RSJ International Conference on Intelligent Robots and Systems, IEEE, 2005, p.2468-2473.

J.P. Merlet (1994), "Trajectory verification of parallel manipulators in the workspace", Proceedings of 1994 IEEE International Conference on Robotics and Automation, 1994, vol.3, p.2166-2171

J.P. Merlet (2006), Parallel robots, Springer.

N.H. Miller (1999), "Cause and natural history of adolescent idiopathic scoliosis", Orthopedic Clinics of North America 30(3): p.343-352.

S.A. Mior, D. R. Kopansky-Giles, E.R. Crowther, J.G. Wright (1996), "A comparison of radiographic and electrogoniometric angles in adolescent idiopathic scoliosis", Spine 21(13): p.1549-1555.

F. Montgomery and S. Willner (1997), "The natural history of idiopathic scoliosis: Incidence of treatment in 15 cohorts of children born between 1963 and 1977", Spine 22(7): p.772-774.

A. Moran and R. Lipczynski (1994), "Automatic digitization and analysis of moiré topograms on a personal computer for clinical use", Medical engineering and physics 16(3): p.259-264.

R. Morrissy, G. Goldsmith, E. Hall, D. Kehl, G. Cowie (1990), "Measurement of the Cobb angle on radiographs of patients who have", Journal of Bone and Joint Surgery American 72: p.320-327.

U.G. Narayanan (2008), Concerns, Desires and Expectations of Surgery for Adolescent Idiopathic Scoliosis: A Comparison of Patients', Parents'& Surgeons' Perspectives, University of Toronto.

S. Negrini and A. Negrini (2007), "The three-dimensional easy morphological (3-DEMO) classification of scoliosis-Part III, correlation with clinical classification and parameters", Scoliosis 2(5).

C.C. Nguyen and F. J. Pooran (1989), "Dynamic analysis of a 6 DOF CKCM robot end-effector for dual-arm telerobot systems", Robotics and Autonomous Systems 5(4): p.377-394.

C.C. Nguyen, Z.L. Zhou, S.S. Antrazi, C. Campbell (1991), "Efficient computation of forward kinematics and Jacobian matrix of a Stewart platform-based manipulator", IEEE Proceedings of Southeastcon'91, 1991, p.869-874

T.F. Niaritsiry, N. Fazenda, R. Clavel (2004), "Study of the sources of inaccuracy of a 3 DOF flexure hinge-based parallel manipulator", Proceedings of ICRA'04 2004 IEEE International Conference on Robotics and Automation, 2004, p.4091-4096

M. Nissinen, M. Heliövaara, M. Ylikoski, M. Poussa (1993), "Trunk asymmetry and screening for scoliosis: a longitudinal cohort study of pubertal schoolchildren", Acta Paediatrica 82(1): p.77-82.

Optitrack, F. V100 and Rigid Body Tracking Software Library, NaturalPoint, Inc.

N. Oxborrow (2000), "Assessing the child with scoliosis: the role of surface topography", Archives of disease in childhood 83(5): p.453-455.

V. Parenti-Castelli and R. Di Gregorio (1999), "Determination of the actual configuration of the general Stewart platform using only one additional sensor", Journal of Mechanical Design 121: p.21.

V. Parenti-Castelli and R. Di Gregorio (2000), "A new algorithm based on two extra-sensors for real-time computation of the actual configuration of the generalized Stewart-Gough manipulator", Journal of Mechanical Design 122: p.294.

P.J. Parikh and S.S. Lam (2005), "A hybrid strategy to solve the forward kinematics problem in parallel manipulators", IEEE Transactions on Robotics, **21**(1): p.18-25.

A.J. Patel and K. Ehmann (1997), "Volumetric error analysis of a Stewart platform-based machine tool", CIRP Annals-Manufacturing Technology **46**(1): p.287-290.

P. Patias, T. B. Grivas, A. Kaspiris, C. Aggouris, E. Drakoutos (2010), "A review of the trunk surface metrics used as Scoliosis and other deformities evaluation indices", Scoliosis **5**(1): p.12.

P. Patias, E. Stylianidis, M. Pateraki, Y. Chrysanthou, C. Contozis, T. Zavitsanakis (2006), "3D digital photogrammetric reconstructions for scoliosis screening", Proceeding of the ISPRS Company Symposium, Dresden, Germany. The International Archives of the Photogrammetry, remote Sensing and Spatial Information Sciences, Vol. 36.

D.J. Pearsall, J. G. Reid, D.M. Hedden (1992), "Comparison of three noninvasive methods for measuring scoliosis", Physical Therapy **72**(9): p.648-657.

K. Pehrsson, S. Larsson, A. Oden, A. Nachemson (1992), "Long-term follow-up of patients with untreated scoliosis A study of mortality, causes of death, and symptoms", Spine **17**(9): p.1091-1096.

S. Pellanera, M. Mangone, P. Raimondi, M. Paoloni, A. D Michele, S. D. Renzo, M. Vanadia, M. Dimaggio, M. Murgia, V. Santilli (2013), "Vertebral rotation in adolescent idiopathic scoliosis calculated by radiograph and back surface analysis based methods. Correlation between the Raimondi method and Rasterstereography", European Spine Journal 22(2): p.367-371.

R. Perdriolle and J. VIDAL (1985), "Thoracic idiopathic scoliosis curve evolution and prognosis", Spine **10**(9): p.785-791.

P. Poncet, S. Delorme, J.L. Ronsky, J. Dansereau, G. Clynch, J. Harder, R.D. Dewar, H. Labelle, P.H. Gu, R.F. Zernicke (2001), "Reconstruction of laser-scanned 3D torso topography and stereoradiographical spine and rib-cage geometry in

scoliosis", Computer Methods in Biomechanics and Biomedical Engineering **4**(1): p.59-75.

G. Pritschow, C. Eppler, T. Garber (2002), "Influence of the dynamic stiffness on the accuracy of PKM", Chemnitz Parallel Kinematic Seminar, p.313-333.

J. Pruijs, M. Hageman, W. Keessen, R. V. Meer, J.V. Wieringen (1995), "Spinal rotation meter: development and comparison of a new device", Acta orthopaedica belgica **61**: p.107-107.

W. Pun, K. Luk, W. Lee, J. Leong (1987), "A simple method to estimate the rib hump in scoliosis", Spine **12**(4): p.342-345.

C. Reboulet and T. Berthomieu (1991), "Dynamic models of a six degree of freedom parallel manipulators", 'Robots in Unstructured Environments' Fifth International Conference on Advanced Robotics , IEEE, 1991, p.1153-1157.

P. Renaud, N. Andreff, J.M. Lavest, M. Dhome (2006), "Simplifying the kinematic calibration of parallel mechanisms using vision-based metrology", Robotics, IEEE Transactions on **22**(1): p.12-22.

T.S. Renshaw, (1993), "Idiopathic scoliosis in children", Current Opinion in Pediatrics **5**(4): p.407-412.

E.J. Riseborough and R. Wynne-Davies (1973), "A genetic survey of idiopathic scoliosis in Boston, Massachusetts", The Journal of Bone and Joint Surgery **55**(5): p.974-982.

C. Robinson and M. McMaster (1996), "Juvenile Idiopathic Scoliosis. Curve Patterns and Prognosis in One Hundred and Nine Patients", The Journal of Bone and Joint Surgery **78**(8): p.1140-1148.

E.J. Rogala, D. S. Drummond, J. Gurr (1978), "Scoliosis: incidence and natural history. A prospective epidemiological study", The Journal of Bone and Joint Surgery, American volume **60**(2): p.173-176.

T. Ropponen and T. Arai (1995), "Accuracy analysis of a modified Stewart platform manipulator", Robotics and Automation, 1995. Proceedings, 1995 IEEE International Conference on, Vol. 1, p521-525

M. Ruggerone and J. H. Austin (1986), "Moiré Topography in Scoliosis Correlations with Vertebral Lateral Curvature as Determined by Radiography", Physical Therapy **66**(7): p.1072-1077.

T. Sahlstrand (1986), "The clinical value of Moire topography in the management of scoliosis", Spine **11**(5): p.409-417.

S.P. Samagh, C. D. Rosen, K. Otarodifard, M. Kornswiet, G. Palmer, T.Q. Lee (2011), "New method for determining apparent axial center of rotation of lumbar and thoracic spine segments", Journal of Rehabilitation Research and Development **48**(5): p.587-595.

J.O. Sanders, D. W. Polly Jr, W. Cats-Baril, J. Jones, L.G. Lenke, M.F. O'Brien, B.S. Richards, D.J. Sucato (2003), "Analysis of patient and parent assessment of deformity in idiopathic scoliosis using the Walter Reed Visual Assessment Scale", Spine **28**(18): p.2158-2163.

N. Shankar, K. Bridger, M.E. Regelbrugge, W. Winfough (1998), "Smart spindle unit for active chatter suppression of a milling machine: I. Overview, fabrication and assembly", 5th Annual International Symposium on Smart Structures and Materials, International Society for Optics and Photonics, 1998, p.160-166.

D. Stewart (1965), "A platform with six degrees of freedom." Proceedings of the institution of mechanical engineers **180**(1): p.371-386.

I.A. Stokes (1994), "Three-dimensional terminology of spinal deformity: a report presented to the Scoliosis Research Society by the Scoliosis Research Society Working Group on 3-D terminology of spinal deformity", Spine **19**(2): p.236-248.

I.A. Stokes and D. D. Aronsson (2006), "Computer-assisted algorithms improve reliability of King classification and Cobb angle measurement of scoliosis", Spine **31**(6): p.665-670.

I.A. Stokes and M. S. Moreland (1989), "Concordance of back surface asymmetry and spine shape in idiopathic scoliosis", Spine **14**(1): p.73-78.

Y.Q. Sun, D. Samartzis, K.M. Cheung, Y.W. Wong, K.D. Luk (2011), "The “X-Factor” Index: a new parameter for the assessment of adolescent idiopathic scoliosis correction", European Spine Journal **20**(1): p.144-150.

N. Suzuki, K. Inami, T. Ono, K. Kohno, M. Asher (1999), "Analysis of posterior trunk symmetry index (POTSI) in Scoliosis. Part 1", Studies in Health Technology and Informatics: p.81-84.

N. Suzuki, T. Ono, M. Tezuka, S. Kamilshi (1992), "Moire topography and back shape analysis-clinical application", International Symposium on 3-D Scoliotic Deformities, Éditions de l'École Polytechnique de Montréal Montréal, p.124-128.

W.C. Sweatt, C. A. Boye, S.M. Gentry, M.R. Descour, B.R. Stallard, C.L. Grotbeck (1998), "ISIS: an information-efficient spectral imaging system", SPIE's International Symposium on Optical Science, Engineering, and Instrumentation, International Society for Optics and Photonics, 1998, p.98-106.

B.V. Reamy and J.B. Slakey (2001), "Adolescent idiopathic scoliosis: review and current concepts", American Family Physician **64**(1): p.111-117.

H. Takasaki (1970), "Moiré topography", Applied Optics **9**(6): p.1467-1472.

Y. Takeda, G. Shen, H. Funabashi (2004), "A DBB-based kinematic calibration method for in-parallel actuated mechanisms using a Fourier series", Journal of Mechanical Design **126**: p.856.

W. Tanaka, T. Arai, K. Inoue, T. Takubo, C.S. Park (2006), "Calibration method for parallel mechanism using micro grid pattern", ICRA 2006, Proceedings 2006 IEEE International Conference on Robotics and Automation, IEEE, 2006, p.763-768.

T.K. Tanev (2000), "Kinematics of a hybrid (parallel–serial) robot manipulator", Mechanism and Machine Theory **35**(9): p.1183-1196.

M. Tarokh (2007), "Real time forward kinematics solutions for general Stewart platforms", 2007 IEEE International Conference on Robotics and Automation, IEEE, 2007, p.901-906.

T.N. Theologis, J. C. Fairbank, A.R. Turner-Smith, T. Pantazopoulos (1997), "Early detection of progression in adolescent idiopathic scoliosis by measurement of changes in back shape with the integrated shape imaging system scanner", Spine **22**(11): p.1223-1227.

J. Thometz, R. Lamdan, X. Liu, R. Lyon (2000), "Relationship between Quantec measurement and Cobb angle in patients with idiopathic scoliosis", Journal of Pediatric Orthopaedics **20**(4): p.512-516.

J. Thometz, X. Liu, J. Klein (1999), "Functional Classification of Patients with Idiopathic Scoliosis Assessed by the Quantec System: A Discriminate Functional

Analysis to Determine the Patient Group with Different Curves", Studies in Health Technology and Informatics: p.77-80.

J. Thometz, X. Liu, R. Lyon (1999), "Axial Rotation in Idiopathic Scoliosis: A Comparison of the Perdriolle, Scoliometer, and the Quantec Spinal Image System", Studies in Health Technology and Informatics: p.329-331.

T. Thulbourne and R. Gillespie (1976), "The rib hump in idiopathic scoliosis. Measurement, analysis and response to treatment", Journal of Bone & Joint Surgery, British Volume **58**(1): p.64-71.

C. Tischler and A. Samuel (1998), "Predicting the slop of in-series/parallel manipulators caused by joint clearances", Advances in robot kinematics: analysis and control, Springer**:** p.227-236.

S. Treuillet, Y. Lucas, G. Crepin, B. Peuchot, J. Pichaud (2002), "SYDESCO: a laser-video scanner for 3D scoliosis evaluations" Studies in Health Technology and Informatics 88: p.70.

L.W. Tsai (1999), Robot analysis: the mechanics of serial and parallel manipulators, Wiley. com.

L.W. Tsai (2000), "Solving the inverse dynamics of a Stewart-Gough manipulator by the principle of virtual work", Journal of Mechanical Design 122: p.3.

L.W. Tsai, and S. Joshi (2002), "Kinematic analysis of 3-dof position mechanisms for use in hybrid kinematic machines", Journal of Mechanical Design **124**: p.245.

N.H. Tuong, J. Dansereau, G. Maurais, R. Herrera (1998), "Three-dimensional evaluation of lumbar orthosis effects on spinal behavior", Journal of Rehabilitation Research and Development **35**(1): p.34-42.

A. Turner-Smith and B. De Roguin (1984), "Lateral asymmetry index", Annual Report of the Oxford Orthopaedic Engineering Centre, 11Nuffield Orthopaedic Centre, Oxford: p.38-40.

A.R. Turner-Smith (1988), "A television/computer three-dimensional surface shape measurement system", Journal of Biomechanics **21**(6): p.515-529.

A.R. Turner-Smith, J. D. Harris, G.R. Houghton, R.J. Jefferson (1988), "A method for analysis of back shape in scoliosis", Journal of Biomechanics **21**(6): p.497-509.

W. Keessen, J.E.H. Pruijs, M.A.P.E. Hageman, R. van der Meer, J.C. van Wieringen (1994), "Variation in Cobb angle measurements in scoliosis", Skeletal Radiology **23**(7): p.517-520.

H. Wang, C. Xue, W. Gruver (1995), "Neural network control of a parallel robot", IEEE International Conference on Systems, Man and Cybernetics, Intelligent Systems for the 21st Century, 1995, vol. 3, p.2934-2938.

J. Wang and C. M. Gosselin (1998), "A new approach for the dynamic analysis of parallel manipulators", Multibody System Dynamics **2**(3): p.317-334.

J. Wang and C. M. Gosselin (2004), "Kinematic analysis and design of kinematically redundant parallel mechanisms", Journal of Mechanical Design 126: p.109.

S.M. Wang and K. F. Ehmann (2002), "Error model and accuracy analysis of a six-DOF Stewart platform", Transactions-American Society of Mechanical Engineers Journal of Manufacturing Science and Engineering **124**(2): p.286-295.

Y. Wang (2006), "An incremental method for forward kinematics of parallel manipulators", IEEE Conference on Robotics, Automation and Mechatronics, 2006, p.1-5.

S.L. Weinstein, L. A. Dolan, J.C. Cheng, A. Danielsson, J.A. Morcuende (2008), "Adolescent idiopathic scoliosis", The Lancet 371(9623): p.1527-1537.

H.R. Weiss and S. Seibel, "Can surface topography replace radiography in the management of patients with scoliosis?", http://www.oapublishinglondon.com /article/437.

I. Weisz, R. Jefferson, A. Turner-Smith, G. Houghton, J. Harris (1988), "ISIS scanning: a useful assessment technique in the management of scoliosis", Spine **13**(4): p.405-408.

S. Willner (1974), "Growth in height of children with scoliosis", Acta Orthopaedica **45**(6): p.854-866.

S. Willner (1979), "Moiré topography for the diagnosis and documentation of scoliosis", Acta Orthopaedica **50**(3): p.295-302.

K. Wohlhart (1999), "Degrees of shakiness", Mechanism and Machine Theory **34**(7): p.1103-1126.

A. Wojcik, M. Mehta, G. Philips (1994), "Surface imaging of body and spinal shape by the Quantec system", Journal of Bone and Joint Surgery **27**: p.328-333.

S.N. Yurt, M. O. Kaya, C. Haciyev (2002), "Optimization of the PD coefficient in a flight simulator control via genetic algorithms", Aircraft Engineering and Aerospace Technology **74**(2): p.147-153.

X. Zheng, H. Bin, Y. Luo (2004), "Kinematic analysis of a hybrid serial-parallel manipulator", The International Journal of Advanced Manufacturing Technology **23**(11-12): p.925-930.

H. Zhuang and Z. S. Roth (1993), "Method for kinematic calibration of Stewart platforms", Journal of Robotic Systems **10**(3): p.391-405.

A. Zubović, N. Davies, F. Berryman, P. Pynsent, N. Quraishi, C. Lavy, G. Bowden, J. Wilson-Macdonald, J. Fairbank (2007), "New method of Scoliosis Deformity Assessment: ISIS2 System", Studies in Health Technology and Informatics **140**: p.157-160.

A. Zuo, Q. J. Wu, W.A. Gruver (2002), "Stereo vision guided control of a Stewart platform", Proceedings of the 2002 IEEE International Symposium on Intelligent Control, p.125-130.

T.M.L. Shannon (2008), "Development of an apparatus to evaluate Adolescent Idiopathic Scoliosis by dynamic surface topography", Research into Spinal Deformities 6, P.H. Dangerfield (Ed.) Amsterdam: IOS Press, 2008: p.121-7.

J.R. Sanes, and S.L. Zipursky (2010), "Design Principles of Insect and Vertebrate Visual System", Neuron, Volume 66, Issue 1, p.15-36.

F. Chen, G.M. Brown and M. Song (2000), "Overview of three-dimensional shape measurement using optical methods", Optical Engineering, 39(1), p.10-22.

Robert S Wainner, Julie M. Fritz, James J. Irrgang, Michael L. Boninger, Anthony Delitto, and Stephen Allison, "Reliability and diagnostic accuracy of the clinical examination and patient self-report measures for cervical radiculopathy", Spine, 28 no. 1 (2003): 52-62.

I. Busscher, F. H. Wapstra, and A. G. Veldhuizen (2010), "Predicting growth and curve progression in the individual patient with adolescent idiopathic scoliosis: design of a prospective longitudinal cohort study," BMC musculoskeletal disorders, 11(1), 93.

J. S. Smith, C. I. Shaffrey, C. Kuntz, P. V. Mummaneni (2008), "Classification systems for adolescent and adult scoliosis", Neurosurgery, 63.3: A16-A24.

The X—ray images sample are from http://www.pinterest.com/spinecor/scoliosis-x-ray/